PEOPLE'S DEMOCRATIC REPUBLIC OF ALGERIA
MINISTRY OF HIGHER EDUCATION AND SCIENTIFIC RESEARCH

University of Mohamed Boudiaf - M'sila
Faculty of Technology
Department of Electronics

THESIS

A dissertation submitted for the degree of
DOCTORAT

Field**:** Electronics

Option**:** Electronics and Telecommunications

By: TEMMAR Mohamed Nasr eddine

THEME

Analysis and Design of Terahertz Microstrip Antenna Based on Photonic Band Gap Substrate

«Analyse et Conception d'une Antenne Microruban Térahertz Imprimée sur un Substrat Photonique à Bande Interdite.»

Presented and publicly defended on the 18/01/2021

JURY MEMBERS:

MEZACHE Amar	**Professor**	**Univ. of M'sila**	**Chairman**
HOCINI Abdesselam	**Professor**	**Univ. of M'sila**	**Supervisor**
KHEDROUCHE Djamel	**Professor**	**Univ. of M'sila**	**Co-supervisor**
ZEBIRI Chemseddine	**MCA**	**Univ. of Setif**	**Examiner**
KAHLOUCHE Ahmed	**MCA**	**Univ. of M'sila**	**Examiner**
DENIDNI Ahmed Tayeb	**Professor**	**Univ. of Quebec**	**Invited**

2020/2021

Acknowledgments

All gratitude is due to "ALLAH" for giving me the strength, courage, and commitment that enabled me to start and finish this research work.

This thesis work was carried out in the Signal and Systems Analysis Laboratory (LASS), Department of Electronics, University of M'sila, under the scientific direction of Prof. Abdesselam HOCINI.

I would like to express my sincere gratitude and appreciation to my supervisor Prof. Abdesselam HOCINI for all his continuous support, availability, encouragement, and guidance throughout the accomplishment of this research work.

I would like to express my sincere gratitude to my co-supervisor Prof. Djamel KHEDROUCHE for his guidance, motivation, and support throughout the accomplishment of this research work.

I would like to express my sincere gratitude and appreciation to Prof. Ahmed Tayeb DENIDNI for all his support, encouragement, and advice throughout the accomplishment of this research work during the fruitful internship accomplished at the Radio Frequency Laboratory (LRF) in INRS-EMT, Montréal Canada under his guidance.

I would like to express my sincere appreciation to Prof. Amar MEZACHE, professor at the University of M'sila, for his interest in my work by doing the honor of chairing the jury of my defense.

I would like to extend my sincere thanks to all members of the jury:

I would like to thank Dr. Chemseddine ZEBIRI, MCA at the University of Setif, for his interest in this work and for having agreed to examine my work by taking part in the thesis jury.

I would like to thank Dr. Ahmed KAHLOUCHE, MCA at the University of M'sila, for his interest in this work and for having agreed to examine my work by taking part in the thesis jury.

I am thankful to all my colleagues and friends which I have met in LASS and LRF from all around the globe for their encouragement, their useful advice, and support throughout this research work.

Finally, I would like to deeply thank all members of the University of M'sila and all my previously enrolled academic institutions until my small family for all of their overall encouragement and provided support.

Analysis and Design of Terahertz Microstrip antenna based on Photonic Band Gap

by

Mohamed Nasr eddine TEMMAR

January 31, 2021 16:42

Submitted to the Department of Electronics, Faculty of Technology, University of Mohamed Boudiaf - M'sila
on January 2021, in partial fulfillment of the requirements for the
Doctoral Program in Electronics and Telecommunications

الملخص

تركز هذه الرسالة على تحليل وتصميم هوائيات تيراهيرتز الميكروستريب القائمة على الركيزة البلورية الضوئية. تم تصميم وتحليل الركيزة البلورية الضوئية المركبة باستخدام تقنية تعتمد على مزيج من خوارزمية التحسين التطوري مع المحاكي CST Microwave Studio ومقارنتها مع أداء الهوائي القائم على الركيزة المتجانسة و البلورية الضوئية التقليدية. بعد ذلك ، تم تصميم وتحليل العديد من هوائيات تيراهيرتز بناءً على ركائز فجوة الحزمة الضوئية المعدلة والمهندسة. تم كذلك مقارنة النتائج التي تم الحصول عليها من الهوائيات المذكورة مع أوراق بحثية مختلفة. أخيرًا ، تم التحقيق في نظام اتصال داخلي MIMO باستخدام هوائي مصغر مصمم على أساس ركيزة بلورية ضوئية محسنة مع الجرافين في نطاق التيراهيرتز متبوعًا بدراسة سيناريو اتصال داخلي شائع لنظم SISO و SIMO و MISO و MIMO ومقارنتها مع أعمال بحثية أخرى.

الكلمات المفتاحية: تيراهيرتز ، هوائي الميكروستريب، البلورة الضوئية ، خوارزمية التحسين ، CST ، MIMO

Abstract

This thesis focuses on the analysis and design of terahertz microstrip antennas based on photonic crystal substrate. A synthesized photonic crystal substrate is designed and analyzed by using a technique based on the combination of an evolutionary heuristic optimization algorithm with the CST Microwave Studio simulator and compared with homogeneous and conventional photonic crystal substrate-based antennas performance. Then, several terahertz antennas are designed and analyzed based on different modified photonic bandgap substrates. The obtained results from the aforementioned antennas are compared with different research papers in literature. Finally, a MIMO indoor communication system is investigated using a designed microstrip antenna based on an optimized photonic crystal substrate with a graphene load at the terahertz band followed by an indoor communication scenario, which is studied for SISO, SIMO, MISO, and MIMO systems and compared with other researches in literature.

Keywords: Terahertz, Microstrip antenna, Photonic crystal, Heuristic algorithm, CST, MIMO

Résumé

Cette thèse se concentre sur l'analyse et la conception d'antennes microruban térahertz basées sur un substrat de cristal photonique. Un substrat de cristal photonique synthétisé est conçu et analysé en utilisant une technique basée sur la combinaison d'un algorithme d'optimisation heuristique évolutive avec le simulateur CST Microwave Studio et comparé aux performances d'antennes basées sur un substrat homogène et de cristal photonique conventionnel. Ensuite, plusieurs antennes térahertz sont conçues et analysées sur la base de différents substrats de bande interdite photonique modifiés. Les résultats obtenus à partir des antennes susmentionnées sont comparés à différents articles de recherche dans la littérature. Enfin, un système de communication intérieur MIMO est étudié à l'aide d'une antenne microruban conçue basée sur un substrat de cristal photonique optimisé avec une charge de graphène dans la bande térahertz suivie d'un scénario de communication intérieur commun qui est étudié pour les systèmes SISO, SIMO, MISO et MIMO et comparé avec d'autres recherches dans la littérature.

Mots clés: Terahertz, Antenne Microruban, Cristal photonique, Algorithme heuristique, CST, MIMO

Publications

Journal Papers

1. **M. N. Temmar**, A. Hocini, D. Khedrouche, and M. Zamani, "Analysis and design of a terahertz microstrip antenna based on a synthesized photonic band gap substrate using bpso,"Journal of Computational Electronics, vol. 18,no. 1, pp. 231–240, 2019.

2. A. Hocini, **M. Temmar**, D. Khedrouche, and M. Zamani, "Novel approach for the design and analysis of a terahertz microstrip patch antenna based on photonic crystals, "Photonics and Nanostructures - Fundamentals and Applications, vol. 36, p. 100723, 2019.

3. **M. N. Temmar**, A. Hocini, D. Khedrouche, and T. A. Denidni, "Enhanced flexible terahertz microstrip antenna based on modified silicon-air pho-tonic crystal,"Optik, vol. 217, p. 164897, sep 2020.

4. **M. N. Temmar**, A. Hocini, D. Khedrouche, and T. A. Denidni, "Analysis and design of mimo indoor communication system using terahertz patch antenna based on photonic crystal with graphene," Photonics and Nanostructures - Fundamentals and Applications, vol. 43, p. 100867, 2021.

International Communications

1. **M. N. Temmar**, A. Hocini, and D. Khedrouche, "Design and analysis of terahertz microstrip patch antenna based on optimized photonic crystal substrate," in The Third International Conference on Technological Advances in Electrical Engineering (ICTAEE'18), December 2018.

2. **M. N. Temmar**, A. Hocini, and D. Khedrouche, "Design and analysis of terahertz microstrip circular patch antenna based on an optimized polyimide photonic crystal substrate." in The Second International Conference on Electrical Engineering (ICEEB'2018), December 2018.

Other works

1. H. Ben salah, A. Hocini, **M. Temmar**, and D. Khedrouche, “Design of mid infrared high sensitive metal-insulator-metal plasmonic sensor,”Chinese Journal of Physics, vol. 61, pp. 86–97, oct 2019.

2. A. Hocini, H. Ben salah, and **M. Temmar**, “Ultra-high sensitive structure based on a metal-insulator-metal waveguide coupled with metal nano racetrack defects in cavity,”Journal of Computational Electronics (under review), 2020.

Contents

List of Figures

List of Tables

List of Abbreviations

1D 1 Dimension.

2D 2 Dimensions.

3D 3 Dimensions.

BPSO Binary Particle Swarm Optimization.

BWO Backward Wave Oscillator.

CM Cavity Model.

CMOS Complementary Metal-Oxide-Semiconductor.

CST Computer Simulation Technology.

DSP Digital Signal Processor.

FIT Finite Integration Technique.

FSS Frequency Selective Surface.

GA Genetic Algorithm.

IC Integrated Circuit.

Info Information.

IR InfraRed.

ITU International Telecommunication Union.

LoS Line of Sight.

MATLAB MATrix LABoratory.

MIMO Multiple Inputs Multiple Outputs.

MISO Multiple Inputs Single Output.

nLoS non Line of Sight.

OFDM Orthogonal Frequency-Division Multiplexing.

PBG Photonic Band Gap.

PCs Photonic Crystals.

PSO Particle Swarm Optimization.

QCL Quantum Cascade Laser.

RoF Radio over Fiber.

SIMO Single Input Multiple Outputs.

SISO Single Input Single Output.

SoC System on Chip.

TE Transverse Electric.

THz Terahertz.

THz-SoC Terahertz System on Chip.

TLM Transmission Line Model.

TM Transverse Magnetic.

VSWR Voltage Standing Wave Ratio.

List of Symbols

BW Bandwidth.

G Gain.

G_t Gain of the transmitter.

K Medium absorption coefficient.

K_B Boltzmann's constant.

N_0 Noise power spectral density.

Sp_{ij} Distance between receiver j and the wall i.

Δ Surface deviation coefficient.

Θ_I Angle of incidence.

Θ_O Angle of refection.

$\hbar$ Reduced Planck's constant.

λ Wavelength.

μ_c Chemical potential.

ω Angular frequency.

c Speed of light in free space.

e Electron charge.

f Operating frequency.

n_s Carrier density.

sgn Sigmoid function.

t_s Thickness of the substrate.

y Receive signal.

A_{abs} Molecular absorption los.

A_{ref} Reflection loss.

A_{spread} Spread loss.

F_B Fractional bandwidth.

G_r Gain of the receiver.

H Gain matrix.

L_p Length of the patch.

L_{ij} Horizontal distance between transmitters and receivers.

P_i Transmitted power from the i_{th} antenna.

S Scattering parameter.

Sp_i Distance between transmitter i and the wall i.

T Temperature.

V_f Fermi velocity.

W_p Width of the patch.

Γ Phenomenological scattering rate.

ϵ_{reff} Effective dielectric constant.

λ_i Singular values of the gain matrix.

ρ Roughness factor.

σ Surface conductivity.

d Travelled distance.

d_r Spacing between receivers.

d_t Spacing between transmitters.

f_d Fermi-Dirac distribution.

f_r Resonance frequency.

g Surface variation intensity.

h Normal Planck's constant.

h_{ij} Gain matrix element between i_{th} transmitter and j_{th} receiver.

n_{min} Rank of the gain matrix.

w White Gaussian noise.

x Transmit signal.

Chapter 1

General Introduction

1.1 Motivation

Terahertz (THz) research has evolved rapidly over the past 25 years in several fields including spectroscopy, imaging, and engineering[1]. In fact, THz spectrometers and imaging systems have been standard research laboratory devices [2] in combination with recently upgraded terahertz sources and detectors [3, 4]. They have also been utilized by many sectors and applications like pharmacy quality control [5], medicine [6], explosive and hidden arms detection, [7, 8] and industry quality control [9, 10]. Over the last decades, several organizations have taken the possibility of utilizing THz waves as a way to transfer information (Info) into account. In all the aforementioned interesting applications, the terahertz antennas are the most crucial component of these systems. Many papers covering various aspects of the topics such as THz sources and detectors, modulation schemes, and measurements for wireless communication have been published. They also discuss wireless terahertz networking methods in depth. Specific interpretations of the THz frequency spectrum and applications exist in the literature but further enhancements are required for effective and efficient terahertz antennas[11].

1.2 Thesis Contributions and Organization

The contributions and outlines of this thesis are ordered as follows:

In Chapter 2, an overview of THz technology is presented where microstrip antenna importance is discussed and highlighted in this promising technology followed by a general presentation of photonic crystal structures. Finally, a conventional THz antenna based on a photonic crystal substrate is analyzed and discussed.

Chapter 3 presents a designed THz microstrip patch antenna based on a synthesized photonic crystal substrate using Computer Simulation Technology (CST) Microwave Studio combined with the Binary Particle Swarm Optimization (BPSO) algorithm in MATrix LABoratory (MATLAB) as a modern optimization technique to synthesize unique photonic crystal structures that enhance the electrical characteristics of the antenna. First, the microstrip antenna is designed based on a photonic bandgap substrate, using air cylinders embedded in a silicon substrate, by analyzing and designing the substrate separately, then employing it in a microstrip antenna. After that, optimization of the microstrip antenna based on the Photonic Band Gap (PBG) substrate is presented using BPSO and analyzed for two different optimization merit functions, viz. the return loss with gain, and the bandwidth with gain. The impact of this published work [12] is presented by comparing it with literature.

Chapter 4 first presents a designed and analyzed compact THz rectangular microstrip patch antenna with a thick substrate for operation in the atmospheric window around 0.65 THz, where the atmospheric path loss is relatively small, followed by the design of the PBG structure which is employed as the substrate for a conventional microstrip antenna. Then, four different enhancements to the conventional photonic crystal substrate are presented by introducing aperiodic Photonic Crystals (PCs) in order to improve the characteristics of the antennas. After that, modifications of the patch shapes are depicted followed by modifications in the substrate's material of Roger-Air and Silicon-Air PCs. The enhancements of these antennas [13, 14, 15, 16] are presented by comparing it with other research papers throughout the chapter progression.

Chapter 5 presents the analysis and design of the Multiple Inputs Multiple Outputs (MIMO) indoor communication system using a THz patch antenna based on a photonic crystal with graphene. In this chapter, first, graphene load is analyzed

and investigated for its interesting characteristic. Followed by MIMO antenna design based on homogeneous, photonic crystal, and optimized structure with the graphene load. Then, by applying the designed antennas in an indoor communication scenario in which its occurrence is most often established, different analyses and studies for capacity enhancement are conducted [17] and compared with other results in the literature.

Chapter 6 concludes the presented contributions and provides some suggestions for further research.

Chapter 2

Terahertz Antenna Based on Photonic Band Gap Structures: State of the Art

2.1 Introduction

The employment of the terahertz band for potential wireless networking solutions is a fresh field of research aside from the traditional applications [18, 19]. The need for high data rate connectivity systems is increasing due to the monotonous rise in demand for fast transmission and reception with an accelerating population development. In this chapter, an overview of terahertz technology is presented where microstrip antenna importance is discussed in this technology. Finally, a conventional terahertz antenna based on a photonic crystal substrate is analyzed and discussed.

2.2 Terahertz Technology

2.2.1 Terahertz region and characteristics

Indeed, the data rate of wireless communication systems can be increased in two different ways aside from power limitations. Firstly, when the transmission network's

bandwidth increased, but the current devices depend on the narrow bandwidth where, in most situations, the bandwidth of the interface is just around 10% of its operating frequency [11]. The next approach to this is the rise in operational frequency in such a manner that telecom networks will meet the target user with a large data rate, even with the limited bandwidth such as the 60 and 90 GHz wireless systems [20, 21, 22] which have been built to fulfill the high bandwidth specifications but are still inadequate to satisfy the potential demands.

The next possible approach to cope with this issue is for the operating frequency band to be shifted to the terahertz band, sandwiched between the spectrums of microwave and far-infrared as shown in Figure 2.1, which is defined as the band between 300 GHz and 3 THz according to the International Telecommunication Union (ITU) . In fact, it is defined as the band from 100 GHz or 300 GHz to 3,10, or 30 THz in literature [23, 24].

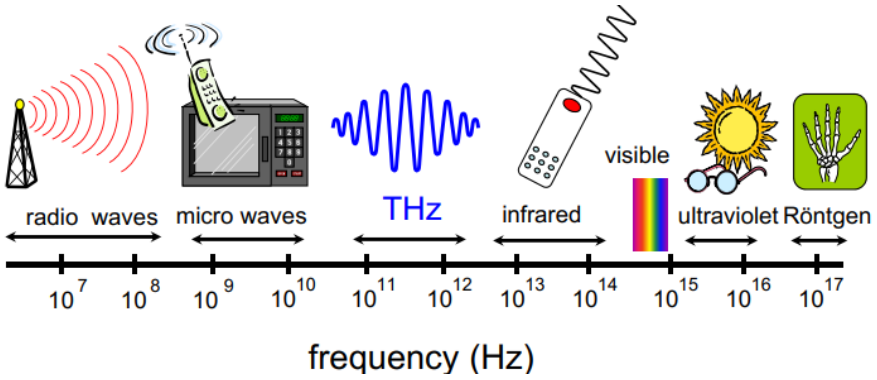

Figure 2.1: Terahertz band location in the frequency spectrum [25].

However, the features of the device vary as the operating frequency rises and the specific aspects of the terahertz wireless communications device need to be evaluated. Besides, since the band sits between the two well-explored spectra systems, all electronic and photonic routes can be used to develop the terahertz spectrum [26].

Over the last decades, the need for a point-to-point wireless communications across an amount of space bandwidth has grown rapidly. One means of achieving these bandwidth criteria is to improve the flexibility of spectral usage by advanced modulation techniques which results in enabling improved point-to-point data throughput, enhancing frequency share, and increasing reuse levels within a space range. The channel bandwidth formula of Shannon indicates a higher limit

for this strategy even if it is generalized to a wireless network in a shared space through a multi-inputs multi-outputs approach. In order to have adequate communication capacity, transmitting bands must be reached at high carrier frequencies beyond the current level. Under the bandwidth rule of Edholm[27], demand has increased every 18 months in the last 35 years for the bandwidth of short-range wireless communication [28].

Mann [29] deems these constraints and points toward a niche in which a very high data rate is needed on a multipoint to the multipoint basis on short distances, i.e. the first mile problems with the ones of the last mile, for commercial operation of terahertz communications networks in cities where the cost of installing optical cables is prohibitively large, for example, where fast dedicated internet connections are a potential solution. Mann also claims that terahertz should conform to stringent community development laws for a streamlined terahertz scheme. A number of high bandwidth technologies can be allowed by means of a terahertz communication system of gigabit or higher rates, including [30] cellular broadband fiber optical networks extensions, a wireless extension to the high-speed wired local network,[31] a link between low data rates, wireless and high-speed optical fiber networks and HDTV [32].

It is important to analyze the benefits and drawbacks of the terahertz waves compared with the microwave and far-infrared before investigating the system characteristics of this work. The different benefits, that this electromagnetic spectrum band provides, are described as follows[33]:

- The spectrum of the microwave is nearly all filled with various utilities. However, a wider spectrum is presented in Terahertz band.
- As a result of less free-space wave diffraction, terahertz communications are inherent to a greater directivity than the micro or millimeter-waves.
- Terahertz communications can be introduced as a connection channel. Terahertz can enable ultra-high frequency bandwidth schemes which can provide secure communication, wide bandwidth, and security against channel attacks such as jamming.
- Terahertz has poor signal attenuation under some ambient environments such

as fog, as opposed to IR.

- The time-dependent refractive index of the atmosphere, scintillation, raised in the IR can be decreased via the terahertz channel.
- For the last and first mile solutions, terahertz is a feasible alternative.
- The greatest allocated frequency given in the latest regulation is 300 GHz so it is free of permission at terahertz band.
- Due to the need for new cutting edge modulation techniques, including OFDM, coherent communication, the substantial advancement of the data rate is sluggish in IR wireless communication systems.

While the terahertz communication channel is persuasive and compelling in the almost millimeter-wavelength of the electromagnetic spectrum, the associated network limitations must be resolved prior to complete commercialization. The atmospheric path loss remains the biggest obstacle to the introduction of the wireless terahertz commercial network. This impairment is caused by varying ambient environments which are demonstrated by the effects on the spread of the electromagnetic wave across a broad frequency range as shown in Figure 2.2 [34].

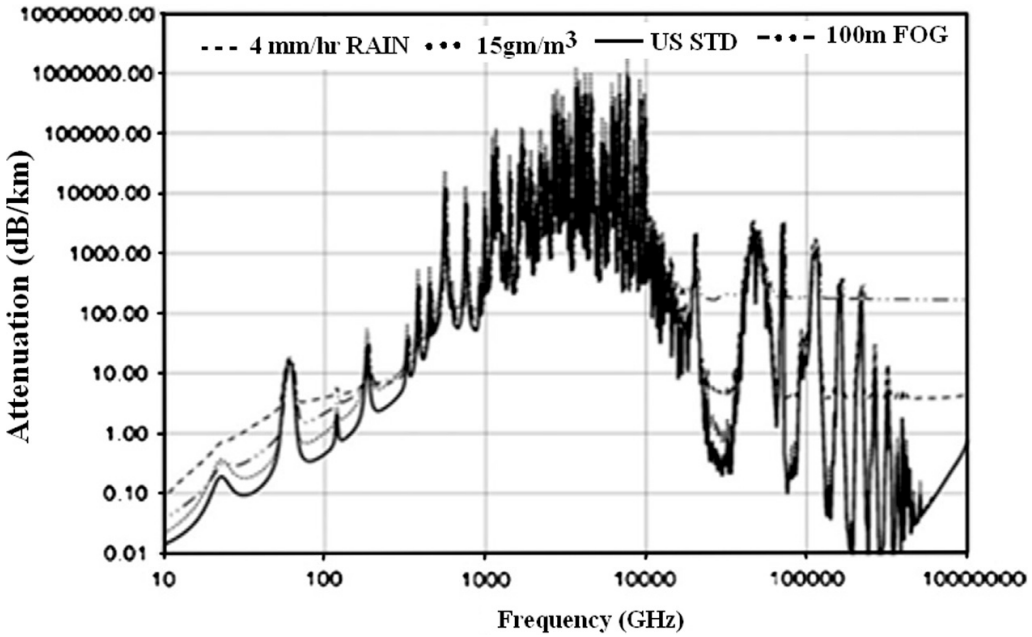

Figure 2.2: Atmospheric path loss in different ambient environments in terahertz band [11].

According to Figure 2.2, the attenuation of the signal decreases with the increase

in the wavelength. The legend's dotted line shows the signal attenuation at sea level in 4 mm/hr rainy weather. The dotted line displays the water level in the soil at 15 gm/m^3. The solid line displays the normal US weather conditions (59% relative moisture), while the dash-dot line indicates 100 m of fog visibility. Based on Figure 2.2, it is noted that the attenuation in the humid environment is the main downside to the Terahertz Communication System. This number, however, is comparatively lower than the IR wave. At 240 GHz, the average foggy attenuation is roughly 200 dB/km and 80 dB/km [35] for the IR and terahertz waves, respectively. In fact, the terahertz link has often been found to undergo higher losses than the microwave. However, in extreme weather conditions, it may be a strong choice against IR. Regardless of the tiny number of contaminants of clouds and pollen in the atmosphere, terahertz loss is limited up to 1 THz. Terahertz propagation primarily depends on the state of the atmosphere and shifts in attenuation frequency due to changes in the height, temperature, etc.

In order to fight against such unfavorable circumstances, it is suggested the need for robust network architecture, otherwise, terahertz connectivity will be limited to either indoor wireless [36] or inter-satellite connectivity only [37]. Fortunately, in the terahertz band, there are several low atmosphere loss windows where wireless connectivity can be built successfully. Such ranges are therefore smaller than $1THz$ with a reduced ambient loss at $300GHz, 350GHz, 410GHz, 650GHz, and 850GHz$,[38] and less than $100dB/km$ for short-range communications. In addition, the attenuation is not important at over $16km$ where the moister impact is marginal and thus inter-satellite connectivity is formed at this height.

Terahertz fiber, such as hollow-glass metallic waveguides[39], bare metal wires[40], and photonic crystal fibers [39], is distinguished by a relatively broad attenuation as compared to near IR wavelengths, which include low-loss optical fibers. As fiber-optic transmission networks will hold very large data rates as high as $100Gb/s$ over tens of kilometers in length, It is impractical that communication systems with terahertz would use terahertz fibers for long-distance propagation. Terahertz fibers may be stronger than the inherent attenuation and dispersal of building materials if the transmission distance is less than a meter, for example through a barrier such as a

wall. However, the Radio-over-Fiber (RoF) approach will use optical fibers for the propagation of terahertz modulated optical signals to the outside of buildings before converting them into terahertz radiation[33].

In free-space, the value of diffractive effects can be analyzed using the Friis equation. According to Brown analysis [33] the load of the receiving antenna is supplied by

$$P_{out} = P_{in}(\frac{\lambda}{4\pi d})^2 G_r G_t F_r(\theta_r, \phi_r) F_t(\theta_t, \phi_t) \tau \epsilon_p \tag{2.1}$$

where the power supplied to the transmitting antenna is P_{in}, G is antenna gain, F is a function of the normalized intensity pattern, τ is the path power transmission factor, ϵ_p is the efficiency of the polarization coupling, λ is the radiation wavelength and d is the spacing between the receiving and transmitting antennas. θ and ϕ are the angles of spherical coordinates at either the receiver or transmitter.

Two factors eventually lead to the free-space loss factor $(\frac{\lambda}{4\pi d})^2$: the presumption that the aerial measurement of the far-field radiation from the transmitting antenna contributes to the transmitter being assumed to produce a spherical wave with a decrease in intensity of $1/d^2$. Furthermore, the second element, λ^2, comes from the diffraction-restricted directivity D_{max} or the solid angle that defines the degree with which the detector is effective in the diffracting intensity pattern featured as $D_{max} = 4\pi A_{eff}/\lambda^2$ with

$$G_t = \frac{P_{rad}}{Pin} D_t \tag{2.2}$$

in which P_{rad} is the radiated power, rely on an antenna gain and directivity. Unless the radiation and the input power are equal, then the antenna gain is identical to the directivity. Equation 1 may be rewritten as

$$P_{out} = P_{in} \frac{A_t A_r}{d^2 \lambda^2} F_r(\theta_r, \phi_r) F_t(\theta_t, \phi_t) \tau \epsilon_p \tag{2.3}$$

where A_t and A_r correspond to the transmitter's and the receiver's effective areas respectively. The received power at the detector changes by $1/\lambda^2$ according to Equation 2.3, thereby increasing detection performance as the wavelength decreases or the frequency of operation rises to terahertz. For calculations of the maximum data

transfer distance of a $400GHz$ relative to a $60GHz$ device, Mann[29] used a simpler form of Equation 2.3. Although terahertz sources are actually less efficient than comparatively large microwave sources, the peak distances for data transmission are $1.9 - 2.0km$. The low power of a $400GHz$ network is compensated by a $400GHz$ radiation diffraction below that of $60GHz$[33].

For the atmospheric attenuation windows of terahertz signals such as the $200 - 300GHz$ or $600 - 700GHz$, Figure 2.2, are readily accessible for terahertz communications. Koch[28] states that the realistic terahertz link distances are restricted to multiple tens of meters by accounting of the high atmospheric attenuation. Therefore, terahertz wireless networks are expected to be restricted to medium and short indoor communication implementations as outdoor situations are far less possible unless unclear weather is uncommon.

As both indoor and outdoor terahertz networks have reduced diffractive effects at terahertz frequencies compared with microwave frequencies, a line of sight between the sender and the receiver is likely to be needed. This restriction is less of a concern for outdoor devices, for instance, where the transmitter and the receivers were mounted on the roofs of buildings.

For indoor structures, non-line of sight paths like reflections from walls will have to be considered. Evidently, the transmission path is significantly disrupted by objects or persons passing along the beam lane. The high gain per antenna demands a strongly directed terahertz emission and a line of sight detection. It should be noted that this terahertz-wireless data link paradigm is quite different from the current wireless indoor communication networks. As an additional illustration of the need for innovative technologies, obstacles may obstruct the line of sight as people walking through the space such that suitability of non-line vision paths such as the reflection of walls is required. Hence, the introduction of indoor terahertz connectivity should therefore not be merely an application of current technology but will require the creation of different techniques and innovations to make it feasible.

Nonetheless, considering that a reflection on usually construction materials [41] causes more losses in the links, highly reflective mirrors are required. Furthermore, controllable high-gain antennas are needed if the primary route is blocked. The re-

flective "wallpaper," which enhances terahertz reflection [42] from walls when there is no visibility in room space is a crucial hardware feature for the implementation of indoor terahertz communications. Real refractive indices 1.7 and 1.59 were implemented in the first edition of the reflective paper[43]. Stacked alternative layers provided a comparatively high 76% reflectivity with a bandwidth of $16GHz$ at $187GHz$. One of the advantages of these dielectric mirrors is that they are versatile since they can be constructed of versatile plastics. The maximal reflectivity is therefore constrained by the index difference of the different layers. An enhanced mirror version mentioned in reference[44] is composed of alternative polypropylene $n = 1,53$ stacks and silicone $n = 3,418$ with high resistivity. These mirrors have 95% high reflectivity for the s-polarization as well as p-polarization and independent of the angle of incident owing to the tremendous index disparity between adjacent classes. Subject to the change of the reflecting band in p-polarization with an angle of incidence, the bandwidth is reduced to $56GHz$. Dispersive properties reports of the mirror show that the group delay is in the range of $5ps$, [45] with a variation between 0.25 and $0.4THz$ of both the terahertz frequency and polarization. Unfortunately, the crystalline silicon layers of $63\mu m$ thickness are not versatile. However, a flexible high index dielectric may be generated with the combination and coextrusion of high resistance silicone or TiO_2 powder with polypropylene [46]. This will increase the efficiency and standardization of the flexible dielectric terahertz mirror.

Studies on terahertz transmission problems rely primarily on indoor and outdoor channel modeling, propagation impacts analysis, modulation schemes assessment, and hardware components of terahertz. Compared to microwave or millimeter-wave networks, the inherent benefit of terahertz communications networks is wider bandwidth. Yet, what about the other set of opposing frequencies, including IR.

The most common optical transmission carrier with a limited distance of up to $10km$ is established as the IR free space transmission connection with a $1.5\mu m$ wavelength. The recorded data rate is $155Mb/s$ [47] as previously stated by Koch,[28] despite the fact that wireless IR devices are 30 years old. A research review [33] has found no little progress over the $155Mb/s$ data rate. Recently, a data limit of $10GB/s$ was shown in an atmospheric simulation environment [48]. Improved

modulation technologies such as orthogonal frequency division multiplexing have been essential to growing the IR wireless data limit to $10Gb/s$. Multi-Inputs multi-Outputs (MIMO) processing with coherence detection are employed for $100Gb/s$ per channel connection [33].

The transceiver misalignment attributable to air turbulence and moisture variations in the beam trajectory, i.e. scintillation, as well as ambient absorption of the IR signal are two of the most critical problems for IR free-space connectivity [49]. Changes in environmental turbulence and moisture induce differences in the real ambient refractive index in time and space. The position of the IR beam on the recipient thus continues to shift in time, resulting in a scintillation impact.

Another possible advantage of terahertz is that intensity modulation and detection utilizing IR photodetectors is not as susceptible as terahertz heterodyne detectors relative to IR communication systems presented in [28]. In comparison, IR light noise is typically more dominant than terahertz noise. Finally, for IR wavelengths, the eye safety concern demands that the transmitted strength of the IR be restricted to eye-safe intensity [33].

2.2.2 Terahertz channel models

The research in [50] reveals that both the molecular structure of the media and the propagation length have an intense effect on the terahertz transmission channel. The main influence on the conduct of terahertz waves is the high absorption from the molecules of water vapor that not only decreases the emitted signal but also creates colored noise. The terahertz band can be perceived as a single transmitting window of $10THz$ in the very short range, i.e. for a transmitting length of many tens of millimeters. That is the greatest distinction from current communications networks that utilize a single transmitting window below $350GHz$. In addition to promoting extremely high transmission speeds, the very high terahertz band channel capacity allows modern encoding and modulation technologies as well as innovative networking protocols for resource-limited nano-applications which are more convenient. The researcher realize that a nano-transceiver is still facing multiple obstacles to incorporate or integrate this communication scheme in a nanoscale system, but it

is considered that the anticipated effect of nano-networks would undoubtedly inspire and promote its growth in our society.

Figure 2.3 from [51] demonstrates the layout of the test benches for terahertz communications. They are divided into three groups and support each category by the "averaged" fit, which indicates the development depending on the communications distance. The data were replicated in part from [52] and augmented by the latest records. The researcher emphasize on the following three key points in evaluating these results. For both shown groups, the reached data rate is continuously rising. Secondly, the growth rate is then supposed to be inversely proportionate to the transmission distance. In other terms, the smaller the distance is, the higher the data rate is reached. Lastly, as can be noted, the midline development, distance from 1 to $10m$, permit us to predict that $100Gbit/s$ solutions will be possible by 2020.

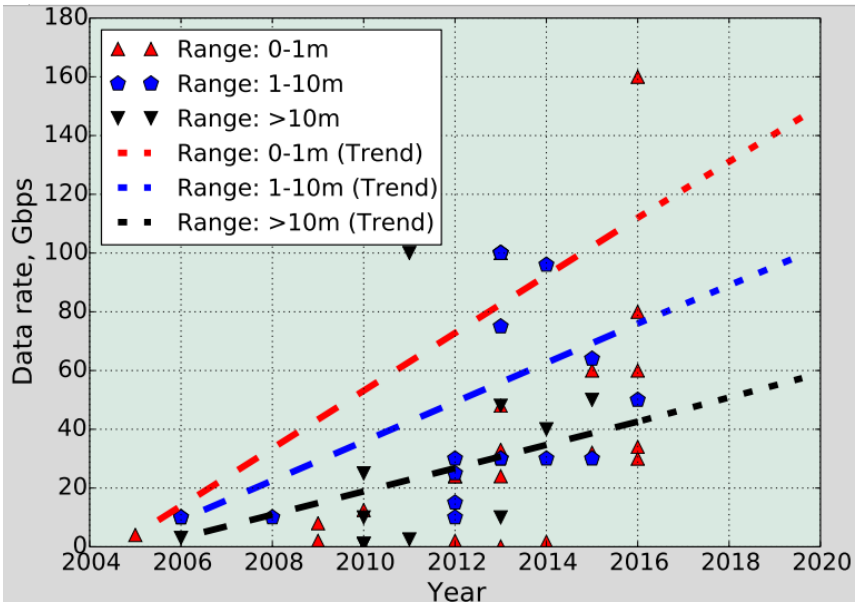

Figure 2.3: The layout of the test benches for terahertz communications [51].

The terahertz networking standardization began in 2008, with the creation under $IEEE802.15$ family of a Terahertz Interest Group (IGterahertz). The NTT, $NICT$, $AT\&T$, $TUBS$, and $Intel$ Alliance explored the inherent shortcomings of the terahertz spectrum in $2008-2013$. The main goal is to create a PHY-MAC layer approach for communications in the lower terahertz range, $252-325GHz$,[53]. In the course of 2014 the $IEEE802.13.3d$ Task Group on $100Gwireless$, TG100 G was

Table 2.1: IEEE 802.15.3d vision of terahertz wireless communications prospective application summary [53], [53], and [51].

Application	Topology	Antennas directivity	Range m	Data rates, Gbit/s
Wireless backhaul	Point-to-point	Extremely directive (>50dBi each side)	500	10-100
Wireless fronthaul	Ad hoc	Highly directive (Base station: >20dBi)	200	10-100
Data centers	Point-to-point	Highly directive (>20dBi each side)	100	1/10/40/100
Kiosk downloading	Point-to-point	Directive (>10dBi kiosk side)	0.1	1-100
Intra-chip networks	Ad hoc	Deployment specific	0.03	1-100

updated. Table 2.1 outlines the $IEEE$ outlook on potential terahertz networking technologies and related technical specifications. The situations vary from wired communications to backhaul and fronthaul lines for cell networks within 5G and afterward. The scope of distances from $3cm$ to $500m$ is exhibited. The specification list, foreseen in the group $IEEE802.15.3d$, has a gap distance of 0.1 to $100m$, which is remarkable. However, it is believed that the indoor wireless connectivity through a terahertz-band in the range of 0.1-10m has to be tackled as one possible application according to the advances in terahertz technology, as well as the growing demand for higher wireless data rates.

2.2.3 Applications and systems

One of the interesting applications is in the research work [51], the idea of an Ethernet socket directly configured with a terahertz cable which is a system functioning in the terahertz frequency range illustrated in Figure 2.4.

Figure 2.4: Terahertz application for Indoor wireless communication systems with massive data transfer capacity [51]

Combining a gigabit Ethernet with the proposed wireless terahertz interfaces will allow massive transfers of wireless data. A step-by-step guide is provided towards the deployment of the planned indoor wireless multi-gigabit connectivity for first and last-mile access in the terahertz band. In both $IEEE802,15.3d$ ($50GHz$ bandwidth and frequency center of $300GHz$) with real terahertz situations where a huge bandwidth of $500GHz$ between $1-1.5THz$, the first phase of the proposed Roadmap are presented [51]. In spite of the target capacity and data bandwidth values, a strong terahertz attenuation and scattering level limits the transmission distance and has to be mitigated with adequate directive beam shaping antennas in both *LoS* and *nLoS* situations. The development of these antennas in the attached transceivers reflect the main challenge to seize the advantage of the terahertz frequency band's extraordinary ability.

Another application is the conducted study in [54] which revealed a detailed simulation analysis on the utilization of Terahertz ($0.8-1.2THz$) MISO technique inside human tissues. The skin model is divided into three layers: stratum corneum, dermis, and epidermis. The impact of sweat ducts and the crudity between layers are taken into account. As a receiving antenna, one dipole antenna was implanted in the epidermis layer while the dermis region contains the transmitting antenna with two dipole antennas. In-vivo channel spatial diversity approaches have been studied. The spacing between transmitters was chosen to ensure that the interconnection, coupling, between the antennas is often lower than $-17dB$. In order to analyze the distance influence, the distance from the two Tx antennas and the receiver was varying. Although it is not beneficial to use multiple antenna strategies for Vivo nano-communications, except under interference circumstances, fading and multipath. The MIMO antenna system provides improved data performance. This early inference illustrates the disparity between in-vivo and traditional communications networks. The work also presented an analysis of applications and advantages for the usage of MIMO in terahertz bands for in-vivo nano-communication. Study to develop terahertz biomedical applications in vivo connectivity with the MIMO antenna system is still a challenge in order to reach full channel efficiency through the analysis of the spatial relationship inside the body medium and the deployment

of MIMO antenna systems in the body.

Furthermore, the application of terahertz radiation for plant control is illustrated in Figure 2.5 [55], as terahertz propagation offers practically real-time hydration and dry stress details. Furthermore, the non-destructive property of T rays enables water supply monitoring to the plant breeding industry with intelligent irrigation approaches and control for selective cultivation which was laboratory restricted before.

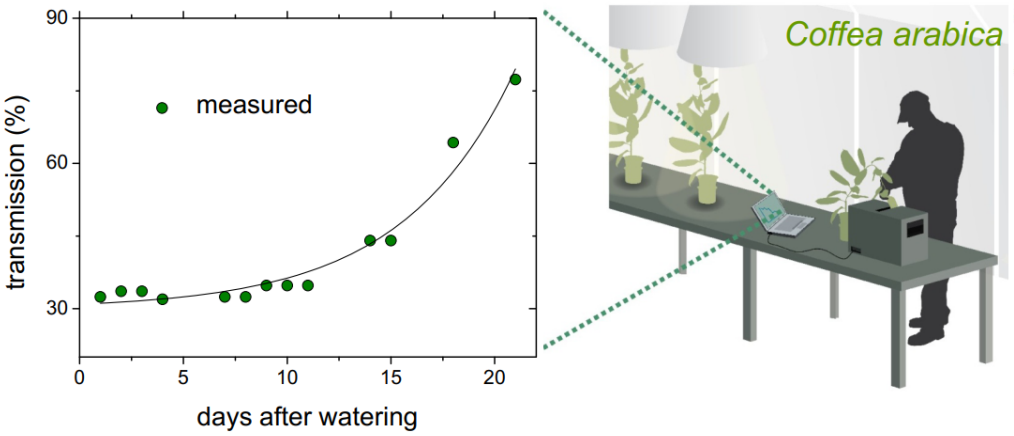

Figure 2.5: Terahertz application for real time hydration and dry stress details

In most terahertz literary papers either terahertz sources, detectors, or components are addressed where they commonly encourage the research with the right to believe that terahertz could be employed for secure communications. Safe connection situations may involve stealthy interaction between unmonitored or controlled cars and personnel. Unmonitored cars need short-haul safe connectivity links to be able to obtain instructions or data until they deploy and execute their autonomous or remote operated task. Unauthorized staff would not be able to recognize the data through eavesdropping on communications networks or the existence of a transmission link in order to protect the Information (Info) [33].

A primary factor for safe terahertz wireless connectivity within the United States Department of Defense (DoD) could be for Project [56] of broadband mobile-on the-move techniques leveraged by both terrestrial and satellite networks. This transition in strategy represents DoD's intention to switch from a manual to autonomous for the spectrum management framework. Through utilizing this latest technology, DoD

intends a military network that connects land, sea, air, and space operations with layered flexibility, persistent communication, and adaptable to the situation. High bandwidth and safe communications are obviously important for such a device. Terahertz connectivity links may deliver each of these essential characteristics as part of a full network. These features include highly directive beams in comparison with microwave transmission, lower radiation scattering in comparison with wireless IR, restricted atmospheric attenuation propagation range, and channel encryption, wide link bandwidth for spread spectrum techniques that enable anti-jamming and low likelihood of sensing systems and activate concealed terahertz signals within the background noise.

As the frequency of terahertz is greater than microwaves, terahertz radiation rays can diffract less naturally. Thus, terahertz links are typically a line of sight, as discussed before. Due to the fact that terahertz transmission beams are strongly directed, the region in which terahertz radiation can track can be concentrated. Microwave transmission is less directional; thus, unauthorized workers will more readily sense side lobes. On the other side of the spectrum, IR transmission with a higher carrier spectrum and smaller realistic beam width are more spatial than terahertz. Nevertheless, ambient objects actively scatter IR radiation. Scattered IR radiation from ambient objects may be measured, thereby undermining the link of communication.

Inherently atmosphere attenuation of terahertz radiation may also act as an advantage for safe channels, thus reducing the total range for wireless transmission. Wave propagation is monitored by air absorption and thus reduces the range for identification. For secure communications, it might be feasible to use attenuated wavelengths of IR links $5 - 7m$ [49]. Due to the strong directive radiation, the transmission of data to the target detector for a limited distance will easily be made feasible. Data transmission to the target detector for short distances may be supported since the emission is strongly directional. The channel is however safe over longer lengths because the atmosphere attenuates the radiation. Likewise, the terahertz radiation is heavily absorbed by the environment outside of the desired propagation space, rendering it very difficult to identify unwanted info. Through

consuming of such geographical regions, the connectivity of such networks may be restricted, and the identification and analysis of signals in such regions may become even more complicated even though the network is operating in a broadcast mode. A technical benefit of an ultra-bandwidth communication network will minimize the chances of an adversary to effectively attack a protected channel in addition to the inherent transmission characteristics that permit safe terahertz communications.

For instance, terahertz's wide channel bandwidth enables different channel security measures against numerous standoff threats, such as jamming. In addition to protection from jamming attempts, the wide bandwidth terahertz systems may also deliver the possibility of fully shielding the exchange of Info . In fact, three specific protection classes of techniques can be classified for communications networks. Techniques for data encryption are well-known and can only be decrypted or interpreted by a recipient with the appropriate key. Such an approach will not, therefore, inform the recipient whether the communication is eavesdropped or not. Quantum cryptography enables the exchange of data on the basis of entangled particle states. Such systems reveal probable eavesdropping operations for the target. However, the sender and recipient sharing of data is conducted as minimum Info for eavesdroppers and other illegal third parties. A third and modern technique of safe terahertz communication is the wide terahertz channel bandwidth that enables low detection probability, such that transmission links are completely concealed and a third party doesn't even know that signals are exchanged. A central frequency of about $240GHz$ gives a bandwidth of about $100GHz$ in the atmospheric terahertz transmitting windows. The distribution of data over $100GHz$ allows it to be quite complicated to jam the device as an attacker must produce enough power to defeat the terahertz received power[33]. The trick to this anti-jamming strategy is to effectively disseminate data using high-speed modulators and demodulators over the terahertz wide bandwidth.

For all the discussed applications, the conventional terahertz systems and hardware requires further enhancements. In fact, while a few reduced attenuation windows are below $1THz$, the signal attenuation in this band is greater than the typical microwave channel. To overcome this constraint, the channels of the wireless com-

munications must be configured with different hardware and software parameters. However, more researches are needed for higher power emitting sources, sensitive detectors, high gain antennas, and low-loss interconnects among the hardware equipment. Work in this area will contribute to the creation of a lightweight, cheap terahertz wireless communication network with low profiles. As stated earlier, terahertz remained a breach since high energy sources were not available.

Different terahertz sources above $1THz$ were recorded in the science and engineering domain, but they cannot all be specifically included in transmission as wireless communication in lower attenuation windows below this frequency is required to be established. Using the optical photo-mixing method, two laser offset frequencies are combined to create the terahertz signal above 1 THz [57, 58, 59, 60]. The terahertz signal may therefore also be produced by means of a Backward Wave Oscillator (BWO) below 1 THz [61]. However, owing to the need for a strong magnetic field, the volume of the unit is extremely immense. Besides this, several other instruments may build a terahertz signal with low power [62, 63, 64, 65, 66]. Since tiny terahertz device specifications are desirable, semiconductor systems must be engineered because low power systems are inevitably present. Numerous semiconductor systems have historically been utilized for the generations of low to medium power on microwaves and millimeters, such as the IMPATT, the schottky diode, the Diode of tunneling, and the gunne diode. Nevertheless, they cannot be used explicitly at the terahertz frequency due to the manufacturing constraints. At the floor of the terahertz range, less than $1THz$, multiple sources were analyzed, but with the change in operating wavelength, the output power declines. In Figure 2.6 [67], the difference in the performance of different semiconductor sources are shown at the terahertz range.

The output power is approximately $0.01mW$ at $1THz$ in traditional sources such as IMPATT diode, Gunn Diode, Tunnel Diode, and Schottky Diode. Schottky diodes with less than $1THz$ were recorded [68, 69] that can be used for both modulation and detection. In comparison, the SiC IMPATT diode was able to achieve a power density of $2.5 \times 10^{-11} W/m^2$ at $0.7THz$ [70, 71]. The Quantum Cascade Laser (QCL) will produce a power of up to $90mW$, but it works beyond $1THz$ [72, 73, 74].

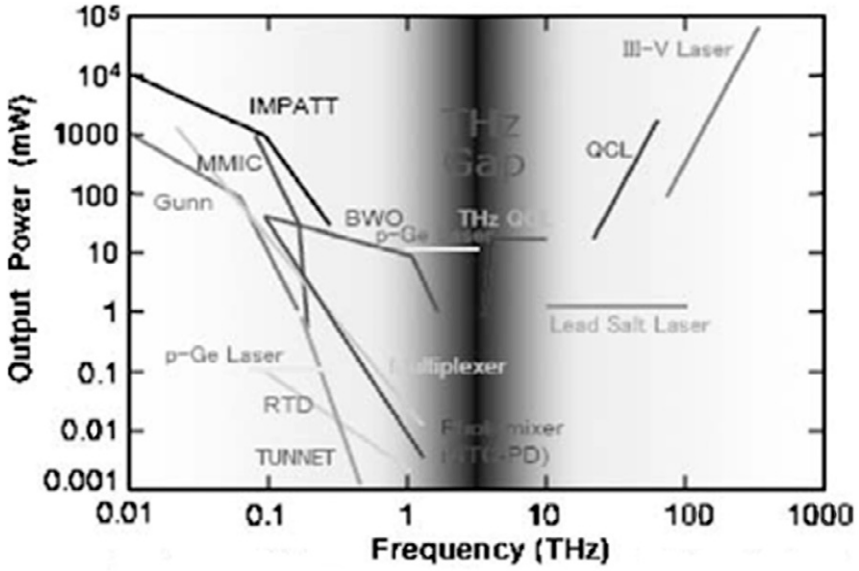

Figure 2.6: The performance of different semiconductor sources at the terahertz band [25]

On the other side, the approach of microwave frequency multiplication for terahertz signal production has been typically employed. This method utilizes solid-state devices to produce a low-frequency output and the carrier frequency is transferred to the greater value by means of frequency multipliers [75, 76, 77]. Terahertz semiconductor sources are still being optimized in industry and it will definitely eliminate the terahertz band gap [78]. Moreover, the solid-state broadband mixer has also been designed for $835 - 900GHz$ [79]. The mixer's output is evaluated in $120K$ and is higher than the sub-harmonic pumped mixer as introduced in [62]. In fact, the use of solid-state instruments as the source of scanning radars with $580GHz$ was demonstrated [80]. This radar configuration shows that solid-state equipment can be extended to terahertz connectivity. The production power in the mW scale is still restricted. Moreover, in terahertz radiation [81, 82, 83, 84] the photoconductive antennas are still utilized but are similarly influenced by poor performance efficiency and mismatching of the impedance between antenna and the attached feeding networks. In fact, the terahertz measurement is correlated with the method of generation. For frequency multiplication methods the signal can be transformed to the intermediate frequency range and the baseband signal can be restored after [75, 77, 80]. Besides, multiple detecting methods have been presented by Hirata et al

[85]. Typically speaking, the reception of the baseband signal through the terahertz channel is feasible [33] with the implementation of the heterodyne rule.

As stated earlier, the key limitation of the terahertz communication network is the atmospheric depletion. The high-power transmitters and powerful detectors have to be established to solve such problems as mentioned above. Though, only a certain amount of the source power can be increased and the power produced by most sources is confined to only the milliwatt scale. As the sources are restricted, there are several folds that are enhanced by the function of the antenna in a wireless communication network. The essential feature of wireless transmission is the antenna [29], on the other side. The antenna can also be used in the sensory and vision system [86, 34]. According to the power constraint, antenna gain in the terahertz network has to be raised in order to extend the signal over a longer range. Though, many terahertz antennas have been designed for other research purposes long before the concept of using terahertz in communication was conceived[81].

Different antennas, including planar and lens antennas were also published in the millimeter or terahertz bands [87, 88, 89, 90, 91, 92]. However, as the length is expanded, the antenna's compactness becomes affected and all sorts of primary sources can hardly be inserted into the lens. Furthermore, the shock wave reflects an external limitation on the antenna of terahertz lens where material with high relativity is used. The shock wave is produced by the difference between the permittivity of the air and the substrate.A low permittivity material based antenna was analyzed [93], which indicates that the size needs to be increased in order to meet the particular criterion for directivity. In addition, the corner reflector array antenna was also published at high-frequency [94].

Further, for wide-band applications with terahertz frequencies[95], the central-fed bow-tie antenna may even be used in bi-conical shape. In addition, the carbon nano-tube is also expected to be an adequately radiating nominee at the terahertz frequency[96, 97, 98]. Besides, the integrated horn antenna, which consists of two stacked wafers, was also developed. Within the first wafer is the horn cavity shaped, and a dipole is mounted at the end. The second wafer serves as a mirror [99]. This form of antenna demonstrates high performance. Furthermore, the corner cube

reflector antenna was addressed in [100, 101]. In [102] a twin slot antenna with $600GHz$ operating frequency has been published for a hot-electron bolometer.

Though, the key issue with such antennas is the system-on-chip specification to operate at higher frequencies. Koch [18] has proposed to utilize the waveguide horn and the planar antennas for the potential wireless communications networks despite the subsistence of different varieties of terahertz antenna. The planar antenna system has more promise and is consistent with planar equipment. In the short distance wireless communication network, the implementation scenario of this kind of antenna was further addressed.

However, the directivity and gain of the antenna are low against the requirement. It indicates the need for a complex feeding technique and the low-loss feeding networks. Nevertheless, the simplicity in design, low cost, and low-profile of the planar antenna motivate the scientists and engineers to further enhance the directivity of the microstrip antenna to meet the future wireless communication requirements. Moreover, various microstrip terahertz antennas have also been studied in the recent past [103, 104, 105, 106, 107] in which design issues of this kind of antenna have been addressed. In most cases, the directivity of the antenna has remained low, yet it can be increased by using the array of antennas in place of a single patch. The gain and directivity of the antenna are, however, poor. It demonstrates that a low-loss feeding is important. But, the versatility with which the planar antenna is built with inexpensive cost and small footprint enable researchers to increase the gain of the microstrip antenna to fulfill the potential wireless connectivity demands.

The microstrip antenna will find its appropriate employment in the monitoring services in addition to the usage of wireless communications. In [108], a dual-frequency band (600 and $800GHz$) antenna has been studied. The fact that different materials are characterized by terahertz as the power level is absorbed differently at specific frequencies is well known. Thus, it may be utilized to identify the dangerous hidden substances.

By eliminating the conductor and the substrate losses, the antenna output can be improved. Because of the presence of the metallic radiator, the loss of the conductor in any kind of antenna remains. Though, a better selection of the substrate material

also decreases the loss of the substrate. In the terahertz antenna development, this defines the specifications for the low permittivity of the substrate. The loss of substrate is also a challenge to the patch antenna in millimeter and sub-millimeter range[109]. The photonic band-gap layer would then be employed as the antenna substrate instead of using the traditional substrate, as the surface wave losses are minimized due to defects in the substrate, thereby improved the performance of the antenna. In the development of the microwave and the millimeter-wave antenna, the photonic bandgap structure is utilized.

Early antenna radiation at the terahertz frequency of this sort was published in [110]. This sort of $610GHz$ array antenna is the model in which an air cylinder is inserted regularly within a homogeneous substrate to decrease its effective permittivity[111]. In this study, the effective permittivity of the material was obtained, in addition to an evaluation of the antenna performance, and the benefit of utilizing the proposed structure as the substrate was addressed over a naturally established positive epsilon substrate. The published antenna directivity is similar to the antenna radiation pattern of the standard substrate in that work. This demonstrates that when utilizing the photonic bandgap substrate instead of the standard substrate material can greatly decrease the number of array components. Nevertheless, the multiple layered substrates in contrast to the conventional substrate is another approach to this challenge where the microwave and millimeter-wave have studied this principle thoroughly. The multiple layered substrate increases both the antenna bandwidth and directivity. In the terahertz antenna system, the implementation of the multi-layered substrate material was discussed[112] where authors obtained a bandwidth of up to 34% -10 dB, i.e. a wide bandwidth.

The manufacturing of such an antenna typically poses the academic community with an obstacle. Various engineering methods have been utilized, which is developed for the design of the nano-meter size, to even fabricate the terahertz microstrip antennas [113, 114, 115]. Furthermore, the measuring challenge of this sort of system can also be overcome by the methods of near-field measurement[116, 117, 118]. Therefore terahertz communication devices will be used in future lightweight high speed to overcome the shortness of wireless communication networks bandwidth.

2.3 The Microstrip Antenna

The traditional two-wire transmission lines were simplified to planar structures by incorporation of the ground plane and by progress in the printed circuit board technology. Planar designs also created modern microwave techniques. The advantages of utilizing planar structures such as designs in the microstrip involve low expense, small-size, small-weight, and particularly excellent electrical and electromagnetic features. A transmission line from the double-wire transmission system has effectively formed. Figure 2.7 illustrates the principle of the parallel line. When the ground plate has an infinite size between the two wires, the image theorem indicates that the top metal picture resides in the bottom metal also. Thus, the bottom conductor may also be dropped. The top conductor can be covered by a strip mounted on the ground floor, and a dielectric substrate between the ground and the top conductor can be wedged, creating a microstrip line [119].

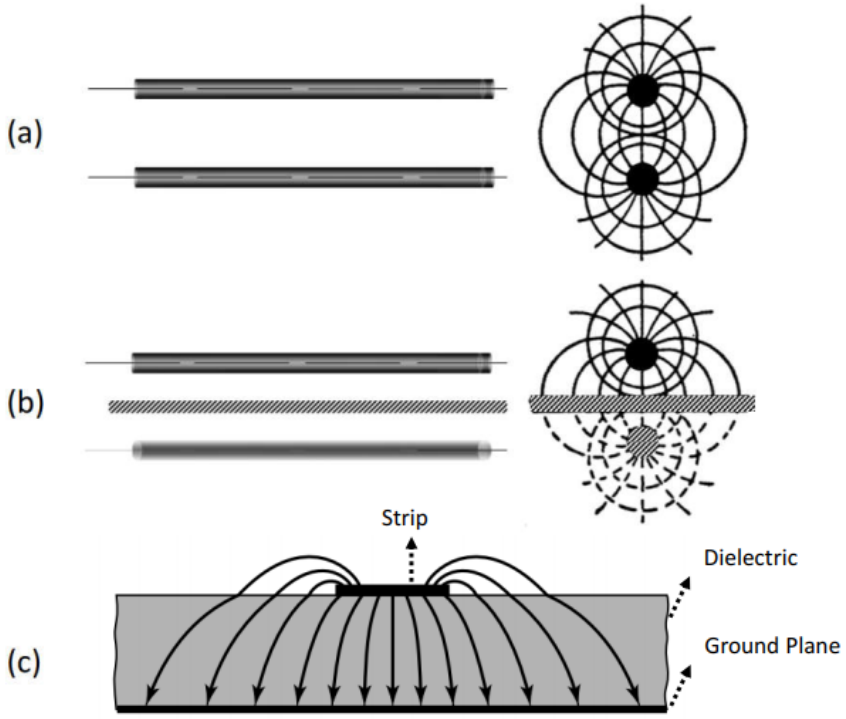

Figure 2.7: Evolution of microstrip transmission line; (a) Two-wire, (b) ground plane bellow a conductor,[119] (c) Microstrip line [120] .

In [119], Grieg and Englemann proposed microstrip patch antennas for the first time as the extensions of microstrip lines in 1952. The microstrip antenna is shown

in Figure 2.8. There are also other feeding methods available other than the presented microstrip line. Microstrip patch antennas have some attractive features equivalent to microstrip transmission lines. The antennas, for example, are easy and affordable to manufacture with state-of-the-art printing systems, suitable for flat and non-planar conditions. Even, conformal antennas with non-electromagnetic specifications are possible with versatile substrates.

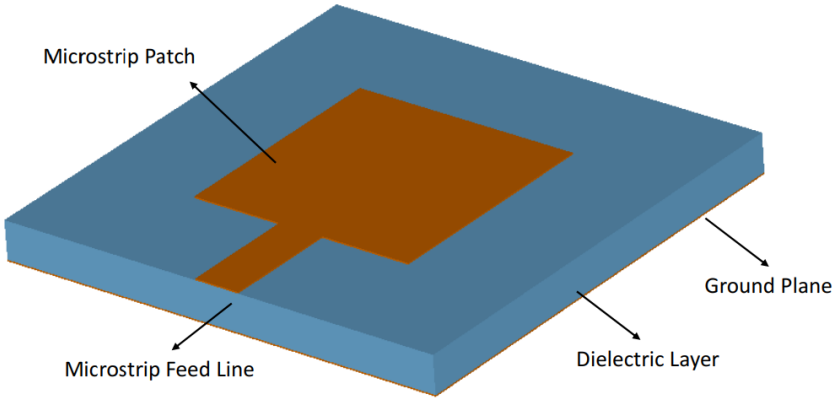

Figure 2.8: The structure of microstrip patch antenna.

Transmission line model, Cavity Model (CM), and full-wave analysis including incorporated equations and moment method are different approaches to model patch antenna. The empirical approaches, TLM and CM, offer a more realistic interpretation of the operation mechanism while the computational approaches give more precise data.

The surface wave effects in the microstrip antenna will enhance the cross-polarization and scalp the radiation patterns as surface wave diffracts from the edges of the ground plane. The surface wave is therefore a source of antenna performance degradation.

In fact, surface waves are propagation modes that are assisted by a grounded substrate which in antennas propagate across the excitement point cylindrically with a reduction in field intensity with distances r, more precisely $1/\sqrt{r}$. The refection of surface waves occurs in the grounded dielectric substrate, that is, as they hit the ground in the bottom and the dielectric-air interface at the top. The wave becomes stuck within the substrate and consumes most of the signal energy, decreasing the target signal strength and lowering the output of the antenna characteristics. Sur-

face waves only affect radiation efficiency on an indefinitely wide ground. Surface waves or currents in fact are reflected and diffracted as they extend to the antenna extremity. A further contribution to radiation is generated by the diffracted waves by affecting the antenna radiation pattern, creating side lobes, and rising cross-polarization.

Moreover, there are mainly two types of surface wave modes, TM surface waves, where the electric field forms loops that spread vertically from the surface of the ground and TE surface waves, where the electric field is parallel to the ground surface and the magnetic field forms vertical loops out of the air. All substrate-based antennas comprise that fact. The lowest TM_0 surface wave mode has a zero cut-off frequency. The cut-off frequencies for the different surface wave modes $n = 0, 2, 4, ...$ for TM modes, $n = 1, 3, 5, ...$ for TE modes are related as follows:

$$f_c = \frac{n}{4h\sqrt{\epsilon_0\mu_0}\sqrt{\epsilon_r\mu_r - 1}} \tag{2.4}$$

Furthermore, decreasing the dielectric thickness and permittivity results in less coupled energy into the surface waves that reduces the magnitude of the surface waves. But, low substrate thickness implies a reduction in antenna bandwidth and antenna efficiency and low permittivity substrate increases antenna size [121].

2.4 Photonic Crystals

The photonic bandgap [121] are periodic structures constructed from either dielectric, metal, or metallodielectric materials that are often referred to as Photonic Crystals (PCs). These periodic materials are developed artificially to prevent the transmission of electromagnetic waves in the engineered "bandgap" frequency band. Moreover, the lattice constant and the permittivity of the structure are the primary parameters in photonic crystal design.

Initially, PBG is employed for the control of the optical properties of materials, i.e. controlling the emission and propagation of light. the first fabrication of the Yablonovite structure [122] was in 1991 with a complete 2D photonic bandgap. On

the other hand, photonic bandgaps are scalable structures with frequency. Thus, shifting from the optical frequency down into the microwave frequency is possible. PCs are primarily categorized into the following groups: 1D, 2D, and 2D PCs based on the dielectric periodicity, as can be seen in Figure 2.9.

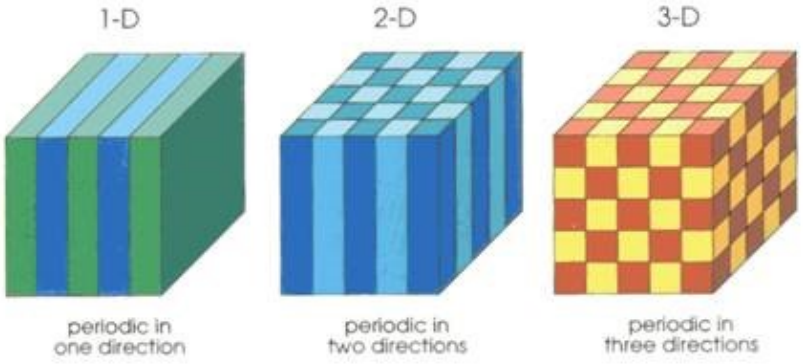

Figure 2.9: Classification of Photonic Crystals (PCs) 1D, 2D, and 3D structures [123].

The structure of the lattice, air holes forming a 2D photonic crystal, is determined by the parameters ϵ, a and r, where ϵ is the permittivity, a the lattice constant and r is its radius. Besides, several research papers have concluded that modifications in the form and positioning of the periodic elements provide an infinite range of varieties of the lattice. However, two popular forms of 2-dimensional photonic crystal, square and hexagonal lattices, are widely employed for technical causes [124, 125].

Many research papers have highlighted the advantages of PCs through time which have unique and favorable properties that attract different applications including their suitability for antenna gain enhancement and radiation pattern shaping applications.

2.5 Design of Terahertz Microstrip Antenna Based on Photonic Crystal Substrate

In this section, a terahertz microstrip antenna is designed and analyzed by investigating a photonic bandgap structure using its different control parameters at

$0.6THz$. After that, it is used as a substrate for a traditional microstrip antenna. In the following subsections. The results are with good agreement with [12, 25] in Chapter 3.

2.5.1 Photonic bandgap design

The air-cylinder-embedded dielectric substrate unit cell is shown in Figure 2.10.a. This squared unit cell has a length of $100\mu m$ whereas the centered air cylinder that is embedded in Arlon AR 600 substrate with ϵ_r of 6.0 and $tan\delta$ of 0.0035 has the same length as the substrate thickness. Multiple duplicates of the unit cell have been concatenated to form PBG structure as shown in Figure 2.10.b.

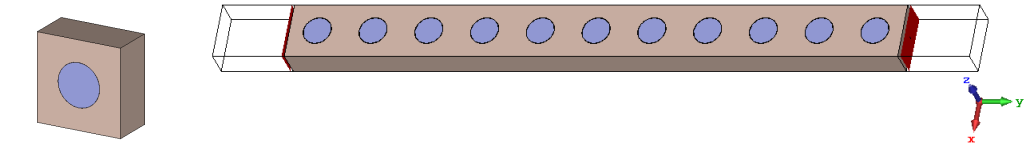

(a) (b)

Figure 2.10: Geometry of PBG structure, (a) unit cell (b) PBG simulated structure

In order to simulate this structure, CST microwave studio environment that is based on Finite Integration Technique (FIT) is used by setting up the electric boundary condition at the top and the bottom of the structure, also the magnetic boundary condition is assigned at the front and the back sides, remaining the right and left sides where the open space boundary condition is established for port excitation of the structure. Simulation results are obtained by sweeping the number of unit cell through $N = 1, 6$, and 11 in $0.5 - 0.8$ THz frequency range.

Simulation results are shown in Figure 2.11. It is noticed that the bandgap property is not achieved when $N = 1$ but as the number of the unit cell is increased, the amount of the insertion loss is also increased that results in the existence of the bandgap property and the increase in its depth for an enhanced PBG performance.

To investigate the effect of variation in substrate thickness, sweeping of the thickness h from $50\mu m$ to $200\mu m$ is simulated. The presented results in Figure 2.12 reveal that there is no significant impact of h on the bandgap property in this range

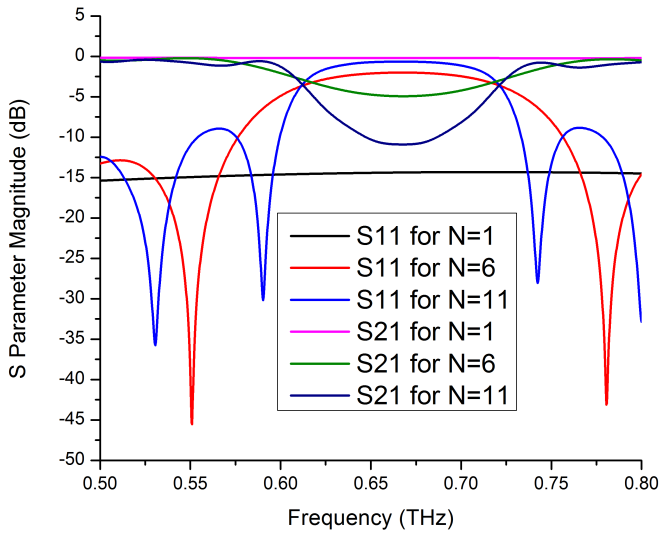

Figure 2.11: S_{11} parameter magnitude in terahertz band for $N = 1, 6$ and 11 using CST microwave studio.

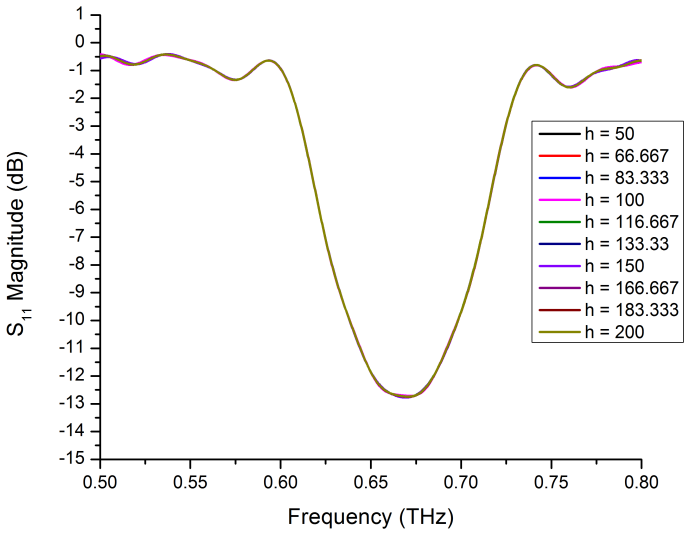

Figure 2.12: S_{11} parameter magnitude in terahertz band for $h = 50\mu m$ to $200\mu m$

of frequency.

Since the length of air holes do not affect the band stop property, investigation of the periodicity a and the radii of air cylinders r for their impact is performed. To do this, the periodicity is fixed and the radius is varied from $5\mu m$ to $45\mu m$.

From Figure 2.13, it is shown that the larger the radius is, the deeper the band

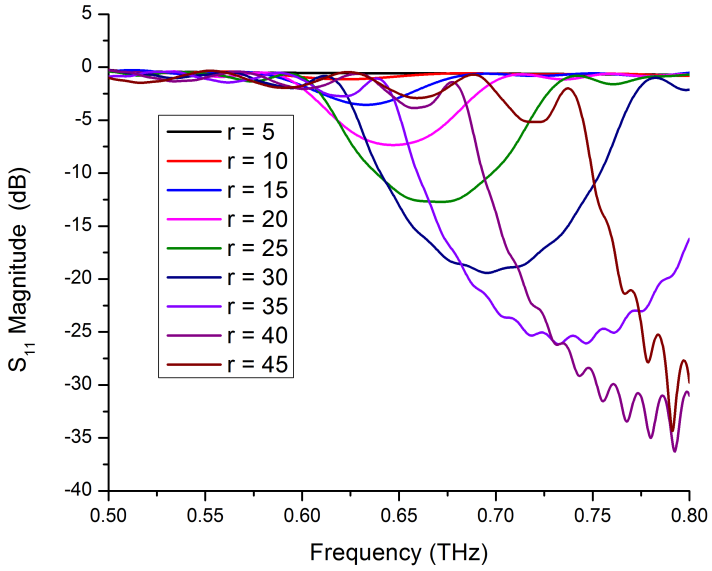

Figure 2.13: S parameter magnitude in terahertz band for $r = 5\mu m$ to $45\mu m$

stop characteristic with a wider shifted bandgap is, and vice versa. As a result, the bandgap property of this structure is controlled by parameters a and r.

In order to design a substrate material with the bandgap property at $0.6THz$, the value of r and a are 25 and $100\mu m$, respectively, with h being $50\mu m$. The S parameters of the design are already shown in Figure 2.11.

2.5.2 Microstrip antenna design

In this section, a microstrip antenna is designed and simulated using the previously selected PBG structure as a substrate. Figure 2.14.b shows the proposed antenna structure with PBG structure used as substrate whereas 2.14.a shows the antenna with a homogeneous substrate. The parameters of the radiating microstrip patch antenna are calculated using the referenced equations [25] then the length and width of the patch are optimized and finally the values of each parameter of the antenna is presented in Table 2.2.

From Figure 2.15 which presents the scattering parameter S_{11} of both antenna configurations, it can be seen that the antenna designed on a PBG substrate material exhibits a narrower $-10dB$ impedance bandwidth and a good resonance is achieved

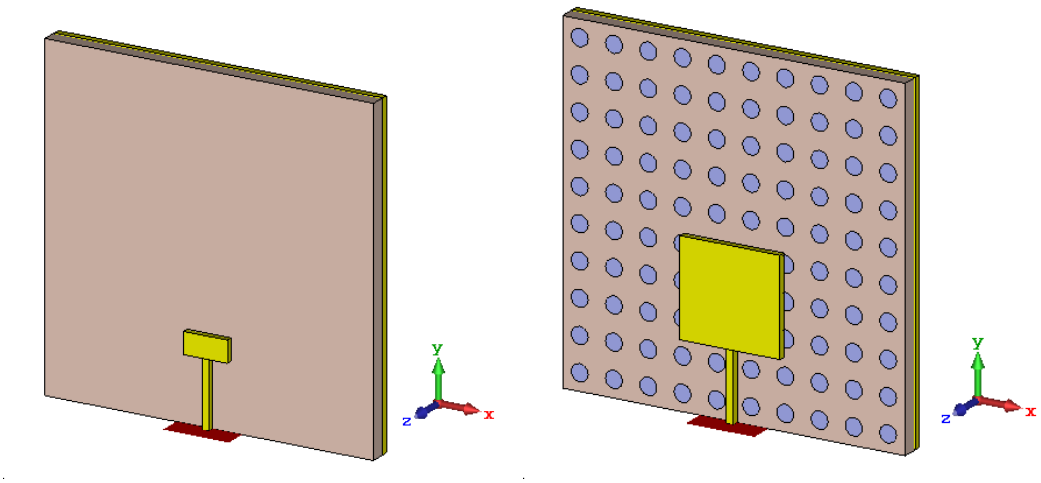

(a) (b)

Figure 2.14: Geometry of the presented antenna based on, (a) homogeneous substrate (b) PBG substrate.

Table 2.2: Parameter values of the presented antennas.

Component	**Parameter**	**Value (μm)**	
Patch of PBG and homogeneous substrate	Width	292	134
	Length	280	65
Feeder	Width	20	
	Length	200	
Ground Plane	Width	1000	
	Length	1000	
Substrate	Width	1000	
	Length	1000	
	Thickness	50	
	a	100	
	r	25	

at $0.609THz$ compared to $0.713THz$ for the antenna designed on the homogeneous substrate. With the decrease in the bandwidth, the quality factor is increased that results in enhanced antenna's other electrical parameters like gain and directivity as shown in Figure 2.16.

From Figure 2.16, it is revealed that in both antenna structures, the maximum directivity is achieved on H-plane with $9.45dB$ for the one designed on PBG and $6.62dB$ for the other one designed on homogeneous substrate material where the difference is 2.83 as an improvement. The maximum directivity on the E plane is $4.79dB$ and $2.99dB$ for the antenna with and without PBG structure, respectively.

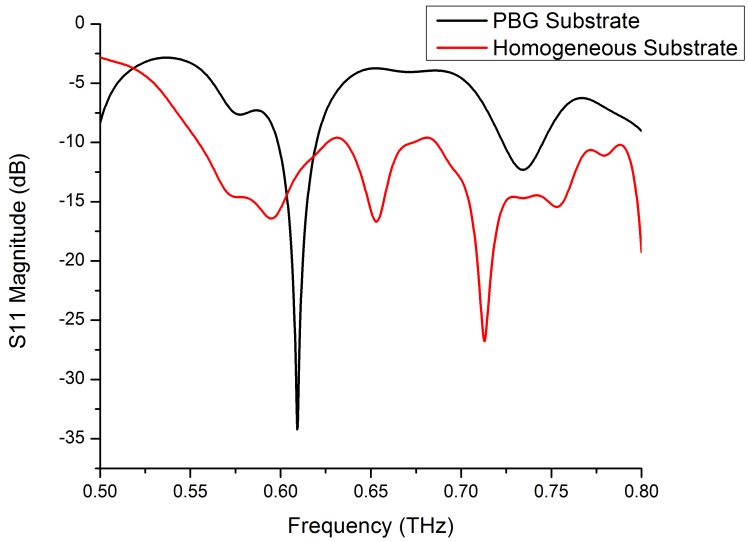

Figure 2.15: S parameter magnitude in terahertz band for the presented antenna structures.

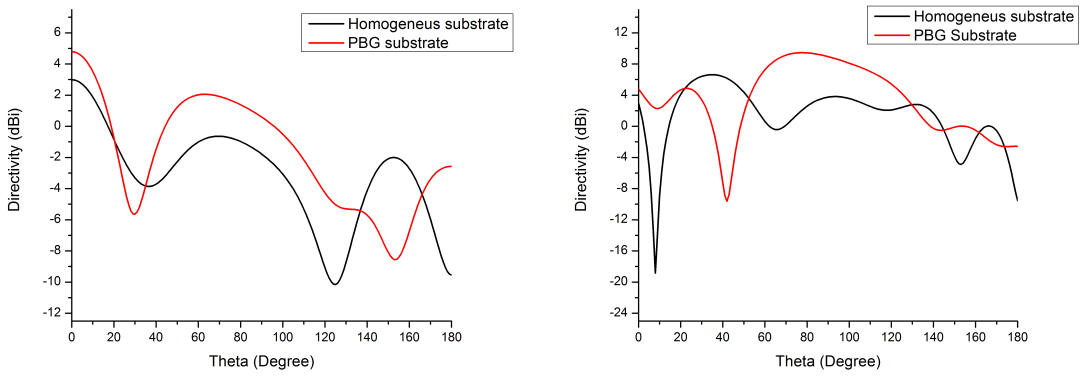

(a) (b)

Figure 2.16: Directivity of the presented antennas at 0.6 THz on, (a) E plane (b) H plane.

However, at terahertz band, the directivity of the antenna is the main concern in comparison with the bandwidth and antenna dimensions because even a narrow bandwidth of the antenna would be able to support the higher data volume. Besides, the dimensions are in order of micrometer.

2.6 Summary

In this chapter, a literature review on the terahertz regime is presented including its potential impact and the main characteristics and challenges. Then, the terahertz channel is investigated and compared with its neighboring bands by showing its added value. Besides, several interesting cutting edge terahertz applications are presented in different fields such as innovative wireless communication networks, biology, agriculture, security and defense. After that, an overview of terahertz hardware is conducted starting from terahertz sources and detectors to the requirement for planar antennas to microstrip antennas basics and some published enhancements and fabrication techniques. Then, an introduction of the photonic crystal is presented followed by simulation work using CST where terahertz microstrip antenna analysis and design procedures are presented and simulated. The photonic crystal structure is separately designed to exhibit the band stop property at $0.6THz$. Then it is used as a substrate of the antenna to enhance its performance at this frequency where there is a low atmospheric attenuation window that makes it suitable for mobile and earth communications. Simulated results obtained for this antenna show that the photonic crystal substrate efficiently enhances the directivity of the traditional microstrip antenna at this band of frequency.

Chapter 3

Analysis and Design of Terahertz Microstrip Antennas Based on Synthesized Photonic Crystals PCs

3.1 Introduction

In the recent decade, the terahertz frequency band has gained various growing applications such as astronomy, space-science [126], next mobile communication system [127], imaging of concealed items [128], time domain spectroscopy [129], medical science [130, 131], and defense applications [132, 133] as discussed in the previous Chapter.

These broad applications of terahertz spectra are due to its unique properties [134, 135] high bandwidth, lower diffraction than microwaves spectra, image resolution, and the fact that terahertz signature of many solid and gaseous materials is in $0.5 - 3THz$ band. Besides, for wireless communication systems, the bandwidth at the terahertz band is capable of establishing a channel with a large conveyed volume of Information (Info) which means higher data bit rates [136].

The microstrip patch antenna is widely used for various applications due to

its low cost, low profile, compatibility with IC technology, ease of fabrication, and installation on shaped surfaces [137].

This antenna, which belongs to standing wave antennas, is a good candidate for terahertz integrated on-chip antenna. The on-chip integrated antenna in silicon technology is promising in terahertz range as it could be even more cost-effective than a conventional packaging of an external antenna with transceivers by considering packaging cost and its compactness at terahertz band. In general, the Terahertz System-On-Chip (THz-SoC) in silicon is very promising in several applications as it requires an intensive analog interface and digital logic for signal processing on-chip for the cost-effective massive production [138].

Nevertheless, the use of the silicon substrate of a conventional digital CMOS technology as an antenna substrate introduces two main loss mechanisms, conduction loss which is due to the low resistivity of the silicon substrate, and the surface-wave mode excitation loss caused by the thick silicon substrate with high relative permittivity of 11.5 [139]. The advantage of using silicon technology is clear when the fully integrated system with analog and logic circuits for baseband and Digital Signal Processor (DSP) is considered.

In order to improve some of the electrical parameters of the microstrip antenna, various researchers have used high dielectric permittivity or thick substrate material [140, 141, 142, 143]. However, the application of high dielectric permittivity material as silicon leads to shock waves at the air-substrate interface in the millimeter and terahertz range of the spectrum [144]. Further, the application of a thick substrate leads to surface wave loss due to the trapping of energy within the substrate [25] and reduction in the substrate thickness reduces the bandwidth and mechanical strength of the antenna. To reduce the surface wave loss, either effective dielectric permittivity or thickness of material has to be reduced. To reduce the effective dielectric permittivity, the property of the material is artificially altered by using the periodic air-defects in the homogeneous host material. This heterogeneous material is called photonic crystal material. In general, the dielectric permittivity of the PBG materials is reduced which is used to enhance its electrical performance [145].

In designing a microstrip antenna at high-frequency, photonic crystal is widely

used as a substrate material and other employments [136, 146, 147, 148, 149, 150]. Photonic Crystals (PCs) have fascinated scientists and researchers as they interact with electromagnetic waves, exciting phenomena appear, and amazing features result. However, due to the complexity of the photonic crystal structures, it is usually difficult to characterize them through purely analytical methods. Instead, full-wave simulators such as CST microwave studio which is based on the Finite Integration Technique (FIT) and HFSS have been used in the analysis. Two-dimensional (2D) PCs take the interest of researches as they are much easier to fabricate than 3D PCs [151, 152, 153] and they have promising applications such as planar waveguides and antennas [154, 155].

MATLAB has become a ubiquitous software package for data manipulation, signal processing, and graphics. Scientists and engineers, worldwide, use MATLAB to analyze and design the systems and products in several fields including antennas. Although electromagnetic simulators can model very complex electromagnetic systems, they lack some of the powerful analysis functions available in MATLAB for numerical optimization problems. Thus, linking programming language MATLAB and electromagnetic simulator CST microwave studio to create a powerful tool for the design and analysis of microstrip antennas is a promising technique. For example, in the design optimization process which involves a large number of parameters. These parameters can be either continuous, discrete, or both, making the design process slow and complicated.

Particle Swarm Optimization (PSO) is a heuristic search method that is based on the idea of collaborative behavior between swarm birds in biological populations. PSO is similar to the Genetic Algorithm (GA) in the sense that they are both population-based search approaches and that they both depend on Information (Info) sharing among their population members to enhance their search processes using a combination of deterministic and probabilistic rules. Heuristic algorithms have been used in antenna optimization with different employments [156, 157, 158, 159]. Researchers report that both PSO and GA have equal effectiveness but superior efficiency for PSO over the GA[160].

3.2 Antenna Based on Periodic Air Holes Photonic Crystal Substrate

3.2.1 Photonic bandgap structure

In this section, the photonic crystal structure is made of air-cylinders embedded in silicon dielectric material whose relative permittivity and electric conduction are 11.9 and $0.00025 S/m$, respectively. The overall dimensions of the structure are $500 \times 500 \mu m^2$ and the thickness is $50 \mu m$ for both dielectrics. Besides, air holes have lattice constant and radius equal to $70 \mu m$ and $28 \mu m$, respectively. Hence the dimensions of the squared unit cell are $70 \times 70 \mu m^2$.

Multiple duplicates of the squared unit cell have been concatenated to form a PBG structure as shown in Figure 3.1. In order to analyze its properties, the simulation is performed with CST microwave studio environment. Because of the structural nature and periodicity, computations can be reduced by setting up the electric boundary conditions at the top and the bottom of the structure, also the magnetic boundary conditions are assigned at the front and the back sides, and for the right and left sides the open space boundary conditions are established.

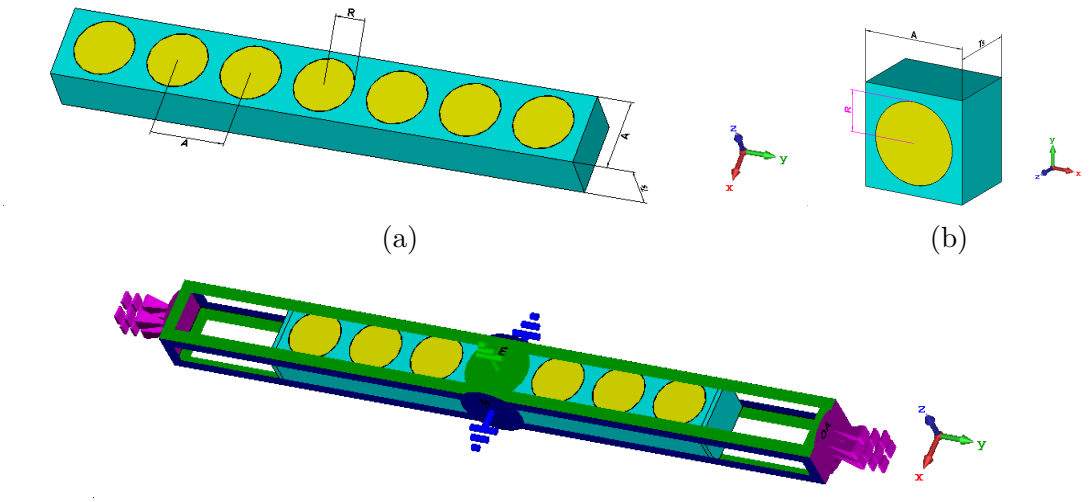

(a) (b)

(c)

Figure 3.1: Geometry of the PBG structure (a) Simulated PBG structure, (b) Unit cell and (c) Boundary conditions of the structure

Simulation results are obtained by taking the number of unit cells equal to 7 in

$0.4-0.8THz$ frequency range. The results are obtained by extracting material properties from the simulated S parameters. The extracted complex relative permittivity is shown in Figure 3.2.

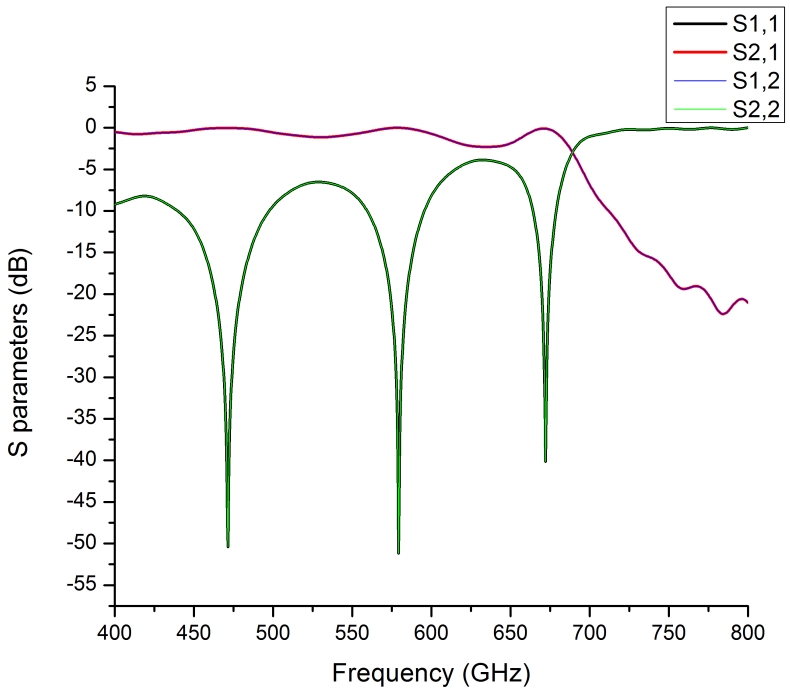

(a)

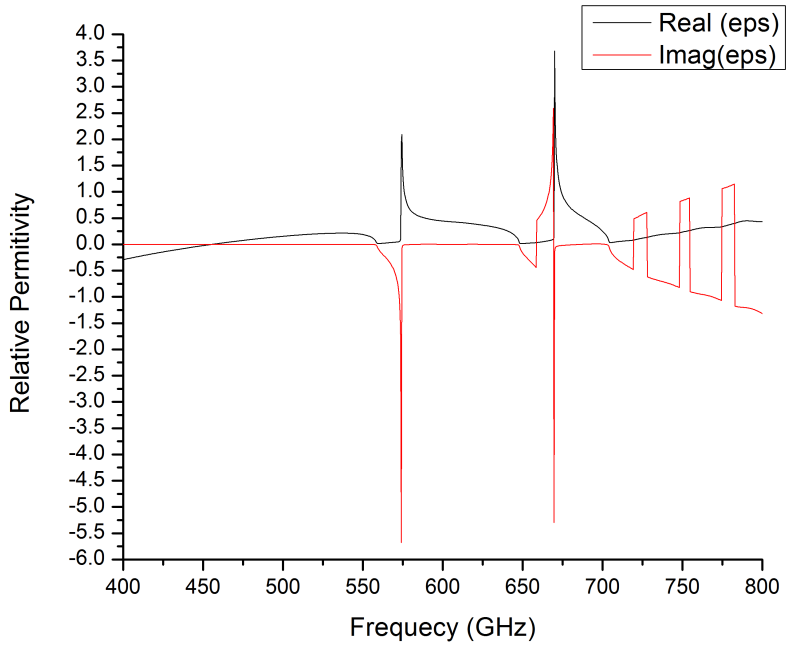

(b)

Figure 3.2: Simulation results of the designed PBG structure (a) S parameters (b) The extracted relative permittivity

Table 3.1: Parameter values of Antenna 1.

Component	**Parameter**	**Value** (μm)
Rectangular patch	Width	319
	Length	245
Substrate	Width	500
	Length	500
	Thickness	50
	Lattice constant	70
	Cylinder radius	28
Feeder	Width	28

To design a substrate structure of the patch antenna that resonates around $0.6THz$, the value of the effective permittivity is taken as 0.44 for next section.

3.2.2 Antenna design

In this section, Antenna 1, namely the patch antenna, is designed and simulated based on the previously analyzed photonic crystal structure as its substrate. First, the width W_p and the length L_p of the rectangular patch are calculated and found to be equal to $295\mu m$ and $223\mu m$, respectively from equation (3.1) and equation (3.2) [145].

$$W_p = \frac{c}{2f_r}\sqrt{\frac{2}{\epsilon_{reff}+1}} \tag{3.1}$$

$$L_p = \frac{c}{2f_r\sqrt{\epsilon_{reff}}} - 2\Delta l \tag{3.2}$$

where

$$\Delta l = 0.412h\frac{(\epsilon_{reff}+0.3)(\frac{W_p}{t_s}+0.264)}{(\epsilon_{reff}-0.258)(\frac{W_p}{t_s}+0.8)} \tag{3.3}$$

Where ϵ_{reff} is the effective dielectric constant, f_r is the desired resonance frequency, c is the speed of light and t_s is the thickness of antenna substrate. Then, an optimization of the calculated values is performed whereas metals are modelled as perfect electric conductors. The value of each parameter of the antenna structure is presented in Table 3.1. Antenna 1 configuration is shown in Figure 3.3.

After that, Antenna 0 namely, a conventional antenna which is based on homogeneous silicon substrate is designed and simulated for comparison and analysis

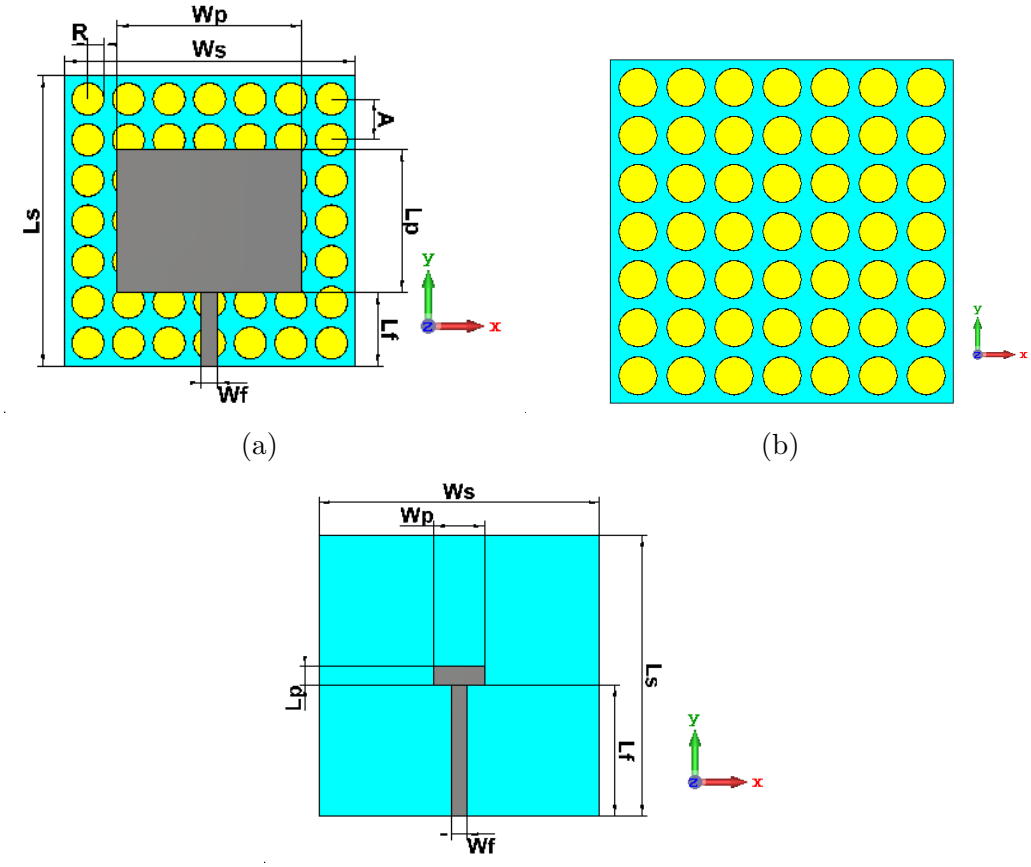

Figure 3.3: Geometry of the designed antennas (a) based on PBG substrate (b) PBG substrate (c) based on homogeneous substrate

purposes. Using equation 3.1 and 3.2, the calculated width and length of the patch are equal to $90\mu m$ and $33\mu m$, respectively.

According to Figure 3.4 which presents the return losses of the presented antennas, it can be obviously seen that the optimized antenna based on PBG substrate exhibits a wider bandwidth of $56GHz$ compared to the antenna based on homogeneous substrate with $41GHz$ and a deeper return loss of $-64.04dB$ is achieved compared to homogeneous substrate antenna with $-11.35dB$. All the resonance frequencies are around $0.65THz$.

For practical reasons, the perfect electric conductor, which was used for metals modelling, is replaced with copper annealed. The maintained return losses and radiation efficiency for copper thicknesses $1.1, 2.1$ and $3.1\mu m$ including the patch, feeder and ground metals are shown in Figure 3.5. Indeed, it is found close results

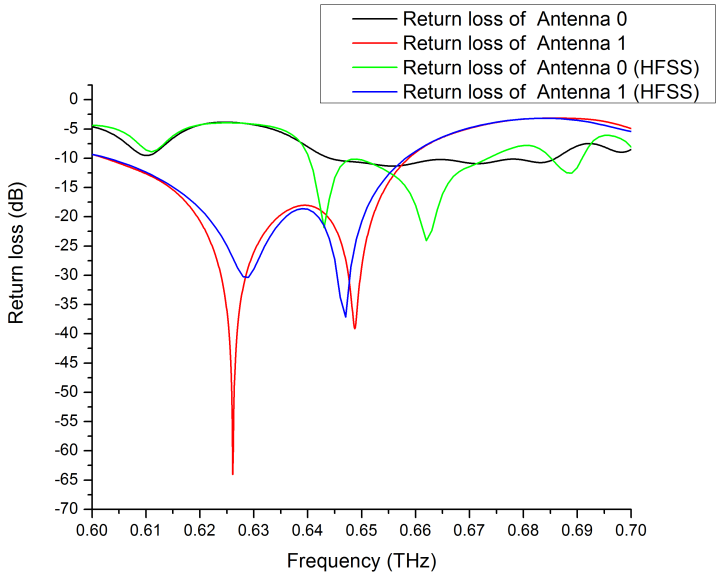

Figure 3.4: S_{11} parameter magnitude in terahertz band of Antenna 0 and Antenna 1

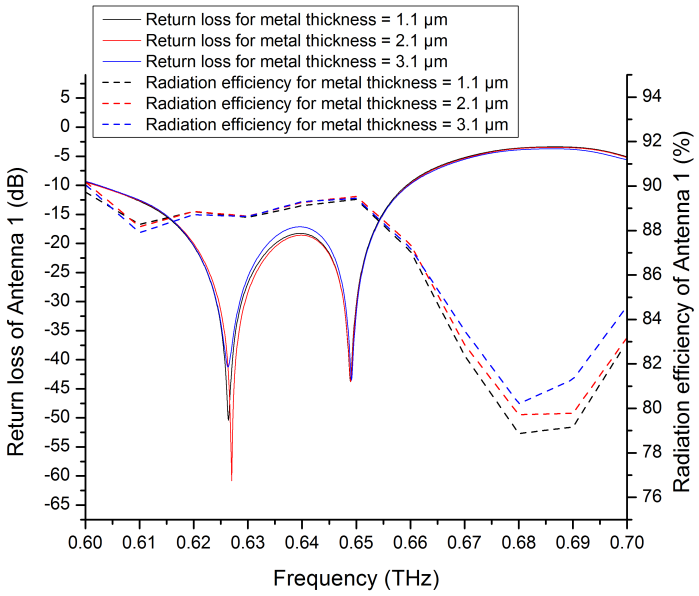

Figure 3.5: S_{11} parameter magnitude in terahertz band of Antenna 1 with different thicknesses of annealed copper

to the obtained ones in Figure 3.4 with the appropriate copper thickness.

It is observed an achievements in the gain and radiation efficiency of Antenna 1 which is based on PBG substrate with a gain of $9.17dB$ and radiation efficiency of 91.08% compared to conventional patch antenna based on the homogeneous substrate with a gain of $3.79dB$ and radiation efficiency 65.4%. Thus, by taking previ-

ous results of the achieved return loss into consideration, the employment of PBG structure is indeed an effective technique to reduce surface waves that results in worthwhile improvements.

The surface current of Antennas 0 and 1 at their resonance frequencies are shown in Figure 3.6. As can be seen, the surface current is presented in both the patch and substrate surfaces due to the fact that the simulated silicon substrate is a lossy dielectric. When the phase is zero, it is shown that the transmitted power from the feeder is dispatched through the patch. But after that, the power is transferred from the patch to out space (air) where most of the power in the substrate is radiated. The advantage of employing a photonic crystal substrate is that most of the power is radiated and a noticeable reduction of the reflected power from air-antenna edge interfaces is achieved. Usually, the reflected power, which is trapped between the edges of the antenna, causes power loss in the form of heat as silicon is a lossy dielectric. Thus, by using the enhanced photonic crystal, the loss in the form of heat is also reduced.

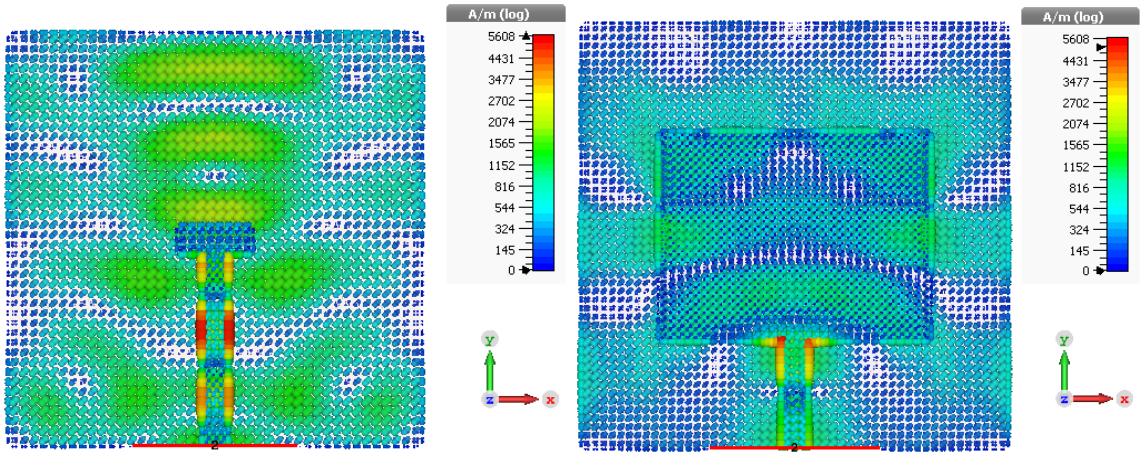

(a) (b)

Figure 3.6: Current distribution frequencies of (a) Antenna 0 at 0.65 THz and (b) Antenna 1 at 0.63 THz.

Figure 3.7 shows the radiation pattern in dB for Antenna 1 at its resonance frequency of $0.62THz$ in XZ and YZ planes. The maximum radiation pattern of this antenna is at $\theta = 0°$and the maximum directivity is $9.58dB$.

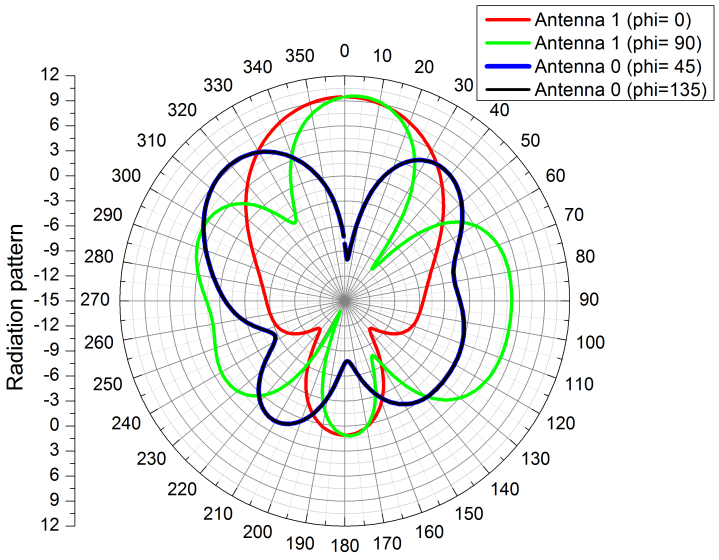

Figure 3.7: Radiation patterns of Antenna 1 based on PBG substrate at 0.62 THz and Antenna 0 at 0.65 THz .

3.3 Antennas Based on Synthesized Photonic Band Gap Substrate

3.3.1 Antenna substrate design by Binary Particle Swarm Optimization (BPSO)

In the present chapter, the researcher uses BPSO to find the best 2D photonic crystal substrate for the presented microstrip patch antenna. As an effective global optimization method, the BPSO algorithm searches for the global minimum in a discrete search space. Hence, the researcher considers a 2D photonic crystal of a square lattice formed by two different materials namely silicon and air with dielectric constants 11.9 and 1, respectively.

In order to apply BPSO, the researcher discretizes the unit cell into many pixels that represent rectangular squares, whereas each square can be filled by one of the two different materials, silicon or air, represented by a binary value, 1 or 0, in the BPSO algorithm. The total number of possible structures of 2D Photonic Crystals increases exponentially with the number of pixels so a full-space search method would not be practical as the number of the pixels increases, in other words, when

the pixels are tiny. In this case, the BPSO algorithm is anticipated to be effective. In the BPSO algorithm, each binary word corresponds to a 2D photonic crystal unit cell formed by pixels, physically just square rods of dielectric material. Each unit cell represents a model candidate in the optimization process. Thereafter, each candidate is analyzed and labeled with a fitness value using a predefined merit function that will be presented in the next sections. After updating position vectors of each binary word in each iteration, the algorithm finds the global minimum, optimal model, of the merit function after a number of iterations. The flowchart of the BPSO implementation with the connected CST microwave studio simulator and MATLAB is shown in Figure 3.8.

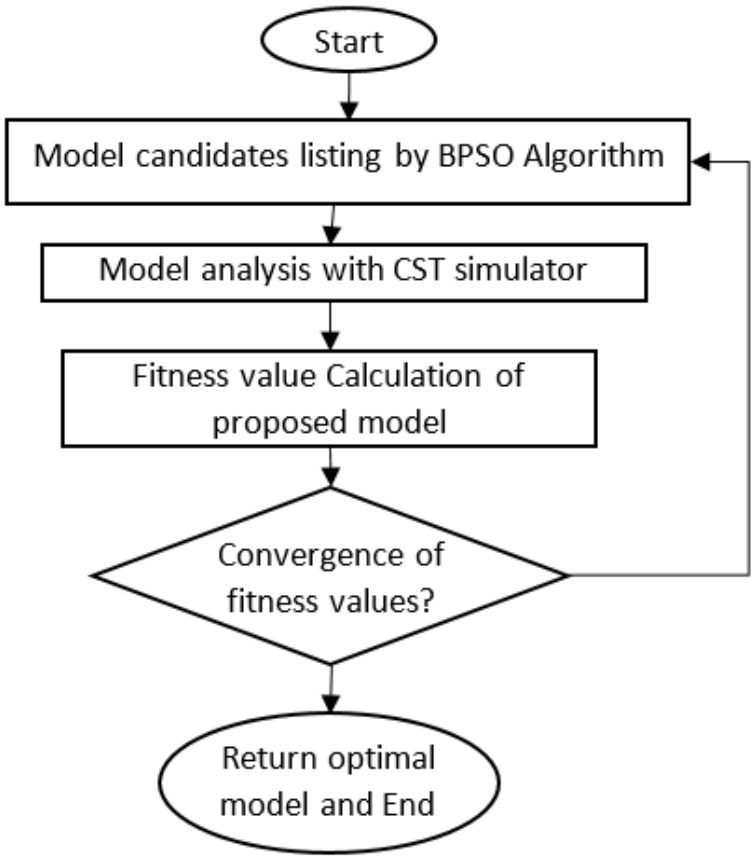

Figure 3.8: Flow chart of the optimization process

To apply the BPSO algorithm to design a 2D photonic crystal, it is required to convert the filling pattern of the unit cell of a 2D structure into a binary word. BPSO steps are used in each iteration to find the global minimum of the merit function. The unit cell is divided into $2N \times 2N$ pixels, each pixel is filled by either

air or silicon dielectric materials.

In this work, the researcher supposes that the primitive unit cell which is centered at the origin, as in Figure 3.9.a, is symmetrical and invariant under the mirror reflection with respect to the horizontal XZ plane and vertical YZ plane shown in bold line.

0	0	0	0	0	0	0	0	0	0
0	0	0	0	1	1	0	0	0	0
0	0	1	1	1	1	1	1	0	0
0	0	1	1	1	1	1	1	0	0
0	1	1	1	1	1	1	1	1	0
0	1	1	1	1	1	1	1	1	0
0	0	1	1	1	1	1	1	0	0
0	0	1	1	1	1	1	1	0	0
0	0	0	0	1	1	0	0	0	0
0	0	0	0	0	0	0	0	0	0

(a)

21	22	23	24	25	25	24	23	22	21
16	17	18	19	20	20	19	18	17	16
11	12	13	14	15	15	14	13	12	11
6	7	8	9	10	10	9	8	7	6
1	2	3	4	5	5	4	3	2	1
1	2	3	4	5	5	4	3	2	1
6	7	8	9	10	10	9	8	7	6
11	12	13	14	15	15	14	13	12	11
16	17	18	19	20	20	19	18	17	16
21	22	23	24	25	25	24	23	22	21

(b)

Figure 3.9: Unit cell optimization grid (frame). (a) The index of each binary word bit in the unit cell geometry (b) Filling pattern of the presented air cylinder unit cell

Thus, the whole photonic crystal structure can be designed by the pixel-filling pattern of a square part of one-fourth of the unit cell, which can be represented by a binary word of $N \times N$ bit. The total number of the possible structures is $2^{N \times N}$, and even for $N = 5$, there is $33,554,432$ different unit cell structure. For such a large searching space, the full-space search method is not practical for finding the best model. In this work, the researcher applies BPSO, a heuristic optimization algorithm, as an effective method for solving this problem. The used BPSO in the present chapter is described as follows.

In step 1, the researcher randomly constructs the initial candidates of $N \times N, 5 \times 5$, binary word, i.e., each bit of the $N \times N$ binary word at the first iteration is set by 0 or 1 randomly. In general, a 2D structure corresponding to a randomly produced binary word results in weak antenna characteristics. To speed up the search, the researcher introduces a special binary word as a special model candidate in the initial

population but the other binary words are all randomly created by the computer. The structure corresponding to the special binary word is a binary representation of the PBG substrate presented in section 3.2 whose structure binary filling pattern is shown in Figure 3.9.b.

In step 2, the researcher computes the fitness value for each binary word. Whereas the fitness of a binary word is predefined by the merit function based on CST microwave studio results of antenna characteristics including gain, return loss, or $-10dB$ bandwidth, the merit function will be defined for each upcoming sections.

In step 3, the researcher updates the position vector of each binary word by: first, computing velocity vectors. Then, calculating the probability vectors for changing the elements of the position vector using a translation function. Finally, updating position vectors, i.e. binary words.

In step 4, the researcher repeats steps 2 and 3 till the optimal structure is reached which corresponds to the minimum fitness value. As a numerical application, In order to avoid the optimal structure becoming impractical for fabrication, having too thin veins or too small holes, and to compromise with computational costs, the researcher takes $N = 5$, i.e., the unit cell is divided into 10×10 pixels. In this case, each binary word has 25 bit, and the researcher chooses 20 particles for each swarm and a maximum number of iteration as 1000.

3.3.2 Return loss optimization

The presented method in the previous section is used to guide the design and optimization of photonic crystal substrate. In order to optimize the return loss, the following merit function of BPSO is selected where S is the scattering parameter, G is the gain and sgn is sigmoid function.

$$M(S,G) = \left[S^3 \frac{sgn(-S-10)+1}{2} + S \frac{sgn(S+10)+1}{2}\right] \times \left[G \frac{sgn(-G+7.5)+1}{2} + G^5 \frac{sgn(G-7.5)+1}{2}\right] \tag{3.4}$$

During the BPSO process, the minimum fitness of the binary words of a swarm does not always decrease. In such a case, the researcher avoids the degradation of the best

binary word. Hence, the researcher gives more rewards when gain or return loss cross threshold values in antenna characteristics, these threshold values of the gain and return loss are assigned in the merit function of 7.5 and $-10dB$, respectively. After long evaluations of more than 65 iterations, more than 1300 consecutive simulations, the achieved minimum of the fitness function is -1.7594×10^{10}. The obtained optimal structure with the minimum fitness value is shown in Figures 3.10(a,b).

1	1	1	0	0	0	0	1	1	1
0	0	0	0	1	1	0	0	0	0
0	1	0	0	1	1	0	0	1	0
0	0	0	0	1	1	0	0	0	0
0	1	1	1	1	1	1	1	1	0
0	1	1	1	1	1	1	1	1	0
0	0	0	0	1	1	0	0	0	0
0	1	0	0	1	1	0	0	1	0
0	0	0	0	1	1	0	0	0	0
1	1	1	0	0	0	0	1	1	1

(a)

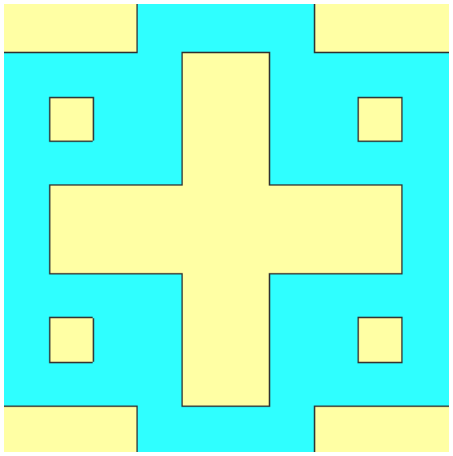

(b)

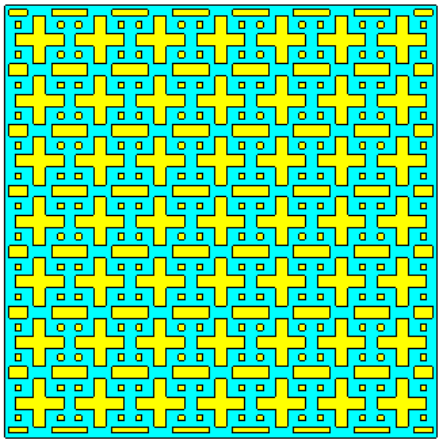

(c)

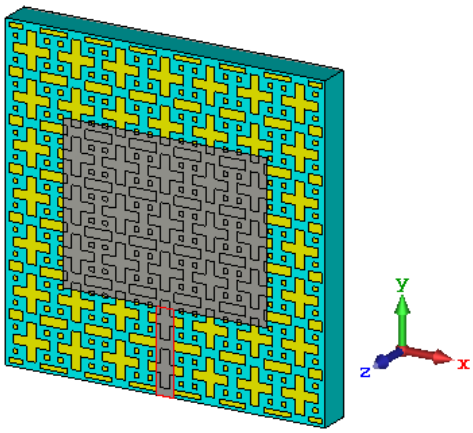

(d)

Figure 3.10: Geometry of the optimized (a) filling pattern of the unit cell, (b) unit cell (c) substrate (d) Antenna 2 using silicon (green) and air (yellow) materials.

It is observed that the structure pixels composed from silicon material are well connected to each other as intended. This photonic crystal structure is used as a substrate to form Antenna 2 as shown in Figure 3.10(c).

From Figure 3.11, the achieved return loss of Antenna 2 is $-67.49dB$ at $0.6THz$ compared to $-64.04dB$ at 0.62 THz with an enhancement of 5.39% and close an-

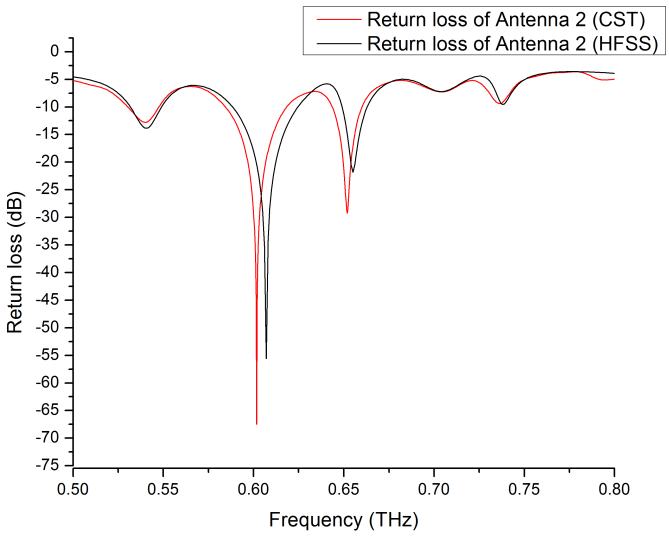

Figure 3.11: S_{11} parameter magnitude in terahertz band of Antenna 2

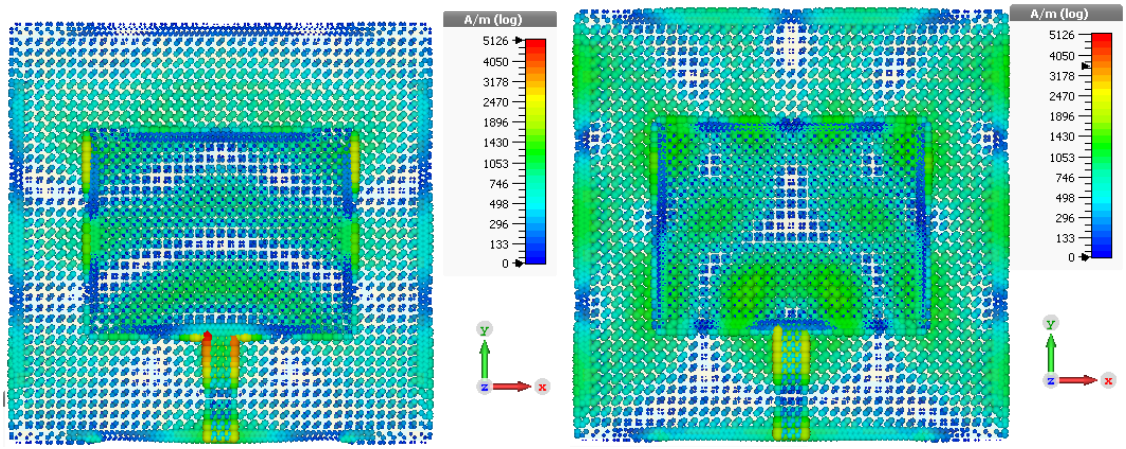

(a) (b)

Figure 3.12: Current distribution of Antenna 2 at (a) 0.6 THz and (b) 0.65 THz

tenna gain performance to Antenna 1 of $9.17dB$. Moreover, another resonance frequency is achieved at $0.65THz$ with return loss of $-29.25dB$. Hence, Antenna 2 becomes dual band antenna around $0.65THz$ with narrower bandwidth suitable for different applications.

The surface current of Antenna 2 at 0.6 and $0.65THz$ are presented in Figure 3.12. The transmitted power from the feeder is dispatched through the patch to out space (air) where most of the power in the substrate is radiated. The advantage from employing PCs substrate is maintained as most of the power is radiated and

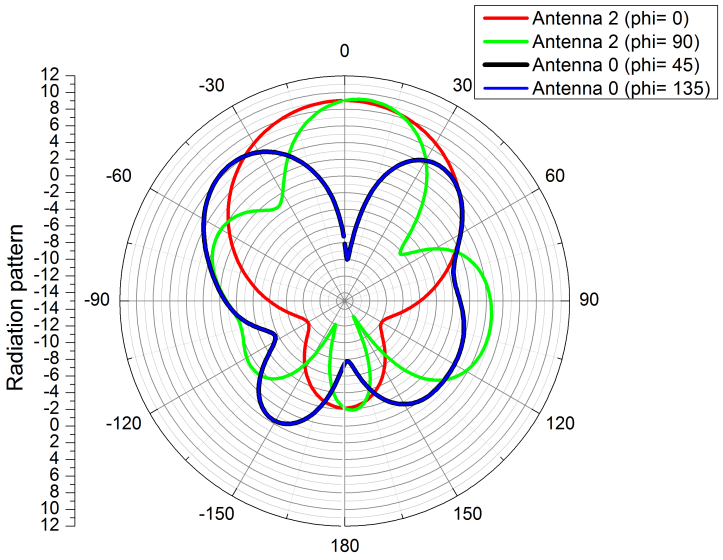

Figure 3.13: Radiation pattern in XZ and YZ planes of Antenna 2 based on PBG substrate at its resonance frequency

a noticeable reduction of the reflected power from air-antenna edge interfaces is achieved.

In Figure 3.13, it is observed the achieved characteristics of side-lobe suppression in the YZ plane of Antenna 2 compared to Antenna 1 in Figure 3.7.

3.3.3 Bandwidth optimization

In this section, optimization of the bandwidth is performed with CST microwave studio controlled by MATLAB using BPSO algorithm as described in previous sections. In order to optimize the bandwidth, the following merit function of BPSO is defined as shown in equation (3.5) and (3.6) where BW is the $-10dB$ bandwidth, F_B is the fractional bandwidth, f_r is the resonance frequency, G is the gain and BW is sigmoid function.

$$F_B = \frac{BW}{f_r} \times 100 \tag{3.5}$$

$$\begin{aligned} M(F_B, G) = -\left[G\frac{sgn(-G+7.5)+1}{2} + G^2\frac{sgn(G-7.5)+1}{2}\right] \times \\ \left[F_B^2\frac{sgn(F_B-10)+1}{2} + F_B\frac{sgn(-F_B+10)+1}{2}\right] \end{aligned} \tag{3.6}$$

As in the previous section, threshold values of the gain and fractional bandwidth

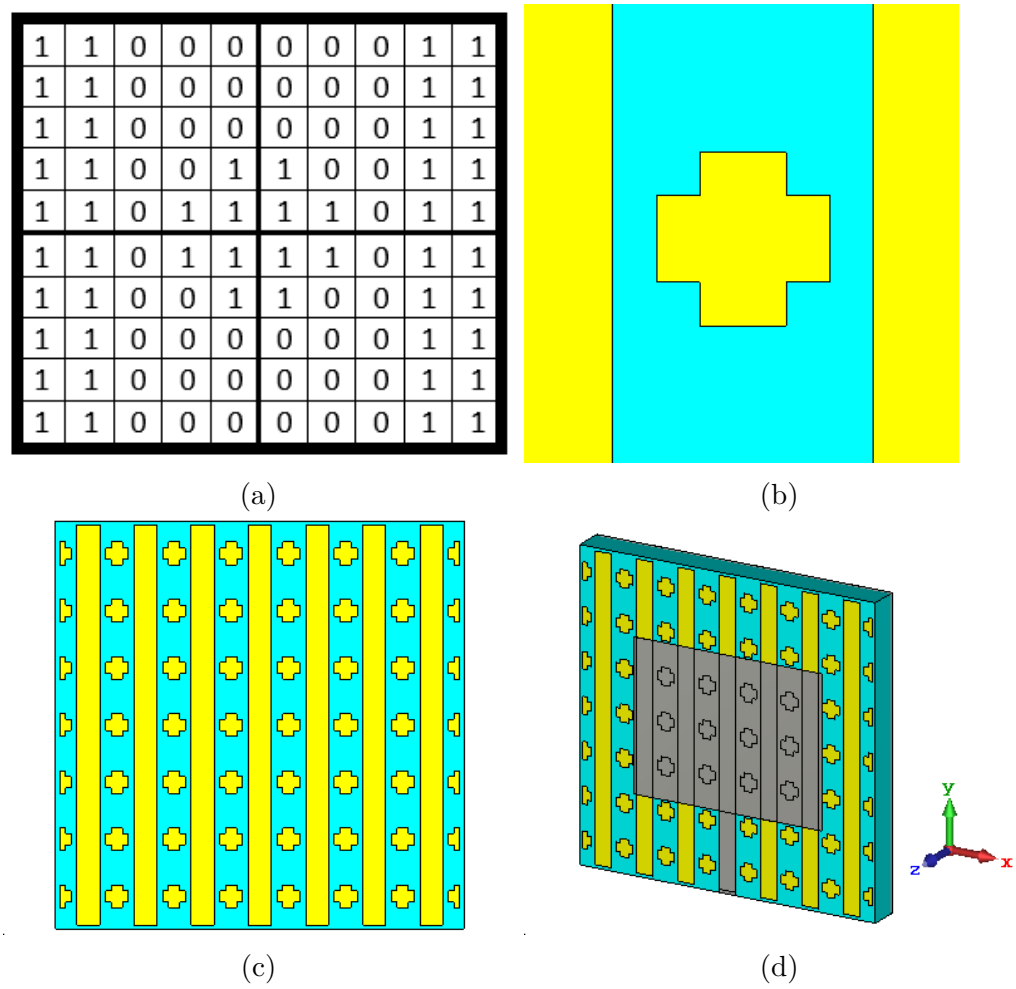

Figure 3.14: Geometry of the optimized (a) filling pattern of the unit cell, (b) unit cell (c) substrate (d) Antenna 3 using silicon (green) and air (yellow) materials.

are assigned in the merit function as 7.5 and 10, respectively. After long evaluations of more than 26 iterations, more than 520 structure simulations, the achieved minimum of the fitness is -7.4307×10^{04}. The obtained optimal structure with the minimum fitness value is shown in Figure 3.14.a,b. it is observed that the structure pixels composed of silicon material are connected to each other as intended. The antenna based on this photonic crystal structure as a substrate is named as Antenna 3 and is shown in Figure 3.14.c.

The achieved $-10dB$ bandwidth of Antenna 3 is $128GHz$ with a resonance frequency of $0.62THz$ compared to $56GHz$ of Antenna 1 with an enhancement of 128.57% as presented in Figure 3.15 and close antenna gain performance to Antenna 1 of $9.17dB$.

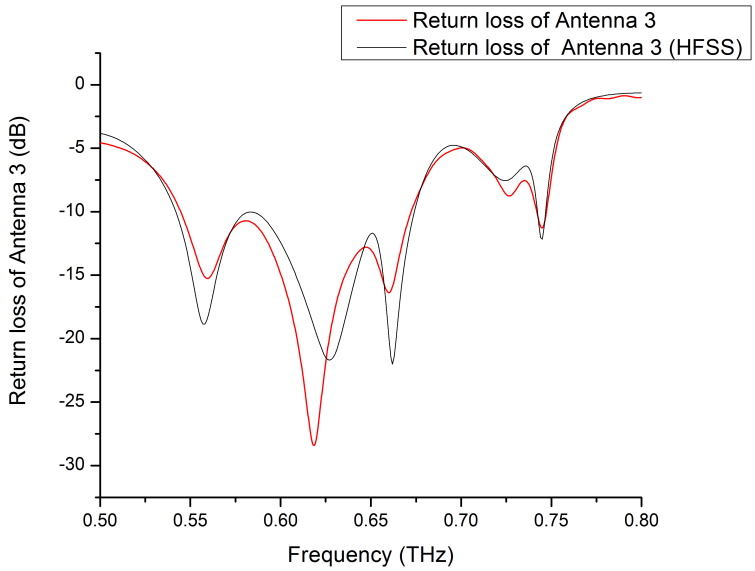

Figure 3.15: Return loss of Antenna 3 in terahertz band

The surface current of Antenna 3 at $0.62THz$ is presented in Figure 3.16 where the advantage from employing photonic crystal substrate is maintained as most of the power is radiated and a noticeable reduction of the reflected power from air-antenna edge interfaces is achieved. According to Figure 3.17, it is observed that the achieved characteristics of Antenna 3 where the reduction of side lobes in Antenna 3 compared to Antenna 1 or 0 in the YZ plane is worthwhile.

The proposed antennas, which exhibit a gain close to $9.17dB$, are compared with the results of the studied antennas in literature offering gain of $7.94dB$ [147],

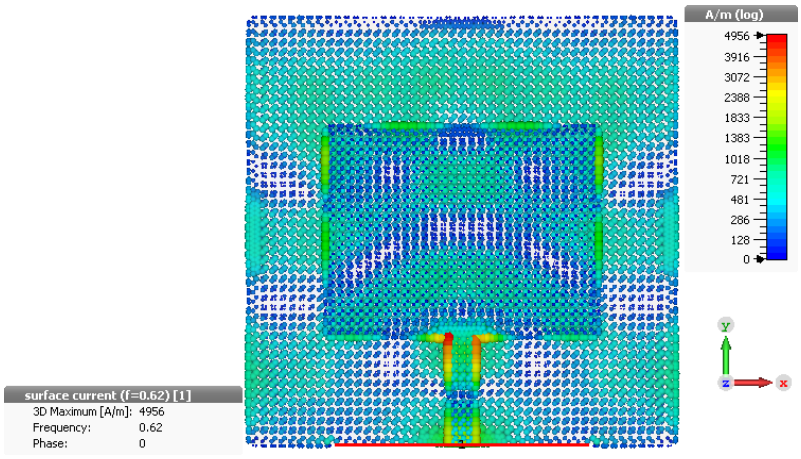

Figure 3.16: Current distribution of Antenna 3

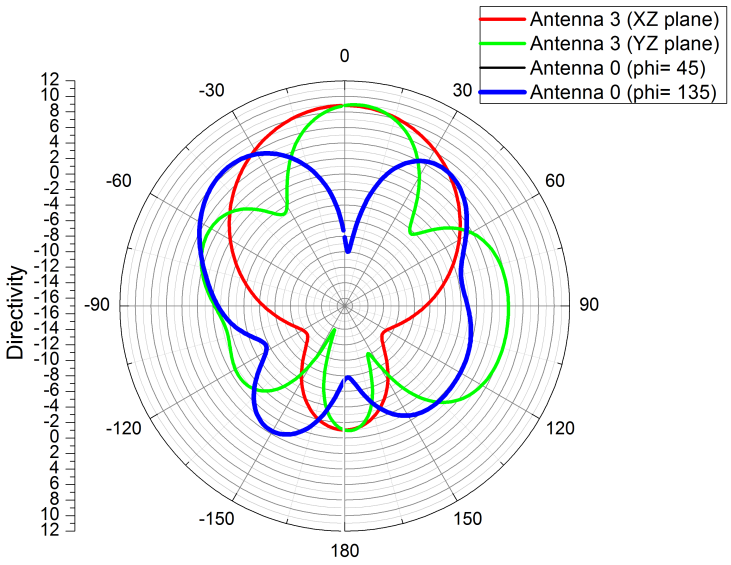

Figure 3.17: Radiation pattern in XZ and YZ planes of Antenna 3 based on PBG substrate at its resonance frequency

3.8dB [146] and 5.09dB [161] and summarized in Table 3.2. As it is shown, this work presents an enhanced antennas which can be selected based on the desired application system requirements.

Table 3.2: Comparison of presented antennas with existing designs

	f_r **(THz)**	S_{11} **(dB)**	**Bandwidth (GHz)**
[147]	0.630	-44.71	36.23
[146]	0.96	-13.05	310
[161]	0.75	-35	50
Antenna 0	0.65	-11.35	41
Antenna 1	0.63	-64.04	56
Antenna 2	0.6	-67.49	32
	0.65	-29.25	16
Antenna 3	0.62	-28.42	128

3.4 Summary

In this chapter, the design and analysis of microstrip patch antenna based on synthesized photonic crystal substrate have been carried out by using a technique based on the combination of BPSO algorithm with CST microwave studio simulator.

The initial antenna is designed by analyzing air cylinders embedded in thick silicon substrate which has high relative permittivity. Indeed, PBG substrate reduces the effect of surface wave losses that results in fruitful antenna electrical characteristics. Furthermore, it can be more beneficial when CST microwave studio has merged with Binary Particle Swarm Optimization (BPSO).

It shows up to be useful to synthesize a well-designed PBG substrate for a terahertz microstrip antenna with the desired characteristics depending on its future application. Also, It has been shown that Antenna 2 becomes suitable for dual band applications around 0.6 and 0.65 THz and the amelioration achieved in return loss is 5.39% compared to Antenna 1. Also, a remarkable improvement over fractional bandwidth for the microstrip patch antenna based on synthesized photonic crystal substrate (Antenna 3), the fractional bandwidth is increased by 128% as compared to the initial antenna (Antenna 1). Further, both optimization results reveal the achieved reduction in side lobes compared to the initial antenna. The enhanced results are due to the presented new synthesized photonic crystal substrates. The obtained antennas have resonance frequencies around $0.65THz$ which is the demand of current wireless communication technology and other different interesting applications.

Chapter 4

Analysis and Design of Terahertz Microstrip Antennas Based on Modified Photonic Crystals PCs

4.1 Introduction

The high data rate required for the development of next wireless communication systems may reach several tens of Gbits per second, as a result, extraordinary real-life applications will emerge. Hence, increasing the available bandwidth is a necessity to establish such a high data rate communication link. Fortunately, terahertz radiation, which usually refers to the frequency band that lies between millimeter waves and InfraRed (IR) light in the electromagnetic spectrum, offers high bandwidth. Besides, it is an unallocated band which is suitable for different new applications [162]. This band of frequency has various interesting applications in wireless communication, medical science [163, 131], imaging of concealed items [164], time-domain spectroscopy [129] and defense applications [132]. This broad application area of THz spectra is due to its unique properties [165, 135] such as high bandwidth, lower diffraction than microwaves spectra, image resolution, and the fact that terahertz signatures of many solid and gaseous materials are in $0.5 - 3THz$ band. However, the main challenge for the realization of a commercial THz wireless communication system in this band is the atmospheric path loss [135] where the amount of loss of

the signal power depends on the atmospheric conditions. This is the reason why terahertz communication systems were limited to space and astronomy applications as discussed in the second chapter.

Since photonic crystal discovery, it takes a great interest that has grown explosively in the design of highly efficient electromagnetic and optical devices for different applications. This new multidisciplinary field of study emerges to have a great promise in different applications. One of these future applications is to build a microstrip patch antenna based on photonic crystal structure as a substrate, in order to suppress the undesirable excited surface waves. As a result, the antenna efficiency is improved, and a reduced side lobe level is maintained due to the diffraction of surface waves at the edges of the antenna substrate [166, 121, 167]. This phenomenon of surface waves is strong when thick substrates are used.

Microstrip patch antenna with a Frequency Selective Surface (FSS) and Photonic Band Gap PBG structures are implemented by Nejati *et al* [148] to enhance the antenna gain in the range of $0.5-0.7\ THz$. Their results exhibit a resonance frequency of $0.67\ THz$ with a minimum return loss around $-18dB$ and a best-achieved gain $8.15dB$ based on previous research on PBG substrate for gain enhancement [168, 111]. On the other hand, the employment of polyimide substance as an antenna substrate for video-rate imaging and homeland defense applications has been reported by Mittala *et al* [169], which results in a gain of $5.22dB$ and resonance frequency of $0.67THz$ with a bandwidth of $40.16GHz$. After that, Kushwaha *et al*[170] introduce the employment of photonic crystal with polyimide substance in the terahertz microstrip antenna. Their results reveal in a gain of $7.934dB$ and a resonance frequency of $0.6308THz$ with a $36.25GHz$ bandwidth. Their antenna is suitable for the application of explosive detection and material characterization [16, 15, 161].

Several research papers have been conducted on microstrip antennas based on metamaterials and electromagnetic bandgap structures [146, 171, 172, 173, 174] which results in interesting improvements. Also, photonic crystal employments in other electromagnetic devices than antennas have been studied and reported [175]. However, all these researches have been performed at a lower frequency than the

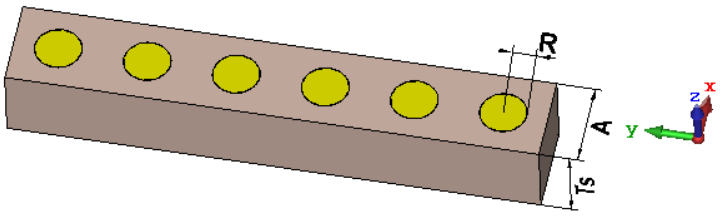

Figure 4.1: Geometry of the simulated PBG structure.

terahertz band which is the spectrum for next wireless communication systems and other quite interesting applications.

4.2 Antenna Based on Photonic Crystal Substrate

4.2.1 Photonic crystal design

In this section, Antenna 1, which is a rectangular microstrip patch antenna, is designed and simulated based on the photonic bandgap substrate. The substrate is made from Polyimide with $\epsilon_r = 3.5$ and $tan\delta = 0.0027$. Figure 4.1 shows multiple concatenated duplicates of air-cylinder-embedded dielectric substrate unit cell. The length of the squared unit cell is $100\mu m$, whereas the centered air cylinder has the same thickness as the substrate ($90\mu m$). In order to extract the substrate electrical properties, simulation results are computed in a $0.5-0.8THz$ frequency range. The extracted real and imaginary parts of the permittivity are shown in Figure 4.2.

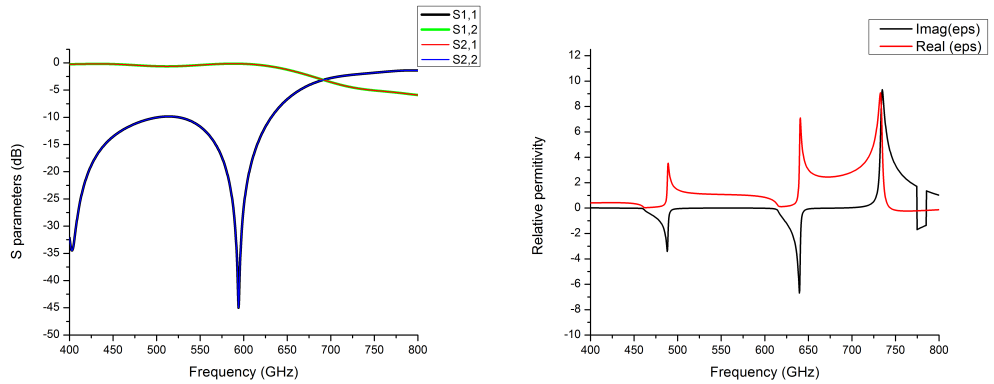

(a) (b)

Figure 4.2: simulation results of the designed PBG structure (a) S parameters, (b) extracted relative permittivity.

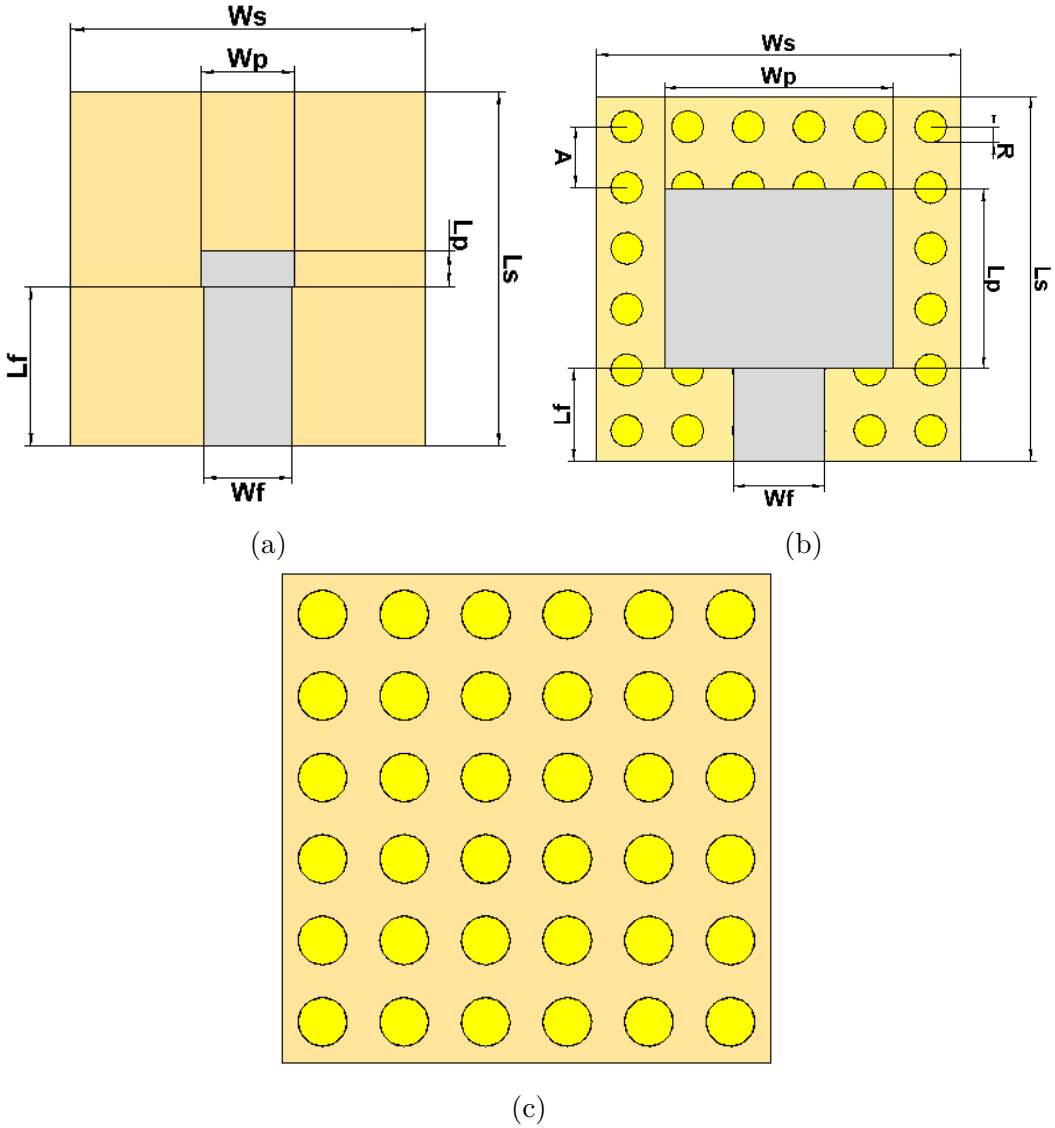

Figure 4.3: Geometry of (a) Antenna 1 based on homogeneous substrate, (b) Antenna 3 based on periodic photonic crystal substrate and (c) photonic crystal substrate.

As a result, for the initial selection of patch width and length to resonate around $0.65THz$, the value of the effective permittivity is 1.4.

4.2.2 Patch antenna design

Figure 4.3 shows Antenna 1 and Antenna 3 structures based on homogeneous and photonic bandgap substrates, respectively. The patch is centered above the substrate and the feed line is designed with a width of $150\mu m$. For conventional microstrip antennas, the thickness of the dielectric substrate t_s should be in the range

($0.003\lambda \leq h \leq 0.05\lambda$) to avoid surface waves excitation [121]. On the other hand, it is found that thick substrates improve the electrical performance, viz. the bandwidth, of microstrip antennas [121]. However, as the substrate thickness exceeds the aforementioned range, shock waves at the air–substrate interface are introduced in the millimeter and terahertz ranges of the spectrum. These surface waves deteriorate antenna performance [121]. As a contribution of this work, the employment of thick aperiodic photonic crystal substrate ($h \geq 0.05\lambda$) is used instead of conventional thick homogeneous substrate to suppress the undesired surface waves and taking the benefits from employing thick substrates. Therefore, the substrate is selected thick enough with $90\mu m$ that excites surface waves in Antenna 1, which is based on a homogeneous substrate. The width W_p and the length L_p of the patch are initially computed using Equation (4.1) and Equation (4.2) [176] where c is the light speed in free space, f_r is the desired resonance frequency, ϵ_{reff} is the effective dielectric constant, and t_s is the substrate thickness. As a summary, the dimensions of Antenna 1 and Antenna 3 are presented in Table 4.1. The employed metal thickness is $25\mu m$.

$$W_p = \frac{c}{2f_r}\sqrt{\frac{2}{\epsilon_{reff}+1}} \tag{4.1}$$

$$L_p = \frac{c}{2f_r\sqrt{\epsilon_{reff}}} - 2\Delta l \tag{4.2}$$

where

$$\Delta l = 0.412h\frac{(\epsilon_{reff}+0.3)(\frac{W_p}{t_s}+0.264)}{(\epsilon_{reff}-0.258)(\frac{W_p}{t_s}+0.8)} \tag{4.3}$$

Table 4.1: Parameter values of Antenna 1 based on homogeneous substrate and Antenna 3 based on periodic PBG substrate

Component	**Parameter**	**Value** (μm)	
		Antenna 1	**Antenna 3**
Patch	Width (W_p)	160	376
	Length (L_p)	60	296
Substrate	Width (W_s)	600	
	Length (L_s)	600	
	Thickness (T_s)	90	
	Lattice constant (a)	100	
	Cylinder radius (r)	26.5	

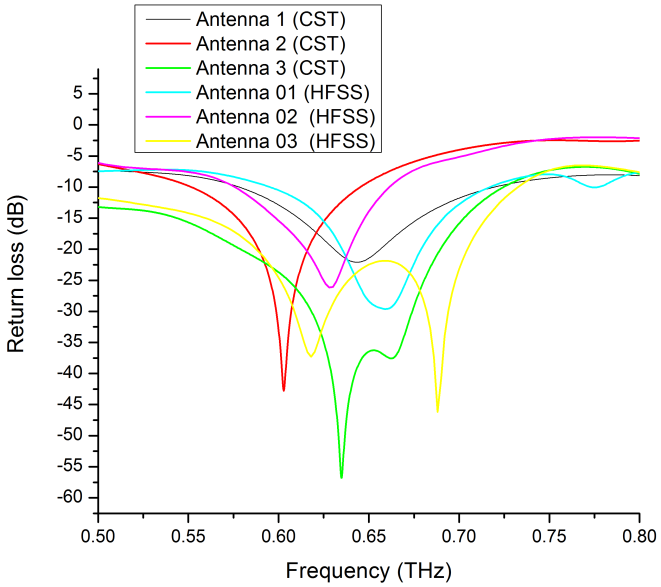

Figure 4.4: S parameter magnitude in terahertz band for Antennas 1, 2 and 3.

From Figure 4.4 which represents the scattering parameter magnitude S_{11} of the antenna configurations, viz. Antenna 1 and 3 with Antenna 2 being the designed antenna using graphene instead of copper annealed, it can be seen that Antenna 3 exhibits a wider bandwidth, quite greater than $230GHz$, than Antenna 1's $140GHz$ with a noticeable improvement. A deep return loss of $-56.81dB$ is also achieved compared to Antenna 1 with $-22.09dB$. All the resonance frequencies of $0.64THz$ and $0.63THz$ for Antenna 1 and Antenna 3, respectively are close to the desired frequency $0.65THz$ within the range of $0.6 - 0.7THz$. Besides, graphene based antenna (Antenna 2) exhibits a resonance frequency at $0.603THz$ and $(-10dB)$ bandwidth of $93GHz$. It is noticed that Antenna 1 based on the employed metal thickness of $25\mu m$ exhibits a wider bandwidth with respect to Antenna 2.

For further analysis, the gain and radiation efficiency are also interesting characteristics of antennas to be taken into consideration, especially for next generation of wireless communication systems in this band of frequency. The gain is plotted versus frequency in Figure 4.5.

It is obviously observed the achieved amelioration of the gain and radiation efficiency of Antenna 2, which is based on photonic crystal substrate, with a gain of $8.95dB$ and radiation efficiency of 89.31% compared to conventional patch antenna,

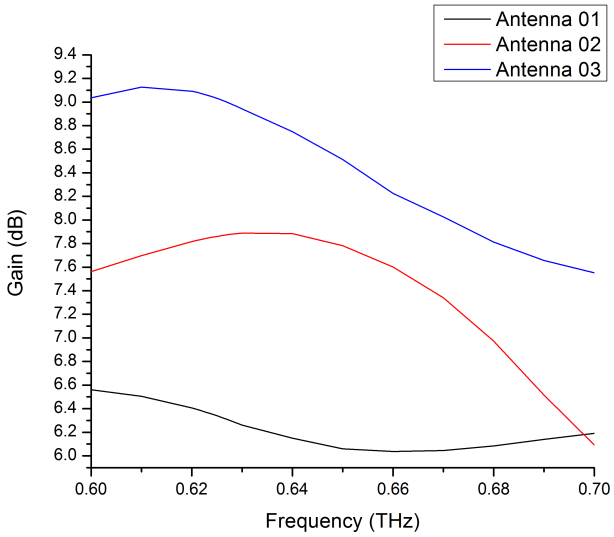

Figure 4.5: Gain versus frequency of Antennas 1, 2 and 3.

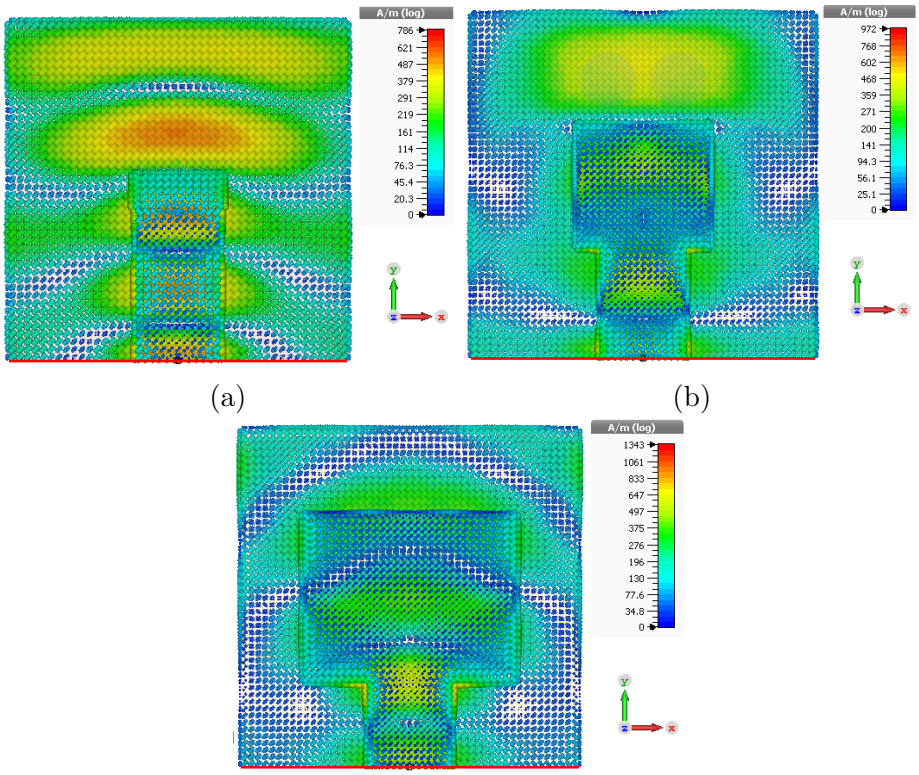

(a) (b)

(c)

Figure 4.6: Current distribution of (a) Antenna 1, (b) Antenna 2 and (c) Antenna 3.

which is based on homogeneous substrate, with a gain of $6.11dB$ and radiation efficiency of 78.94%. Thus, by taking the previous results of the achieved return loss

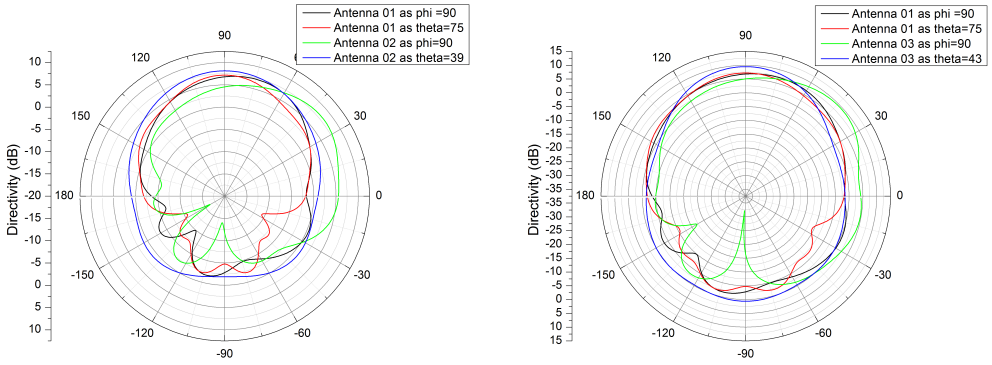

(a) (b)

Figure 4.7: Polar plot of (a) Antenna 1 and Antenna 2 (b) Antenna 1 and Antenna 3, radiation patterns at their resonance frequency for θ and ϕ planes which define the solid angle of maximum radiation.

into consideration, the employment of PBG structure is indeed an effective technique to reduce surface waves that results in worthwhile improvements of different antenna characteristics.

The surface currents of Antennas 1, 2 and 3 are presented in Figure 4.6. The transmitted power from the feeder is dispatched through the patch to out space (air) where most of the power in the substrate is radiated. The advantage from employing photonic crystal substrate is maintained as most of the power is radiated and a noticeable reduction of the reflected power from air-antenna edge interfaces is achieved. The far-field radiation pattern is shown in Figure 4.7 for the three antennas in the planes containing solid angle at which maximum radiation is achieved. It can be easily seen the advantage of Antennas 3 and 2 over Antenna 1 at their maximum radiation solid angle.

4.3 Antenna Based on Aperiodic Photonic Crystal Substrate

In this section, the presented structures of antenna are designed based on Antenna 3 but the air cylinders of the substrate are divided into several sets of air holes. Each set has its own radius as shown in Figures 4.8. Figure 4.8.a represents Antenna 4

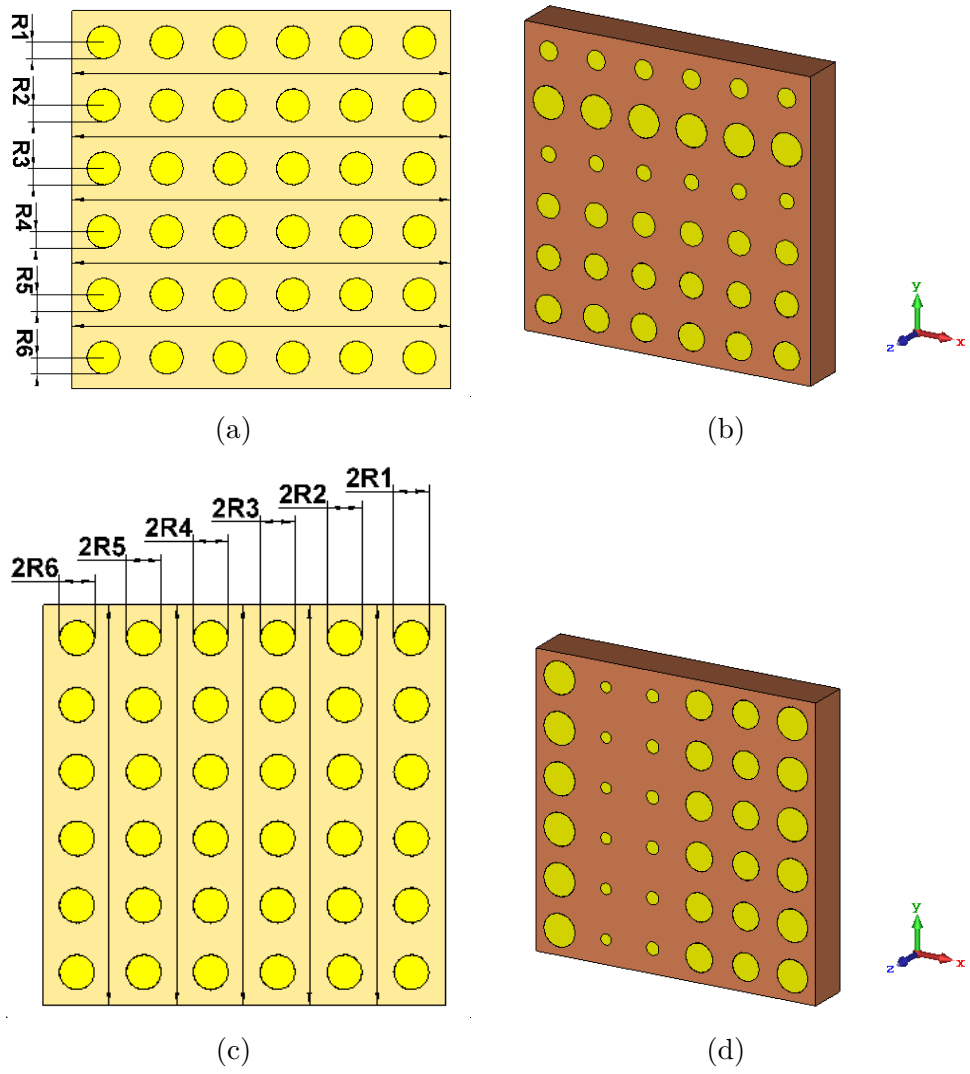

Figure 4.8: Geometry of proposed antenna's substrate based on aperiodic photonic crystal substrate namely (a) and (b) Antenna 4, (c) and (d) Antenna 5

which has six sets of air holes, Figure 4.8.c represents Antenna 5 which has also six sets of air holes, Figure 4.9.a represents Antenna 6 which has three sets of air holes and Figure 4.9.c represents Antenna 7 which has five sets of air holes. By starting from Antenna 3 substrate geometry where all the air cylinders are identical, an optimization of holes radiuses of each set with the merit function that takes S_{11} and gain into considerations is launched for each antenna structure. The results reveal the best combination of air cylinder radiuses which offers the best antenna performance and is summarized in table 4.2 for each antenna geometry.

In this part, the conventional antenna has been compared with the presented antennas which are based on optimized photonic crystal substrate. It is observed, from

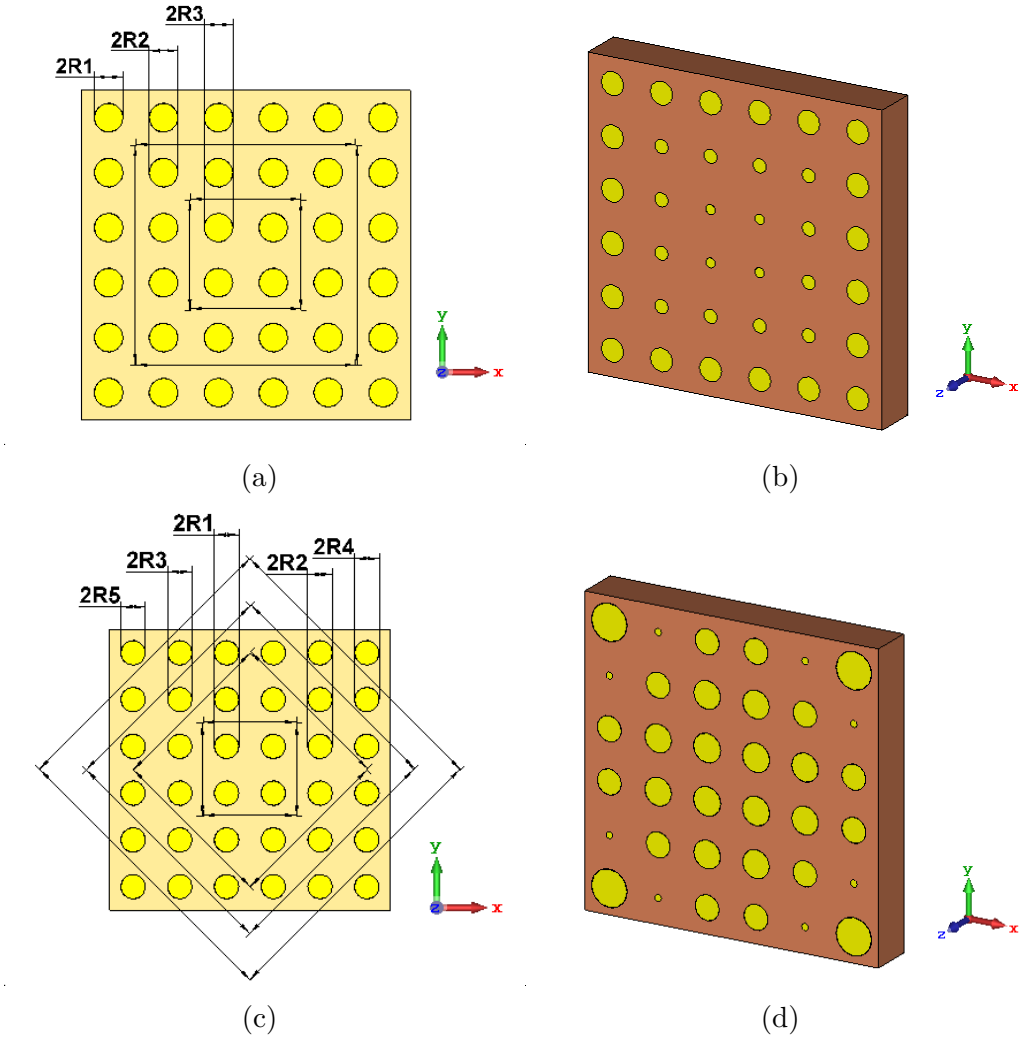

Figure 4.9: Geometry of the proposed antenna's substrate based on aperiodic photonic crystal substrate namely (a) and (b) Antenna 6, (c) and (d) Antenna 7

Table 4.2: The best Parameter values results for the proposed antennas.

	R1 (μm)	**R2** (μm)	**R3** (μm)	**R4** (μm)	**R5** (μm)	**R6** (μm)
Antenna 3	26.5	26.5	26.5	26.5	26.5	26.5
Antenna 4	19.28	32.87	15.57	24.27	25.27	27.68
Antenna 5	33.52	28.71	29.45	13.60	11.50	33.84
Antenna 6	22.81	13.55	9.64	***	***	***
Antenna 7	27.94	27.32	24.66	6.84	36.21	***

Figures 4.10 and 4.11, that all antenna structures including conventional antenna based on homogeneous substrate resonate close to the desired frequency ($0.65THz$) within $0.6 - 0.7THz$ range. The achieved minimal return loss ($S_{11} \leq -10dB$) of Antenna 1, Antenna 3 and Antenna 4 are $-22.09dB$, $-56.8dB$ and $-83.73dB$, re-

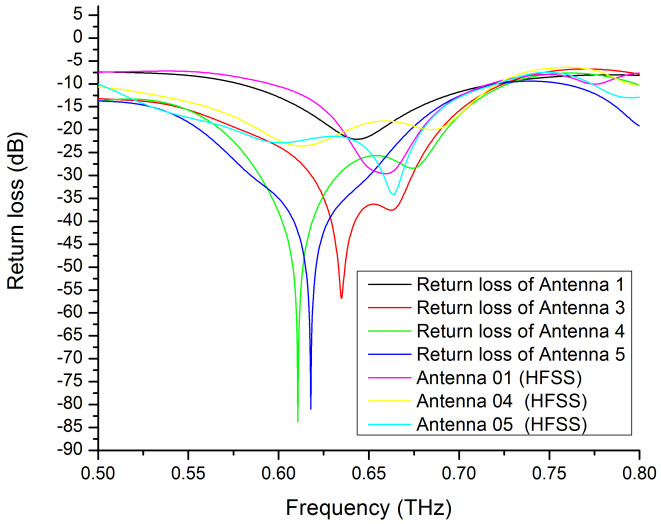

Figure 4.10: S parameter magnitude in terahertz band for proposed antennas based on aperiodic photonic crystal.

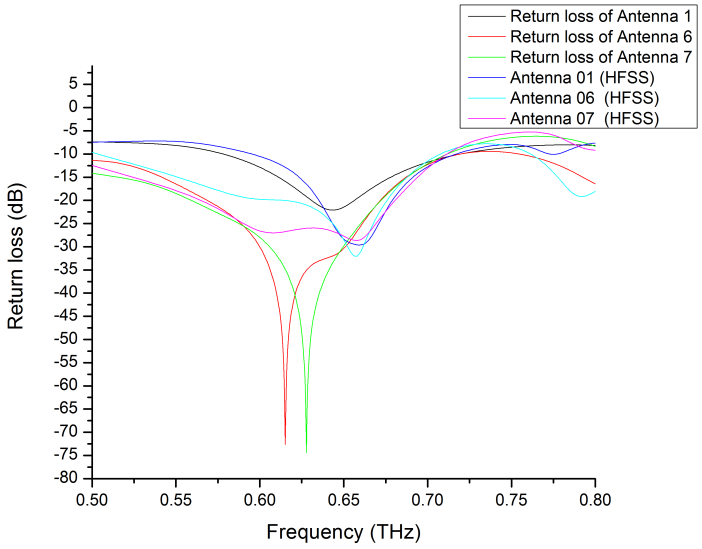

Figure 4.11: S parameter magnitude in terahertz band for proposed antennas based on aperiodic photonic crystal.

spectively with an enhancement of more than 279% with respect to Antenna 1. Also, the achieved gain and radiation efficiency of Antenna 4 based on optimized photonic bandgap, which are equal to 9.19dB and 90.84% respectively, are clearly greater than those of the conventional antenna, which are equal to 6.11dB and 78.94%, respectively. On the other hand, Antenna 5 exhibits a minimal return loss of 80.97dB and

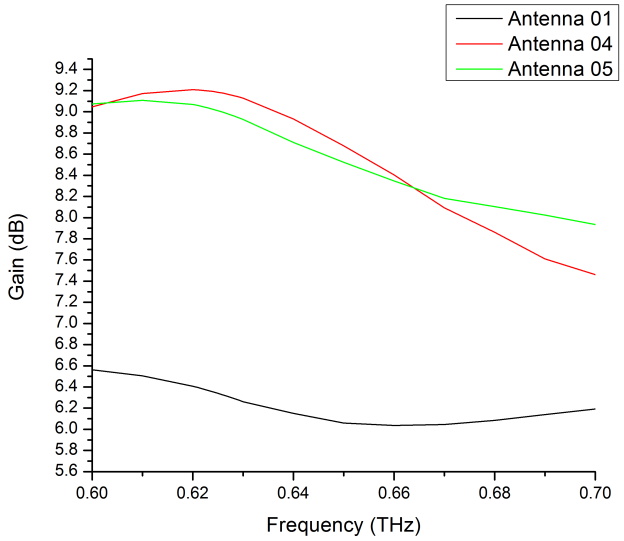

Figure 4.12: Gain of the presented antennas (Antennas 1, 4 and 5).

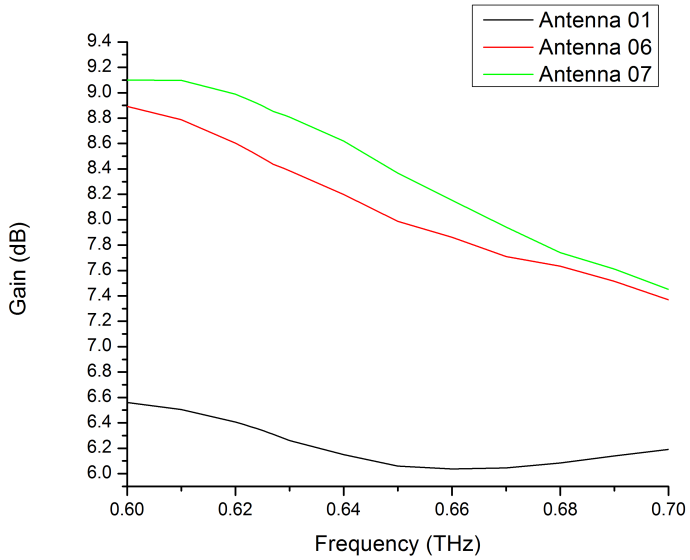

Figure 4.13: Gain of the presented antennas (Antennas 1, 6 and 7).

gain of $9.08dB$ with radiation efficiency of 88.48% which are interesting results as a competitive antenna performance. Antenna 6 reveals good electrical characteristics with the obtained minimal return loss of $-67.79dB$ and achieved gain of $9.04dB$ with radiation efficiency of 90.03%. Finally, Antenna 7 shows a minimal return loss of $-74.45dB$ and an emulative gain of $9dB$ with radiation efficiency of 88.72%. Furthermore, the gain of the presented antennas in frequency range $0.5THz - 0.8THz$ is shown in Figure 4.12 and 4.13 for proper understanding. It is worthwhile to men-

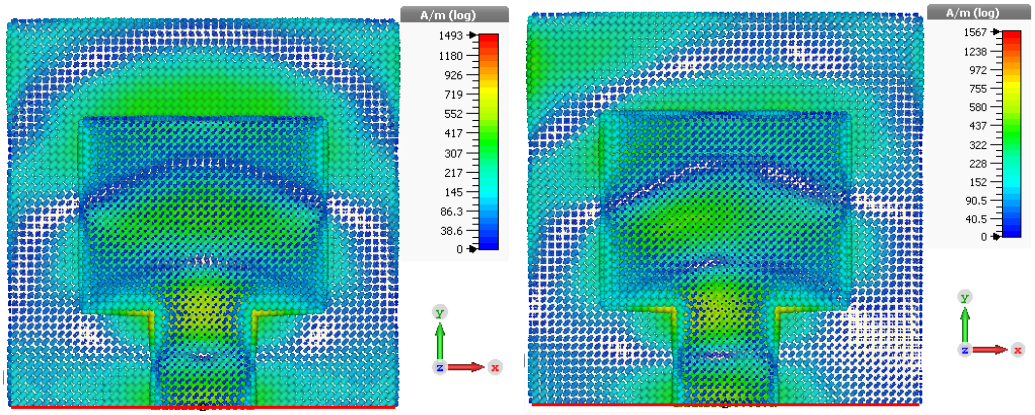

(a) (b)

Figure 4.14: Current distribution of (a) Antenna 5, (b) Antenna 6.

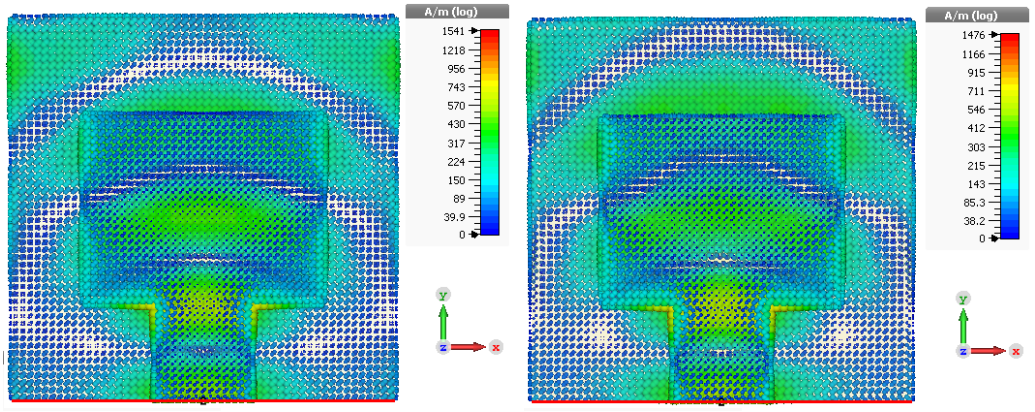

(a) (b)

Figure 4.15: Current distribution of (a) Antenna 6, (b) Antenna 7.

tion that the absolute bandwidths of the Antennas from 3 to 6 are quite greater than the conventional antenna bandwidth of $140GHz$ as it can be obviously seen in Figure 4.10 and 4.11.

The surface current of Antennas 4, 5, 6 and 7 are presented in Figure 4.14 and 4.15. The transmitted power from the feeder is dispatched through the patch to out space, where most of the power in the substrate is radiated. The advantage from employing photonic crystal substrate is maintained as most of the power is radiated and a noticeable reduction of the reflected power from air-antenna edge interfaces is achieved.

According to Figure 4.16 and 4.17, which represents the radiation pattern of the four optimized antennas, it is clearly seen the achieved directivity compared to the

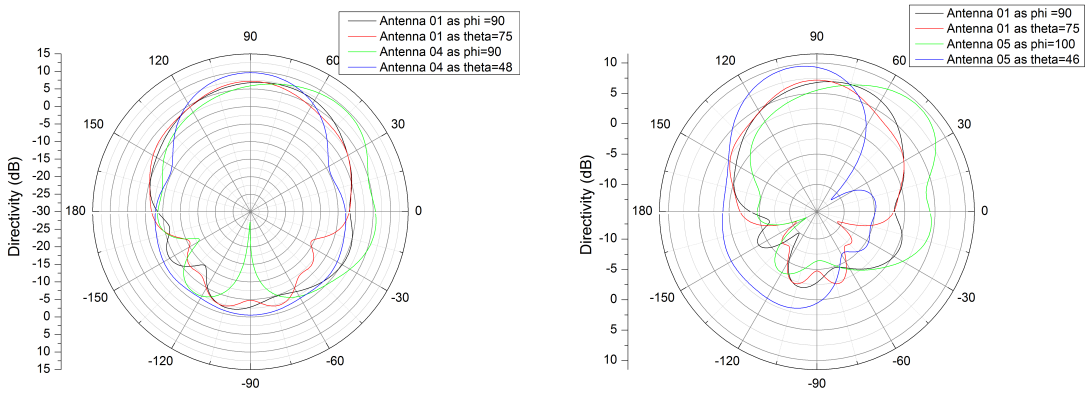

(a) (b)

Figure 4.16: Polar plot of (a) Antenna 1 and Antenna 4 (b) Antenna 1 and Antenna 5, radiation patterns at their resonance frequency for θ and ϕ planes which define the solid angle of maximum radiation.

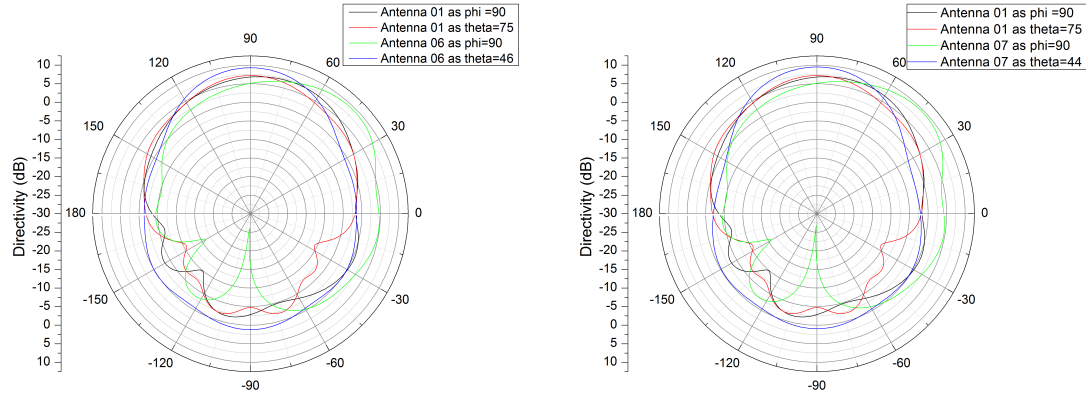

(a) (b)

Figure 4.17: Polar plot of (a) Antenna 1 and Antenna 6 (b) Antenna 1 and Antenna 7, radiation patterns at their resonance frequency for θ and ϕ planes which define the solid angle of maximum radiation.

conventional antenna based on homogeneous substrate. Besides, it is noticed that when the variation freedom of sets radiuses is horizontal as in Antenna 4, the level of side lobe is the greatest compared to the other designs as can be seen in the blue curves of Figure 4.16 and 4.17. However, it is also noticed the vanishing of that side lobe as the variation freedom of sets radiuses is vertical as in Antenna 5 and it is smaller for the other structures namely Antennas 6, and 7 as they are combination of vertical and horizontal variation at the same time. As a result, the more directive the antenna is, the more efficient the communication link can be established.

The simulated results prove that the antenna performance which is based on photonic bandgap substrate including the return loss, radiation efficiency and the gain are effectively improved due to surface wave suppression that exists in the conventional antenna as it is based on the homogeneous substrate. The novelty of this section is the approach to enhance microstrip patch antenna based on photonic crystal substrate as already shown in Figure 4.8 and 4.9. Further exciting results of the proposed antennas and improvements are obtained from this optimization. The proposed antennas are compared with the results of the existing antennas in literature and summarized in Table 4.3.

Table 4.3: Comparison of presented antennas with existing designs.

	f_r **(THz)**	S_{11} **(dB)**	**Bandwidth (GHz)**	**Gain (dB)**	**Radiation efficiency (%)**
[**167**]	0.67	-24	***	7.3	***
[**111**]	0.676	***	***	5.22	***
[**169**]	0.63	-44.71	36.23	7.94	85.71
[**172**]	0.96	-13.05	310	3.8	***
[**173**]	0.75	-35	50	5.09	86.58
Antenna 1	0.64	-22.09	140	6.11	78.94
Antenna 3	0.63	-56.81	>>230	8.95	89.31
Antenna 4 (enhancement %)	0.61	-83.73 (+279%)	>>230	9.19 (+50.41%)	90.84 (+15.1%)
Antenna 5	0.62	-80.97	>>230	9.08	88.48
Antenna 6	0.61	-67.79	>>230	9.04	90.03
Antenna 7	0.62	-74.45	>>230	9	88.72

The proposed terahertz microstrip antennas may have applications mainly in sensing and communication, such as the next generation of wireless communications due to their resonating frequency close to $0.65THz$ where there exist a low atmospheric attenuation window in terahertz range and their electromagnetic characteristics such as high gain, radiation efficiency, return loss and wide bandwidth. These antennas, which belongs to standing wave antennas, are good candidates for terahertz integrated System On-Chip (SoC). The on-chip integrated antenna technology is promising in terahertz range as it could be even more cost-effective than a conventional packaging of an external antenna with transceivers by considering packaging cost and its compactness at terahertz band.

4.4 Antenna Structure of Modified Patch Shapes

4.4.1 Size modifications

In this section, modifications are introduced to patch antenna based on the air-cylinder-embedded dielectric substrate with squared unit cell shown in Figure 4.1 which has a length of $100\mu m$, whereas the centered air cylinder, that is embedded in Polyimide substrate with a relative permittivity of 3.5 and $tan\delta$ of 0.0027, has the same length as the substrate thickness ($90\mu m$). In order to benefit from the property of photonic bandgap in surface wave suppression, the substrate thickness is chosen thick enough to excite these surface waves [121]. To design the substrate structure of patch antenna that resonates around $0.65THz$, the value of the effective permittivity is taken as 1.07.

In this part, a microstrip antenna is designed and simulated using the previously selected photonic bandgap as a substrate. Figure 4.18.a shows the antenna with the PBG structure, viz. Antenna 8, that is used as its substrate whereas the conventional antenna with the homogeneous substrate is shown in Figure 4.3.a. The initial parameters of the radiating microstrip patch antenna are selected close to the calculated ones using the referenced equations in [25] then the length and width of the patch are optimized. The patch is centered above the substrate and the feed line is designed with a width of $150\mu m$. As a summary, the values of each parameter of the antennas are presented in table 4.4.

Table 4.4: Parameter values of the presented Antennas 1 and 08

Component	**Parameter**	**Value (μm)**	
Patch of homogeneous and PBG substrate	Width	160	335
	Length	60	110
Substrate	Width	600	
	Length	600	
	Thickness	90	
	Lattice constant a	100	
	Cylinder radius r	36	

In this work, the presented structure is made of the optimized patch antenna based on photonic bandgap substrate studied previously but the holes are divided

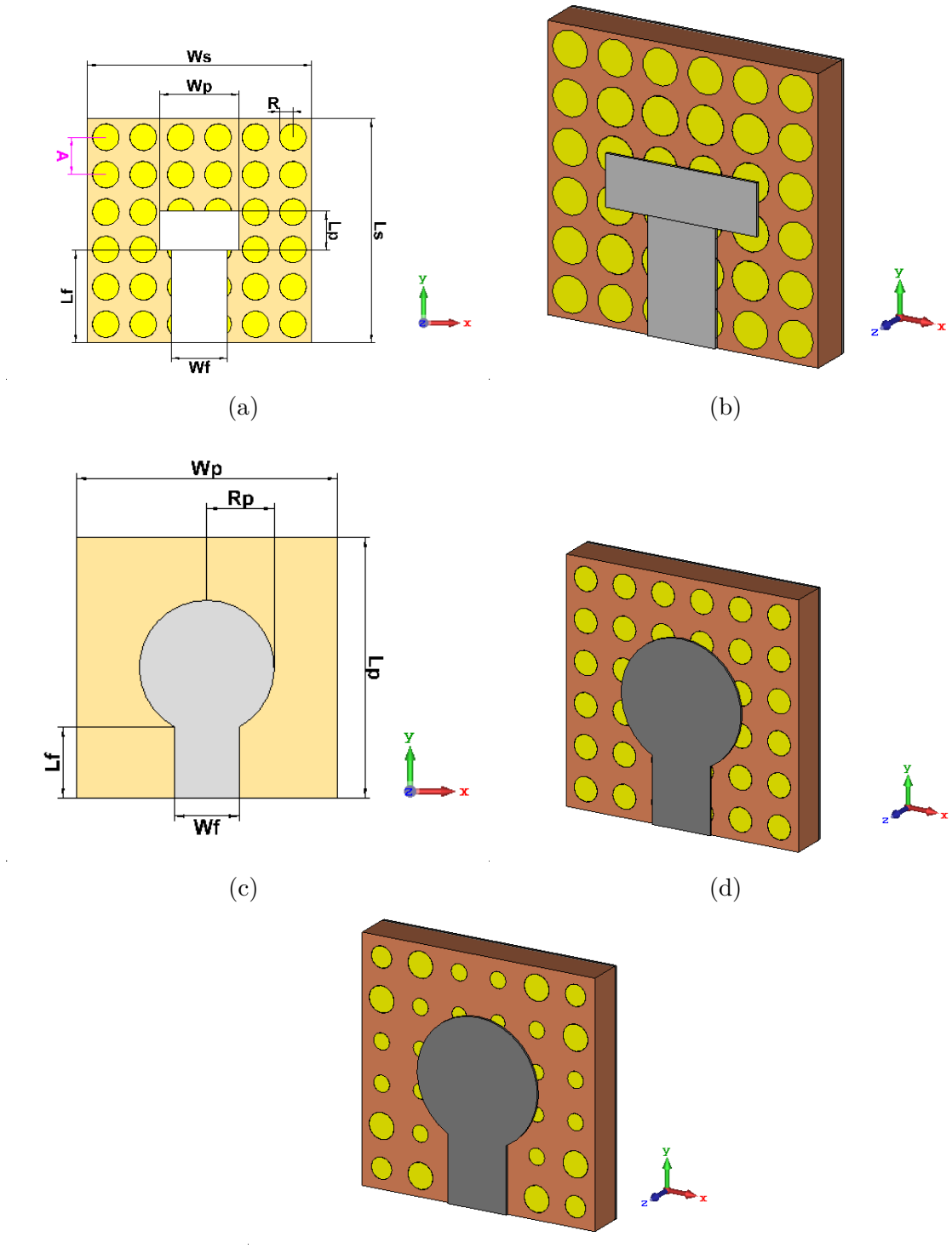

Figure 4.18: Geometry of terahertz antenna based on photonic crystal substrate with different patches (a) Antenna 08 (b) Antenna 09 (c) Antenna 10 (d) Antenna 11 (e) Antenna 12.

into three sets of air holes. Each set has its own radius as shown in Figure 4.18.b of Antenna 9 for the optimized substrate using the square sets of holes similar to Antenna 6 but with different patch size. After optimization of holes radiuses, it is found that R_1, R_2 and R_3 are 38.70, 40.89 and 37.04μm respectively.

4.4.2 Circular Patch Structure

In this subsection, a circular patch microstrip antenna is designed and simulated using photonic bandgap structure as a substrate. The substrate is also made from Polyimide with $\epsilon_r = 3.5$ and $tan\delta = 0.0027$. Figure 4.18.d shows the antenna with the photonic bandgap substrate, Antenna 11, whereas Figure 4.18.c shows the conventional antenna with the homogeneous substrate, Antenna 10; the radius of the circular patch antenna is 155μm. The patch is centered above the substrate and the feed line is designed with a width of 150μm. The substrate is designed thick enough with 90μm that excite surface waves in Antenna 10 which is based on homogeneous substrate. As a summary, the substrate's dimensions of Antenna 10 and Antenna 11, which is based on photonic crystal substrate, are presented in table 4.4. In this work, the presented structure of Antenna 12 is designed based on Antenna 11 but the air cylinders of the substrate are divided into five sets of air holes. Each set has its own radius as shown in Figure 4.9.c. By starting from Antenna 11 substrate where all the air cylinders are identical, an optimization of holes radiuses of each set with the merit function that takes $S_{1,1}$ and gain into considerations is launched. The result reveal that R1, R2, R3, R4 and R5 are equal to $13.37, 18.59, 20.68, 32.39$ and $26.53\mu m$, respectively.

4.5 Results and Discussion of the Modified Patch Antennas

From Figure 4.19 which presents the scattering parameter of the antenna configurations. It can be seen that the antenna designed on the optimized patch based on PBG substrate, Antenna 8, exhibits a wide bandwidth of $216GHz$ compared to

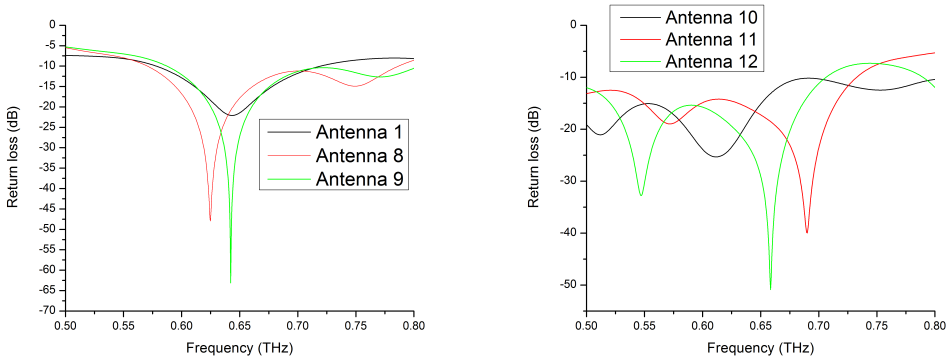

(a) (b)

Figure 4.19: Return loss of the presented antennas in Figure 18 (a) Antennas 1, 8 and 9 (b) Antennas 10, 11 and 12.

the antenna based on homogeneous substrate, Antenna 1, with $140GHz$ and a deep return loss of $-47.92dB$ is achieved compared to homogeneous substrate antenna with $-22.09GHz$. All the resonance frequencies are close to the desired frequency of $0.65THz$. The Voltage Standing Wave Ratio (VSWR) is slightly improved to 1.008.

In this part, the antenna based on enhanced photonic bandgap substrate, Antenna 9, has been compared with the conventional antenna. It is observed from Figure 4.19 that the return loss of both the conventional antenna and the antenna based on enhanced photonic bandgap resonate at a frequency of $0.64THz$ and achieve the return loss ($S11 \leq -10dB$) of $-22.09dB$ and $-63.17dB$ respectively; also, the absolute bandwidth of $140GHz$ and $216GHz$ is maintained, respectively. The improvement is more than $76GHz$.

From Figure 4.19.b which presents the scattering parameter S_{11} of the antenna configurations, it can be seen that Antenna 11 exhibits a wider bandwidth ($288GHz$) than Antenna 10's ($268GHz$) by an improvement of $20GHz$. Also, a deep return loss of $-39.67dB$ is achieved compared to Antenna 10 with $-25.34GHz$. All the resonance frequencies, $0.61THz$ and $0.69THz$ for Antenna 10 and Antenna 11, respectively, are close to the desired frequency $0.65THz$ with a shift of 6% but within the range of $0.6 - 0.7THz$. The ameliorated VSWR is 1.02.

Besides, the conventional antenna has been compared with Antenna 12 which is

based on an optimized PBG substrate. It is observed from Figure 4.19.b that both conventional Antenna 10 and Antenna 12 resonate close to the desires frequency $0.65THz$ within the range $0.6-0.7THz$ but Antenna 12 is the closest with $0.658THz$ resonance frequency. The achieved minimal return loss ($S11 \leq -10dB$) of Antennas 10 and 12 are $-25.34dB$ and $-50.88dB$, respectively; also, the absolute bandwidths of Antenna 10 and Antenna 12 are approximately equal to $268GHz$. The voltage standing wave ratio for Antenna 10 of 1.12 is improved by 0.115; the ameliorated VSWR of Antenna 12 is 1.005.

For further analysis, the gain and radiation efficiency are also interesting characteristics of antennas to be taken into consideration, especially for wireless communication systems in this band of frequency. From Figure 4.20, it can be seen that the gain of the enhanced photonic bandgap antenna, Antenna 9 gain of $8.77dB$ and radiation efficiency 94.05%, is strongly greater than the antenna based on homogeneous substrate, $6.11dB$ and 78.94% respectively, which is also an interesting result as an improvement. Figure 4.20.b shows the gain of the presented antennas.

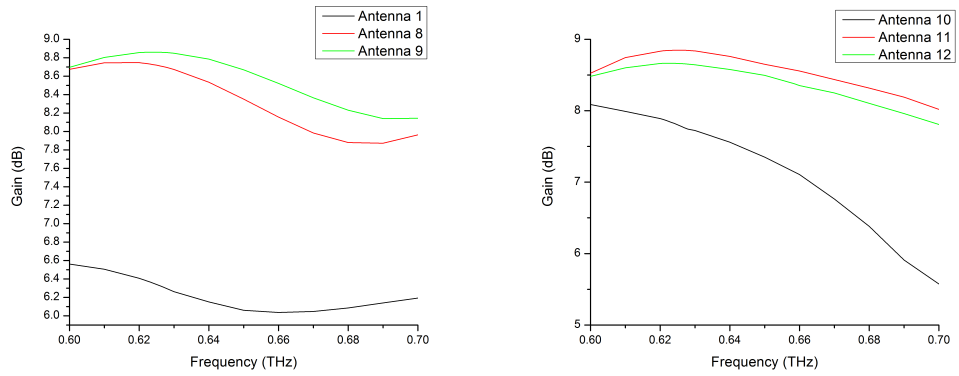

(a) (b)

Figure 4.20: Gain versus frequency of presented antennas (a) Antennas 1, 8 and 9 (b) Antennas 10, 11 and 12.

It is obviously observed the achieved amelioration of the gain and radiation efficiency of Antenna 11 that is based on photonic crystal substrate, gain of $8.18dB$ and radiation efficiency of 92.75%, compared to conventional patch Antenna 10 which is based on the homogeneous substrate with a gain of $7.98dB$ and radiation efficiency of 85.88%. Thus, by taking previous results of the achieved return loss into

consideration, the employment of PBG structure is indeed an effective technique to reduce surface waves that results in worthwhile improvements in different antenna characteristics. It can be seen from Figure 4.20.b that the gain efficiency of Antenna 12 based on optimized photonic bandgap, which are equal to $8.5dB$ and 92.25%, respectively, are strongly greater than the conventional Antenna 10, which are equal to $7.98dB$ and 85.88%, respectively; this is also an interesting result as an improvement. The surface current of Antennas 8,9,10,11 and 12 are presented in Figure 4.21 where the advantage from employing photonic crystal substrate is maintained as most of the power is radiated and a noticeable reduction of the reflected power from air-antenna edge interfaces is achieved.

The achieved spatial directivity of the final optimized photonic bandgap antenna structure at $0.64THz$ is shown in Figure 4.22.b from which the directivity of the antenna can be deduced. The more directive the antenna is, the more efficient the communication link can be established.

The far-field directivity of Antenna 12 based on the optimized photonic crystal substrate at $0.658THz$ is shown in Figure 4.22.d which presents the antenna gain pattern; as a result, the grater the gain of the antenna is, the more efficient the communication link is.

The simulated results prove that the antenna performance which is based on photonic bandgap substrate including the return loss, VSWR , radiation efficiency and the gain are effectively improved due to surface wave suppression that exists in the conventional antenna as it is based on the homogeneous substrate. The novelty in this work is the approach to optimize a microstrip antenna based on photonic crystal substrate as shown in Figure 4.18. Further exciting results of the presented antennas and enhancements are obtained from this optimization. This part presents the closest resonant frequency of $0.658THz$ to the desired frequency of $0.65THz$ for wireless communication technologies.

The proposed antenna is compared with the results of the existing antennas in literature and summarized in Table 4.5. As it is shown, this section presents the closest resonant frequency of $0.644THz$ to the desired frequency of $0.65THz$ for wireless communication technologies. Besides, the proposed Antenna 9 is compared

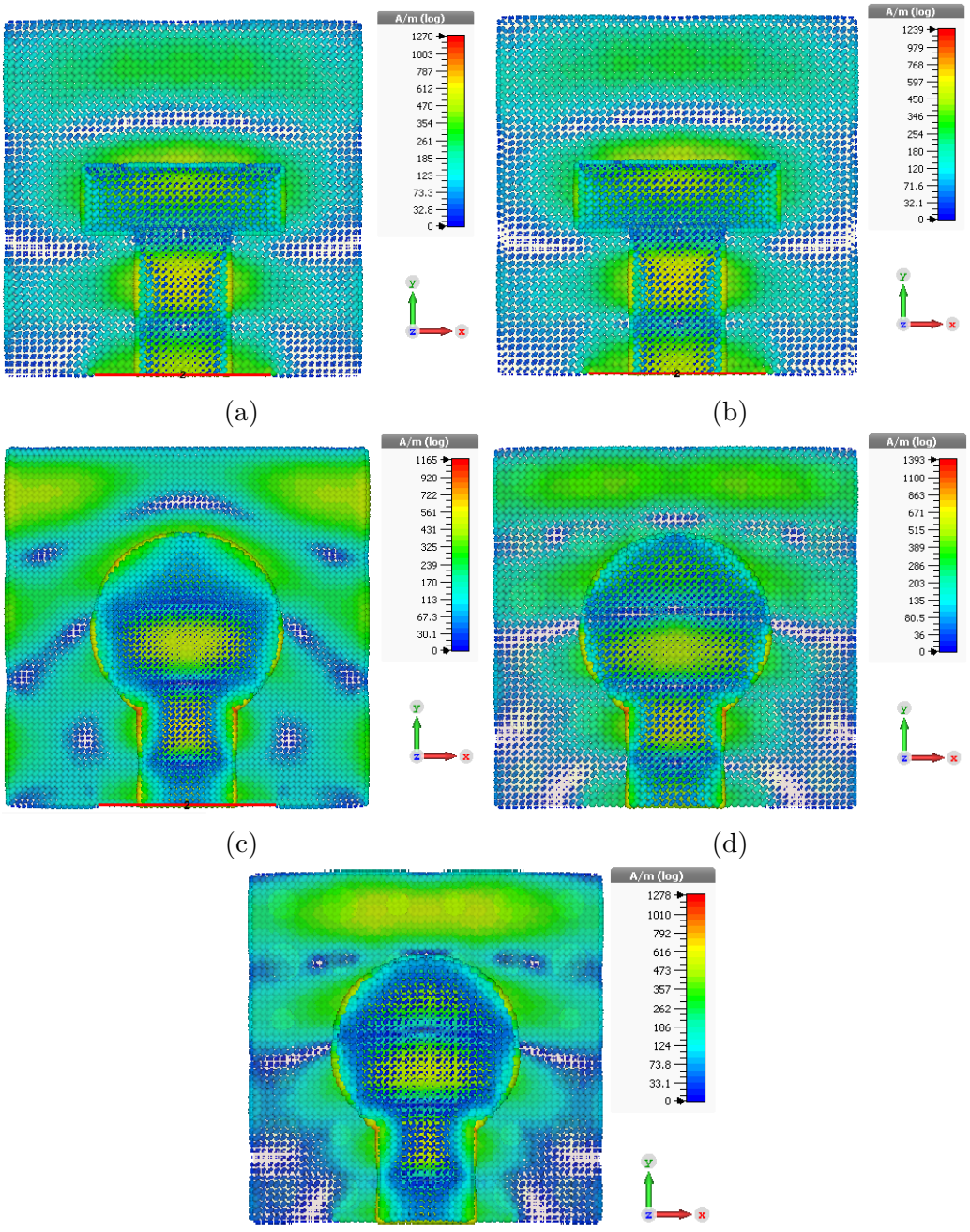

Figure 4.21: Current distribution of the presented antennas (a) Antenna 08 (b) Antenna 09 (c) Antenna 10 (d) Antenna 11 (e) Antenna 12.

with the results of the existing antennas in literature and summarized in Table 4.5.

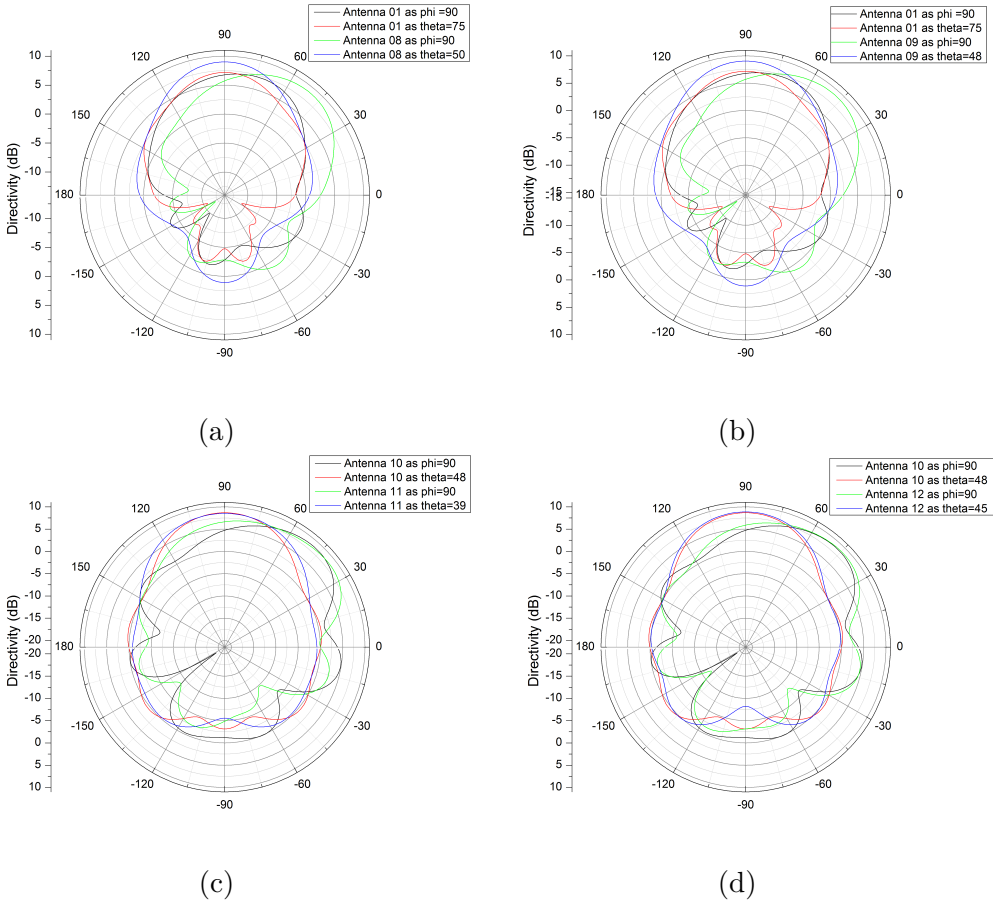

Figure 4.22: Polar plot of (a) Antennas 1 and 8 (b) Antennas 1 and 9 (c) Antennas 10 and 11 (d) Antennas 10 and 12 , radiation patterns at their resonance frequency for θ and ϕ planes which define the solid angle of maximum radiation.

Table 4.5: Comparison of presented antennas with existing designs.

	Resonance frequency fr (THz)	**Return loss (dB)**	**Bandwidth (GHz)**	**Gain (dB)**	**Radiation efficiency (%)**
[167]	0.67	-24	***	7.3	***
[111]	0.676	***	***	5.22	***
[169]	0.63	-44.71	36.23	7.94	85.71
[172]	0.96	-13.05	310	3.8	***
[173]	0.75	-35	50	5.09	86.58
Antenna 1	0.64	-22.09	140	6.11	78.94
Antenna 8	0.624	-47.92	216	8.73	93.94
Antenna 9	0.644	-63.17 (80%)	216 (25%)	8.77 (36%)	94.05 (08%)
Antenna 10	0.61	-25.34	268	7.98	85.88
Antenna 12	0.658	-50.88 (101%)	268 (0%)	8.5 (6.5%)	92.25 (7.4%)

4.6 Antenna Based on Different Substrate Dielectric Materials: RT5870-Air and Silicon-Air

The objective of this section is to investigate the employment of the non-periodic photonic crystal substrate based on materials other than polyimide-air. Rogers RT5870 and Silicon materials which have lower and higher permittivity than polyimide are selected. It should be noted that the antenna based on a homogeneous silicon substrate is already presented in Chapter 3.

In this part, Antennas 14 and 15, which are rectangular microstrip patch antennas, are designed and simulated based on homogeneous and conventional PBG substrate, respectively. The substrate is made from Rogers RT5870 with $\epsilon_r = 2.33$ and $tan\delta = 0.0012$. Figure 4.23 shows the simulated photonic crystal structure geometry. The length of the squared unit cell is $152\mu m$ whereas the centered air

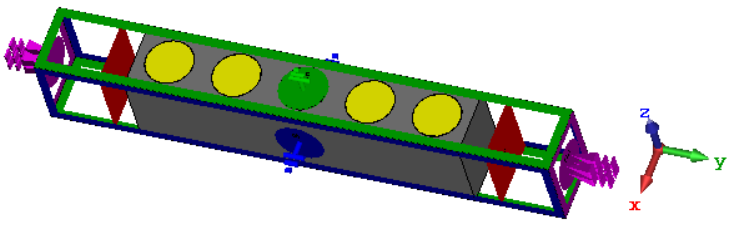

Figure 4.23: Geometry of the simulated photonic crystal structure.

cylinder has the same thickness as the substrate of $186\mu m$ with a radius of $53\mu m$. In order to extract substrate electrical properties, simulation results are computed in $0.35 - 0.75THz$ frequency range. The extracted real and imaginary parts of the permittivity with their corresponding scattering parameters are shown in Figure 4.24.

According to Figure 4.25, which shows Antennas 14 and 15 structures based on homogeneous (Rogers) and photonic bandgap substrates (Rogers-Air), respectively, the patch is centered above the substrate and the feed line is designed with a width of $58\mu m$. The substrate is selected thick enough with $186\mu m$ that excites surface waves in Antenna 14, which is based on homogeneous substrate. The width W_p and the length L_p of the patch are $179\mu m$ and $209\mu m$ based on square substrate surface with $760\mu m$ length.

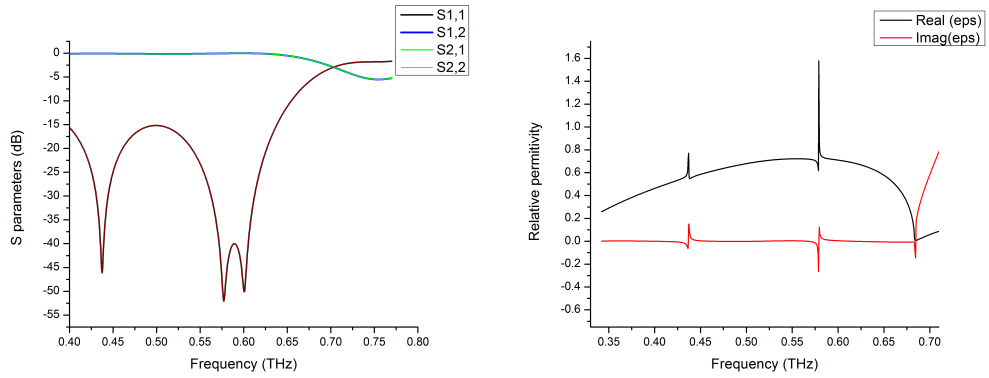

(a) (b)

Figure 4.24: Simulation results of roger photonic crystal substrate (Figure 23) (a) Reflection and transmission coefficients (b) relative permittivity.

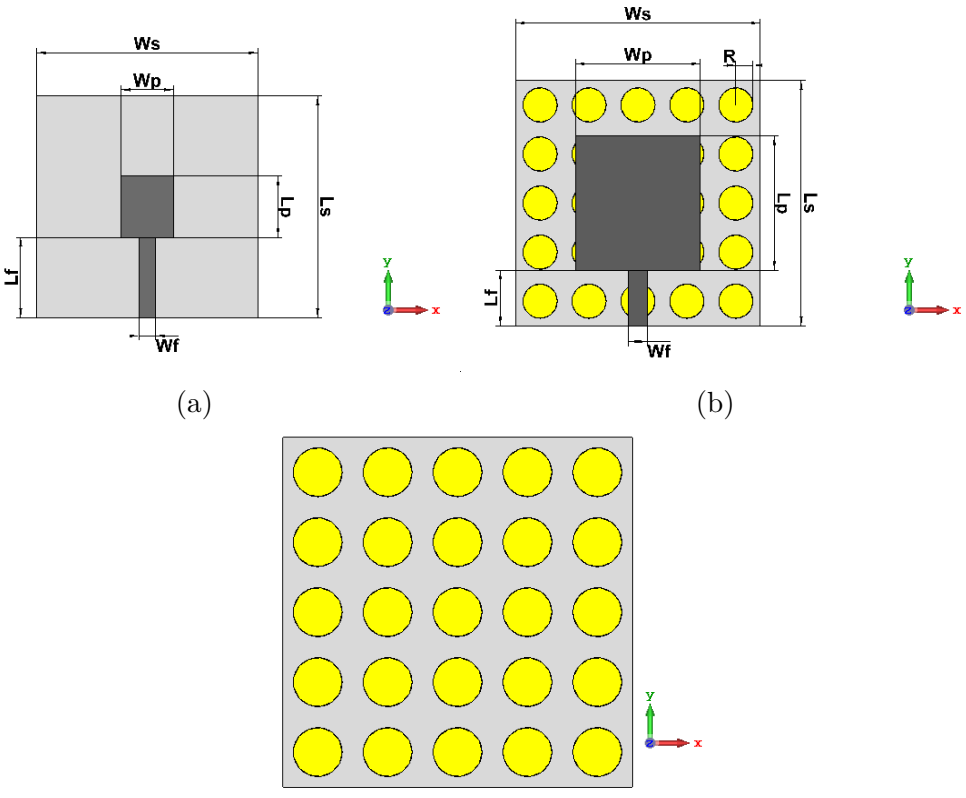

(a) (b)

(c)

Figure 4.25: Geometry of (a) Antenna 14, (b) Antenna 15 and (c) substrate of Antenna 15.

From Figure 4.26, which represents the scattering parameter magnitude S_{11} of the antennas, it can be seen that Antenna 15 exhibits a wider bandwidth, more than $287GHz$, than Antenna 14's $182GHz$ with a noticeable improvement even

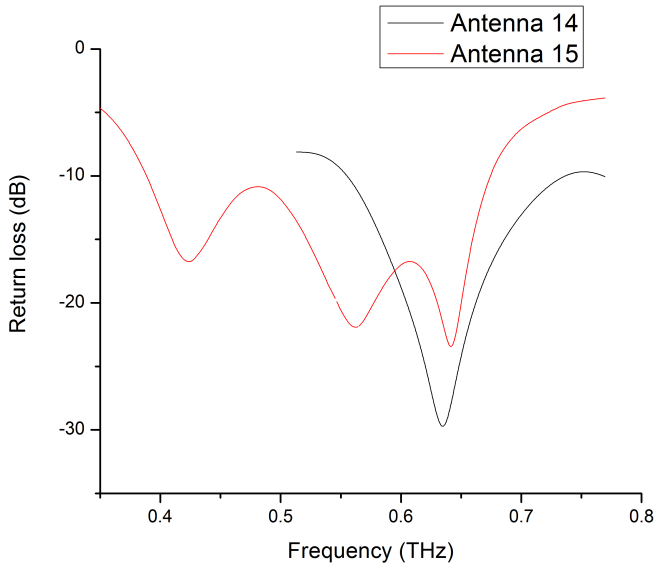

Figure 4.26: Return loss of Antenna 14 and Antenna 15.

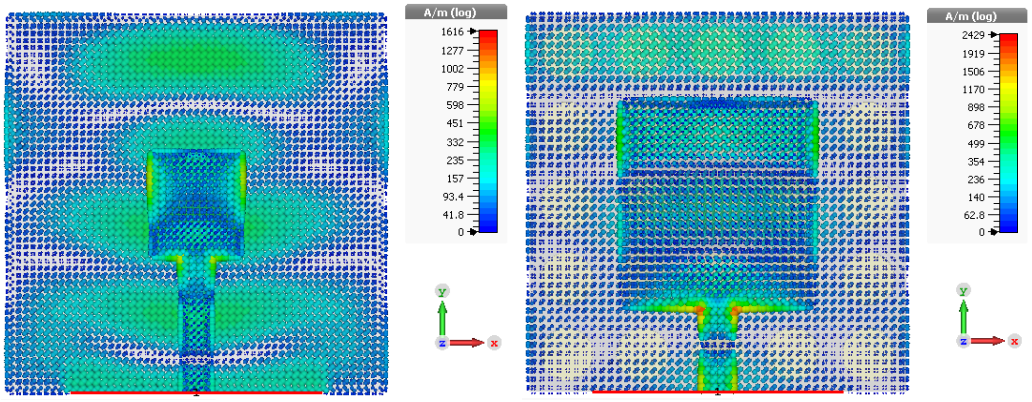

(a) (b)

Figure 4.27: Current distribution of Antenna 14 and Antenna 15.

with different substrate material. Also, a reduced return loss less than $-15dB$ is achievable. All the resonance frequencies around $0.64THz$ for Antenna 14 and Antenna 15 are close to the desired frequency $0.65THz$ within the range of $0.6 - 0.7THz$. The surface current of Antennas 14 and 15 are presented in Figure 4.27 where the advantage from employing photonic crystal substrate is maintained as most of the power is radiated and a noticeable reduction of the reflected power from air-antenna edge interfaces is achieved.

It is obviously observed in Figure 4.28 the achieved amelioration of the gain and radiation efficiency of Antenna 15 that is based on photonic crystal substrate, a gain

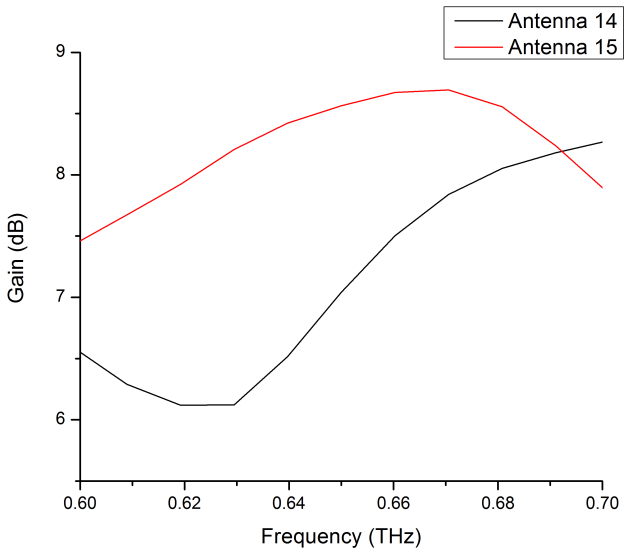

Figure 4.28: Gain versus frequency of Antenna 14 and Antenna 15.

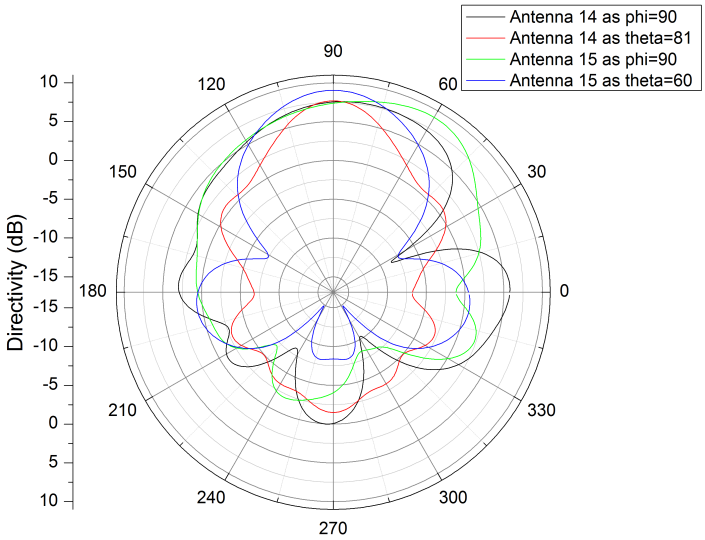

Figure 4.29: Radiation pattern of Antenna 14 and Antenna 15.

of 8.6dB and radiation efficiency of 85%, compared to conventional patch antenna which is based on homogeneous substrate with a gain of 7dB and radiation efficiency of 75%. Thus, by taking previous results into consideration, the employment of photonic bandgap structure is indeed an effective technique to reduce surface waves that results in worthwhile improvements of different antenna characteristics.

The far-field radiation patterns are shown in Figure 4.29 for both antennas in the planes containing solid angle at which maximum radiation is achieved. It can

be easily seen the advantage of Antenna 15 over Antenna 14 at their maximum radiation and the reduced side lobes.

According to Figure 4.30 which shows the substrate of Antennas 16 and 13 structures based on optimized PBG substrate, respectively. The radii for Antennas 16 and 13, viz. R_1, R_2, R_3, R_4, R_5 and R_1, R_2, R_3, R_4, R_5, R_6, R_7, R_8, R_9, R_{10}, R_{11}, R_{12}, R_{13}, R_{14}, R_{15} , R_{16}, has been found to be 57, 57, 15, 64, 47 μm and 29, 14, 25, 30, 22, 27, 25, 15, 29, 29, 25, 15, 30, 27, 24, 19 μm, respectively.

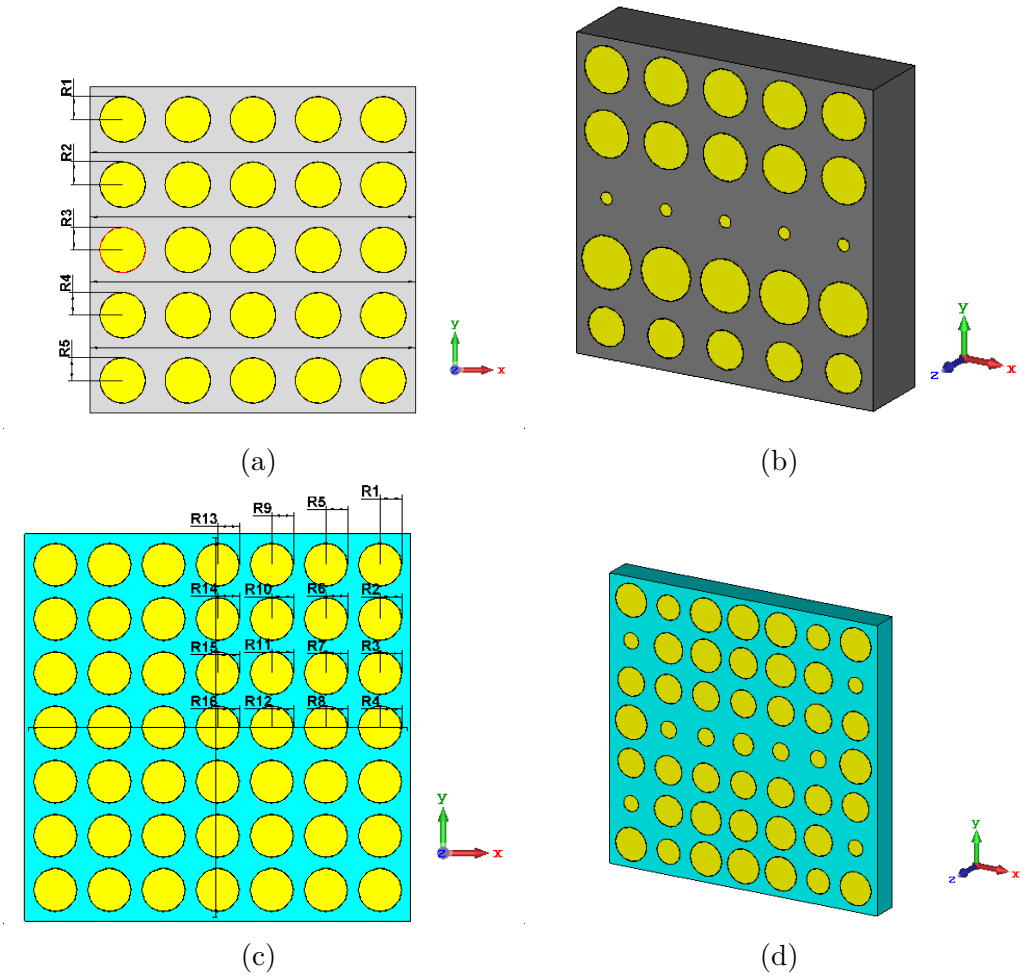

Figure 4.30: Geometry of the optimized substrates for terahertz antennas (a) and (b) Antenna 16, (c) and (d) Antenna 13.

From Figure 4.31, which represents the scattering parameter magnitude S_{11} of the antenna configurations, it can be seen that Antenna 16 exhibits a wider bandwidth, more than $291GHz$, than Antenna 14's $182GHz$ with a noticeable improvement for Silicon based antennas where all resonance frequencies are within

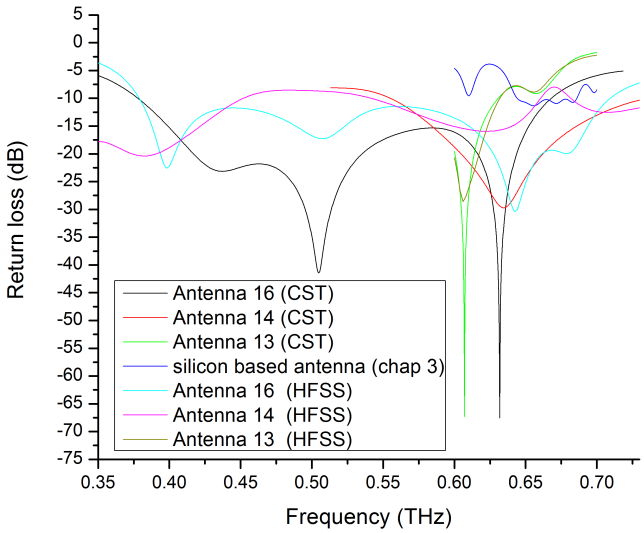

Figure 4.31: Return loss of Antennas 16 and 13 compared to Antenna 14 and conventional silicon based antenna.

$0.6 - 0.7THz$ window even with different substrate material. The surface current of Antennas 13 and 16 are presented in Figure 4.32, where the advantage from employing photonic crystal substrate is maintained as most of the power is radiated and a noticeable reduction of the reflected power from air-antenna edge interfaces is achieved.

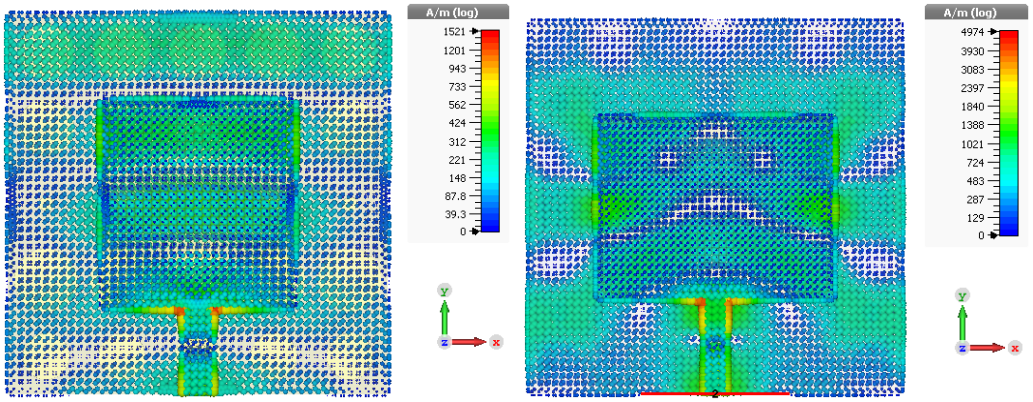

(a) (b)

Figure 4.32: Current distribution of Antenna 16 and Antenna 13.

It is clearly seen, the achieved enhancement of the gain ($8.4dB$) and radiation efficiency (88.7%) of Antenna 16 that is based on modified photonic crystal substrate compared to conventional patch antenna which is based on homogeneous substrate

with a gain of $7dB$ and radiation efficiency of 75%, in Figure 4.33. For silicon based antennas, a gain of $9.75dB$ and radiation efficiency of 89.7% is achieved compared to conventional patch antenna, which is based on homogeneous silicon substrate, with a gain of $5.37dB$ and radiation efficiency of 70%. Thus, by taking previous results into consideration, the employment of modified photonic bandgap structure is indeed an effective technique to reduce surface waves that results in worthwhile improvements of different antenna characteristics.

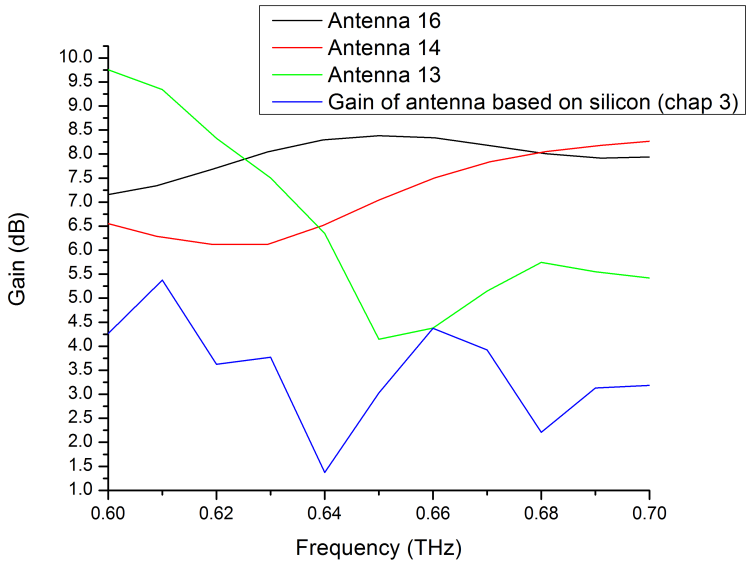

Figure 4.33: Gain versus frequency of Antennas 16 and 13 compared to Antenna 14 and silicon based antenna.

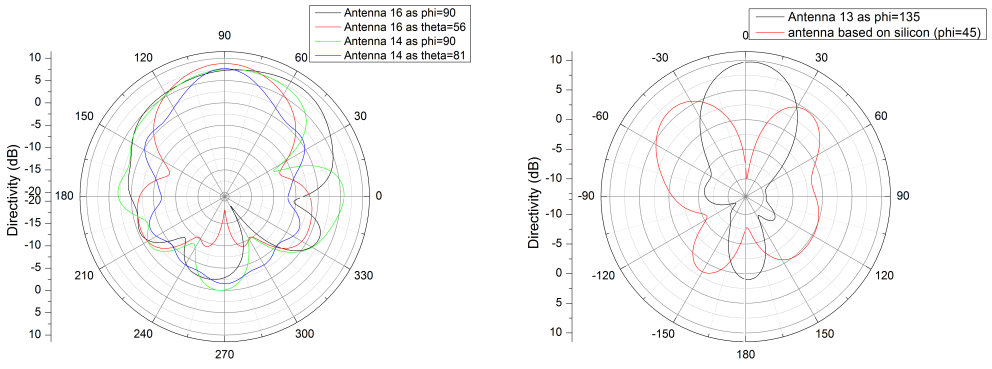

(a) (b)

Figure 4.34: Radiation pattern of (a) Antenna 16 and Antenna 14 (b) silicon based antenna and Antenna 13.

The far-field radiation patterns are shown in Figure 4.34 for both antennas in the planes containing solid angle at which maximum radiation is achieved which corresponds to both silicon and roger based antennas. It can be easily seen the advantage in directivity of Antenna 16 over Antenna 14 at their maximum radiation and Antenna 13 over the antenna based on silicon substrate.

4.7 Summary

In this chapter, several terahertz microstrip patch antennas based on optimized photonic crystal substrate are designed and analyzed. First, the antenna based on photonic crystal substrate is designed and analyzed in order to enhance its performance around $0.65THz$ by suppressing the undesirable surface waves that renders it to a more suitable component for the next generation of wireless communication systems. Simulated results show that the photonic bandgap substrate efficiently enhances the characteristics of the conventional microstrip antenna at this band of frequency. Finally, multiple other investigated antennas based on modified photonic crystal structure are proposed which result in noticeable and worthwhile extra ameliorations of antenna return loss, bandwidth, gain, and radiation efficiency with a great enhancement such as 279%, 50.41% and 15.1% in the return loss, gain and radiation efficiency, respectively.

Chapter 5

Design of MIMO System for THz Indoor Communications

5.1 Introduction

Beyond the next generation of wireless communication systems, the transition of the carrier frequencies to the terahertz band is the viable solution to meet long-term demand for extra-high transmission data rates [177]. This enables fascinating real-life technologies to arise. For the establishment of such a high data rate communication links, increasing the available bandwidth is therefore quite important. However, the terahertz channel has other distinct characteristics, such as a higher transmission path loss and extra molecular loss of absorption [50], compared to the lower band systems. This challenge is addressed by many researchers [178] where highly directional antennas are proposed to defeat the emerged losses and to increase the link capacity for practical indoor environment applications and to build extra high-speed communication systems. Moreover, the reflection and scattering of waves at the lower bands are also different [179, 180, 181]. For terahertz rays, the surfaces of indoor objects should be perceived as rough surfaces rather than smooth as the roughness of the indoor surfaces such as plaster or wallpaper is comparable with the traveling wavelength.

The motion of moving objects in the indoor environment is quite slow compared to terahertz signals through a certain time window. Thus, a moving object can be

considered as a static object between the transmit antenna and the receive antenna [182]. Therefore, the channel may be influenced by fading in most situations and this will impact the bit error rate. Hence, diversity is required for the receive antenna to catch several redundant waves where the probability that all received waves are affected instantaneously is excessively diminished. There are several strategies for raising channel capacity, one of which is to use the MIMO technic to introduce a diversity scheme in communication systems [183]; nevertheless, as MIMO systems suffer from limitations of size, isolation of antennas and spacing. It is critical to tackling other technics to overwhelm such constraints. By using a photonic crystal substrate-based antennas and making them directional [12] is a promising strategy.

Due to the low profile, low cost, simple deployment on molded surfaces, and compatibility with Integrated Circuit (IC) technology, microstrip patch antennas are commonly used for different applications [183]. However, the antenna substrate exhibits two main losses which are the conduction loss of the substrate and the loss of surface wave due to the employed substrate with high permittivity and comparatively large thickness [139]. Some researchers have used a high-dielectric or thick substrate to boost the electrical characteristics of the microstrip antennas [184, 185, 186, 187]. Nonetheless, adding such high-dielectric-permittivity materials with considerable thickness contributes to the excitation of shock waves in the frequency ranges of the millimeter and terahertz [188].In fact, the implementation of a thick substrate contributes to surface waves excitation due to the absorption of energy within the substrate [25], while a decrease in the thickness of the substrate deteriorates the antenna's radiation pattern.

Photonic Crystals (PCs) are commonly employed as a substrate in the design of microstrip antenna for operation at high frequencies to reduce the aforementioned surface wave loss [189, 146, 147, 148, 149, 150]. Besides, researchers have been attracted by the two-dimensional (2D) PCs, as they are much easier to manufacture than three-dimensional (3D) PCs [190, 191, 192] and have wide utilities rather than antennas and planar waveguides [154, 155]. Nevertheless, due to the complicacy of photonic crystal, characterizing those using strictly analytical methods is usually difficult. Alternatively, full-wave simulators such as the finite integral technic-based

CST Microwave Studio were used for these researches to analyze the designed antennas based on a photonic crystal substrate. Besides, the employment of photonic crystals in integrated silicon-based on-chip antennas is appealing in the area of terahertz technology for different applications such as MIMO communication systems because they are more cost-effective in regards to packaging expenses and compactness compared to traditional packaging of separate antennas and transceivers. Generally, the System on chip (THz-SoC) technology for Terahertz band is interesting in many applications which includes extremely high analog interfaces and digital logic for processing and low-cost mass production [138].

Graphene is the first discovered two-dimensional structure made from graphite which was proposed in the last decade [193]. Several devices have been reconstructed based on graphene such as optical sensors [194] and filters [195] due to its special properties. The most interesting feature is that by changing the electrostatic voltage bias, graphene surface conductivity is controlled. Several researchers conducted their researches on the utility of graphene in antennas to improve its radiation characteristics [196, 197, 198, 199, 200, 201].

The scientific community is developing and improving manufacturing techniques. However, in recent years, some techniques were used to fabricate even the structure with the nanometer scale, which can be employed in the construction of the THz microstrip antennas [113, 114, 115]. In addition, the measurement challenges are also an issue that can be overcome by measuring techniques in the near field [116, 117, 118]. This makes it possible to complete the manufacturing and testing of the terahertz microstrip antennas and to be utilized in their desired applications.

In this chapter, first graphene load is analyzed and investigated for its interesting characteristic. Followed by MIMO antenna design based on homogenous, photonic crystal and optimized structure with the graphene load. Then by applying the designed antennas in indoor communication scenario which its occurrence is often, different analysis and studies for capacity enhancement are conducted and compared with other results in literature. Finally, a summary concludes the work.

5.2 Graphene properties

Graphene is a single layer of atoms in a two-dimensional material with a surface conductivity $\sigma(\omega,\mu_c,\Gamma,\ T)$ which is related to the angular frequency ω, chemical potential μ_c, phenomenological scattering rate Γ and temperature T. The Kubo formula [202] describes the graphene conductivity as:

$$\sigma(\omega,\mu_c,\Gamma,T)=\frac{je^2(\omega-j2\Gamma)}{\pi\hbar^2}\times\left[\frac{1}{(\omega-j2\Gamma)^2}\int_0^\infty\epsilon\left(\frac{\partial f_d(\epsilon)}{\partial\epsilon}-\frac{\partial f_d(-\epsilon)}{\partial\epsilon}\right)d\epsilon-\int_0^\infty\frac{f_d(-\epsilon)-f_d(\epsilon)}{(\omega-j2\Gamma)^2-4(\frac{\epsilon}{\pi})^2}d\epsilon\right] \tag{5.1}$$

Where $\hbar$ and h are the reduced and normal Planck's constants, e is the electron charge, K_B is the Boltzmann's constant, and the Fermi–Dirac distribution $f_d(\epsilon)$ is described as:

$$f_d(\epsilon)=(e^{(\epsilon-\mu_c)/k_BT}+1)^{-1} \tag{5.2}$$

The carrier density n_s is related to chemical potential μ_c based on the following relationship [202]:

$$n_s=\frac{2}{\pi\hbar^2V_f^2}\int_0^\infty\epsilon\left[f_d(\epsilon)-f_d(\epsilon+2\mu_c)\right]d\epsilon \tag{5.3}$$

where V_f is the Fermi velocity. Hence, the chemical potential, which is determined by the carrier density, can be tuned up by application of chemical doping and electrostatic bias voltage [202]. The surface impedance of graphene is introduced in Figure 5.1 for different chemical potentials. It is noted that graphene has a low resistance when μ_c=1 and a high resistance when μ_c=0. Therefore, graphene can operates in two different modes which are controlled by adjusting its corresponding chemical potential μ_c. In order to tune the chemical potential a FET or graphene-based electrolytic capacitor should be considered. In fact, the chemical potential is controlled by the carrier density n_s which can be tuned by employing an electrostatic bias voltage and chemical doping [203]. Several researches have been conducted that present a strong capability of electrolyte to control the carrier density in graphene

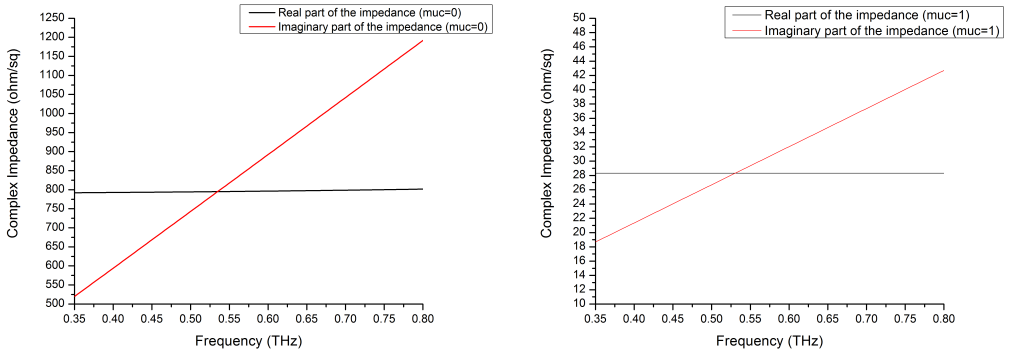

(a) (b)

Figure 5.1: Graphene properties as (a) $\mu_c = 0$ (b) $\mu_c = 1$.

such as [204] and [205].

5.3 Antenna design with graphene load

In this section, the researcher designed and developed three different MIMO antennas which are based on homogeneous and artificial substrates. By introducing a graphene load in the single antenna structure presented in [13] and exploiting its radiation characteristics in such an orientation and spacing, the final proposed MIMO antenna is developed as a rectangular microstrip patches based on a PBG substrate. Figure 5.2 shows the designed MIMO antenna where the width W_p and length L_p of

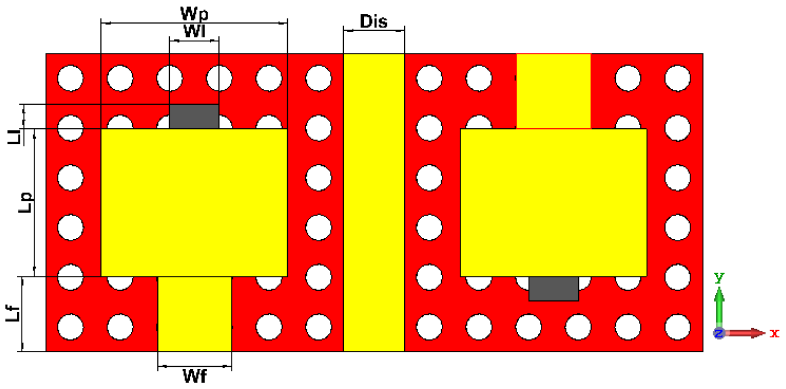

Figure 5.2: Geometry of MIMO antenna design based on PBG for different μ_c).

the patch are $376\mu m$ and $296\mu m$ respectively and the feeder width W_f and length

L_f are selected to be $150\mu m$ and $152\mu m$. The graphene load has a width W_l and a length L_l of $100\mu m$ and $50\mu m$, respectively. The substrate material is chosen to be polyimide where its relative permittivity $\epsilon_r = 3.5$ and $tan\delta = 0.0027$ with a size of $600 \times 600 \times 90\mu m^3$. The first MIMO antenna is based on homogeneous substrate. For the photonic crystal structure, the length of the squared air polyimide unit cell is $100\mu m$ and the air holes have a radius of $26.5\mu m$ of periodic PBG concerning the second MIMO antenna. For optimized PBG, viz. third MIMO antenna, the radii's are $19.28, 32.87, 15.57, 24.27, 25.27$, and $27.68\mu m$, respectively for each row of holes. All holes thicknesses are $90\mu m$ as the substrate. A copy from the antenna, which is fed by another port, is shifted by a distance Dis of $123\mu m$ and rotated by $180°$.

The introduced three antennas are designed and investigated by using CST simulator which is based on the Finite Integration Technique (FIT). The simulations have been performed using CST time domain solver with the number of mesh cells being $250576, 504300$ and 680190 for MIMO antennas based on homogeneous, PBG and optimized PBG substrates, respectively. The graphene has been modelled using a volumetric approach with a thickness of $0.02\mu m$.

The scattering parameters, i.e. the reflection coefficients S_{11} and S_{22} for port 1 and 2 respectively and the transmission coefficients S_{21} and S_{12}, are computed for MIMO antenna based on homogeneous substrate as shown in Figure 5.3 and for MIMO antenna based on photonic crystal substrate with optimized photonic crystal substrate as $\mu_c = 1$ and as $\mu_c = 0$. It is noticed that the transmission coefficients are approximately identical because of the presented geometrical symmetry of MIMO antennas. The same remark still true for reflection coefficients. From transmission coefficients S_{21} and S_{12}, it is shown the low coupling power between port 1 and 2 and vice versa.

For reflection coefficients S_{11} and S_{22}, It is obviously seen the resonance frequency around $0.65THz$ atmospheric window. Also, the $10dB$ bandwidths are $151, 266, 336, 287$ and $356GHz$ for Antenna 1, Antenna 2 as μ_c being 0, Antenna 2 as μ_c being 1, Antenna 3 as μ_c being 0, and Antenna 3 as μ_c being 1. Indeed, the employment of periodic photonic crystal and optimized photonic crystal, i.e. Antenna 2 and 3, enlarge the bandwidth compared to MIMO Antenna 1 which is based

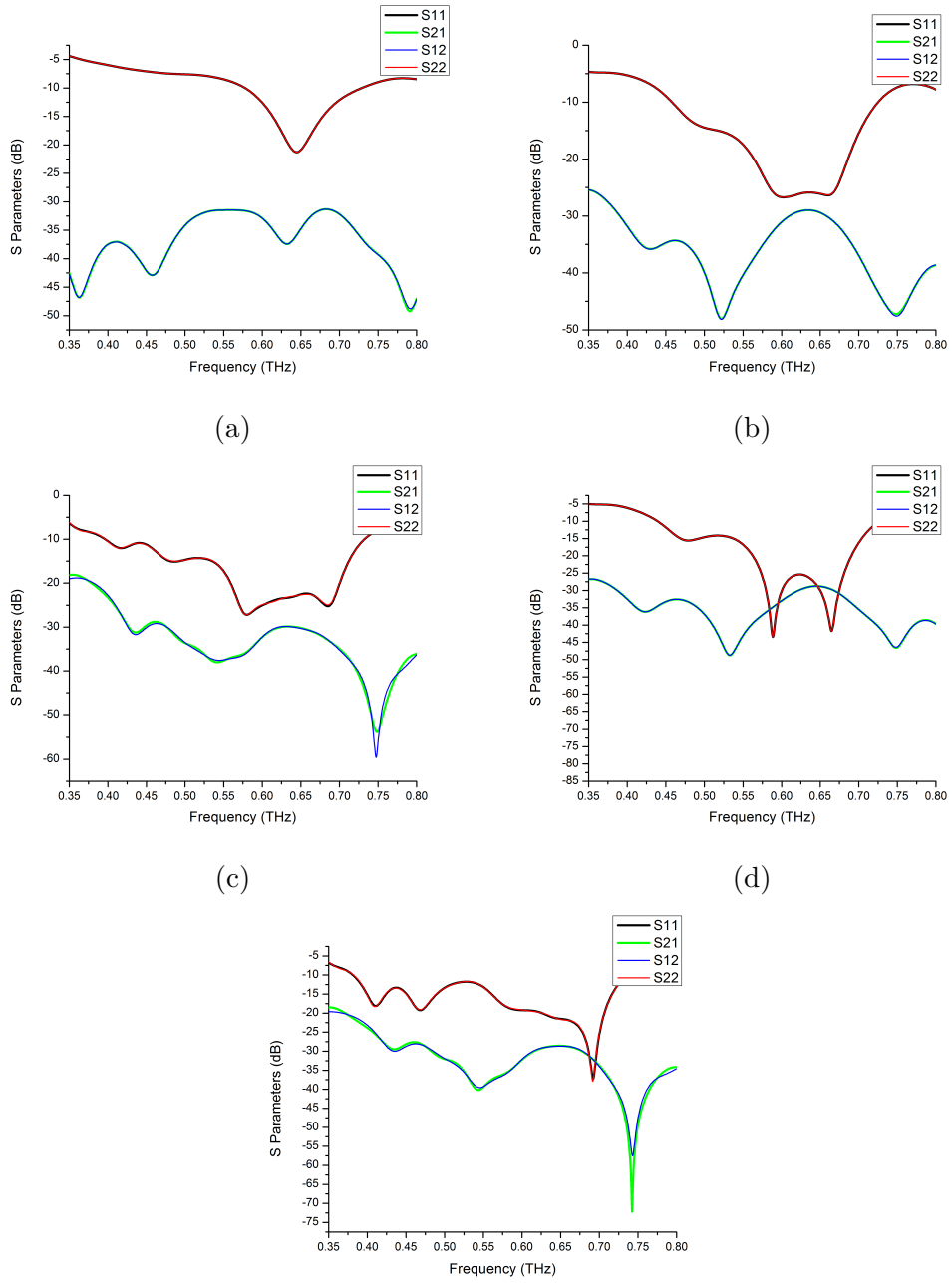

Figure 5.3: Return loss of the designed MIMO antennas based on (a) homogenous, (b) PBG for $\mu_c = 0$, (c) PBG for $\mu_c = 1$, (d) optimized PBG for $\mu_c = 0$ and (e) optimized PBG for $\mu_c = 1$

on homogeneous substrate. Moreover, the introduction of the small sized graphene load has widened the bandwidth which is an important factor for high data rates transmission.

In Figure 5.4, the gains variation with respect to frequency are plotted for the

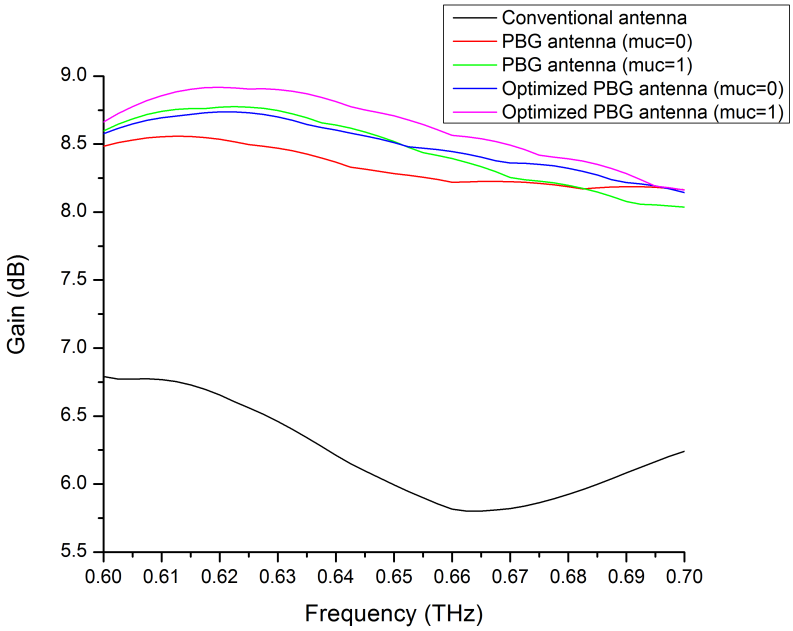

Figure 5.4: Gain versus frequency of the designed MIMO antennas.

different MIMO antennas. It is clearly seen the gain enhancement due to the suppression of surface waves by the photonic crystal substrate compared to Antenna 1, conventional antenna, which is based on homogeneous substrate. Also, the gain is slightly improved when graphene load operates in low resistance mode for both Antennas 2 and 3. The maximum achievable gains around $0.65THz$ are $6.7, 8.55, 8.77, 8.73$, and $8.92dB$ for Antenna 1, Antenna 2 as μ_c being 0, Antenna 2 as μ_c being 1, Antenna 3 as μ_c being 0, and Antenna 3 as μ_c being 1.

The radiation patterns of the MIMO antennas are shown in Figure 5.5. According to Figure 5.5.a and Figure 5.5.b, the directivity of MIMO Antenna 1 reaches its maximum at incidence angle theta of 70° and $-70°$ for port 1 and port 2, respectively at $0.6THz$ where each port is fed separately. However, the direction of maximum radiation is shifted (tilted) to be 50° and $-50°$ according to port 1 and port 2, respectively for MIMO Antenna 2 and 3 at $0.62THz$. It is also remarked the slightly ameliorated radiation as the chemical potential being 1, which corresponds to the low resistive mode of graphene load. The main lobe beam width for MIMO Antennas 1, 2 as $\mu_c = 0$, 2 as $\mu_c = 1$, 3 as $\mu_c = 0$ and 3 as $\mu_c = 1$ are $69.0°, 73.0°, 69.2°, 72.4°$ and $68.6°$.The 2D far field radiation pattern of MIMO

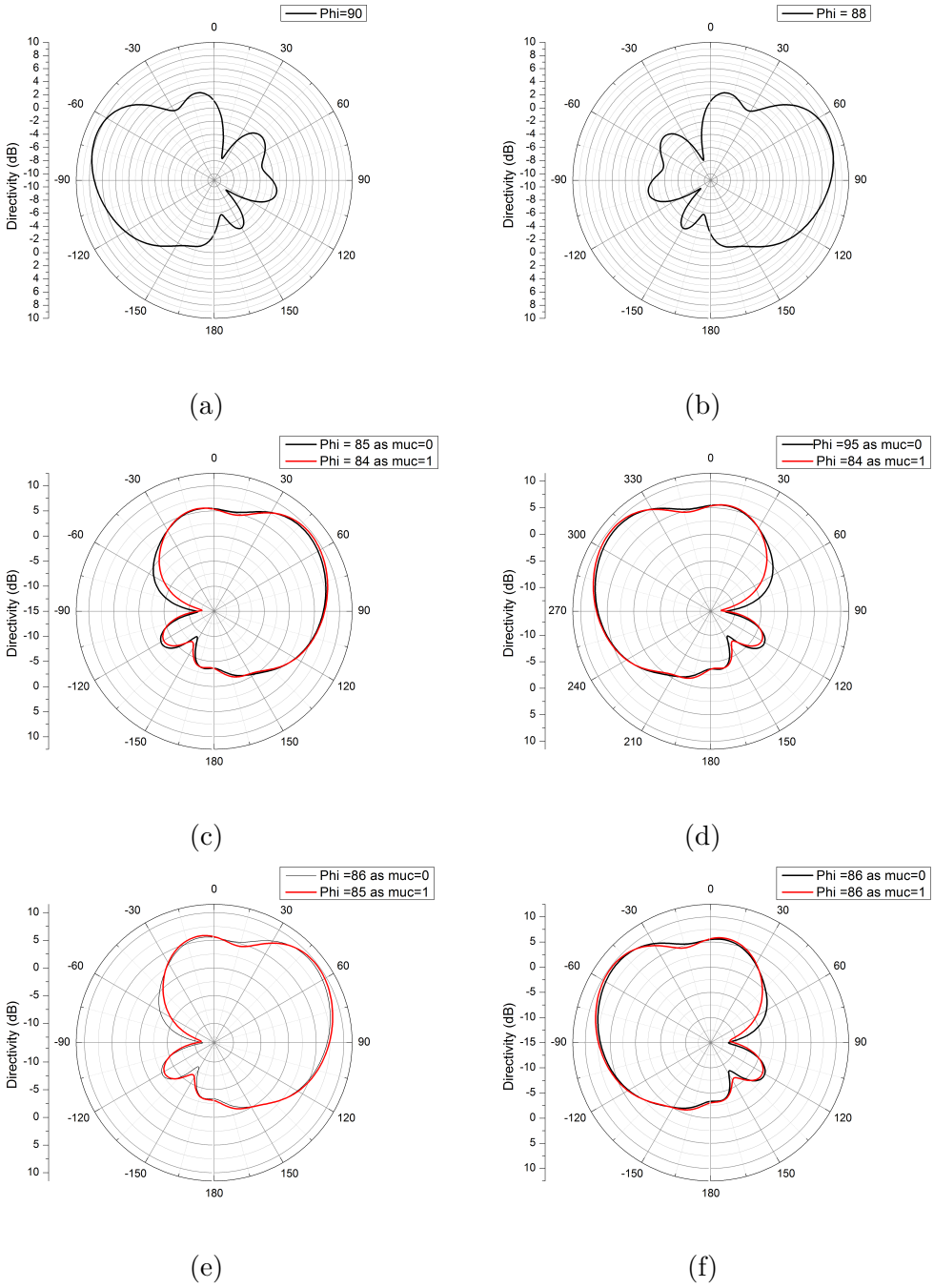

Figure 5.5: Far field radiation pattern of the designed MIMO antennas (a) Antenna 1 for port 1, (b) Antenna 1 for port 2 , (c) Antenna 2 for port 1, (d) Antenna 2 for port 2, (e) Antenna 3 for port 1 and (f) Antenna 3 for port 2

Antenna 3 is shown in Figure 5.6.

Furthermore, the dimension for the graphene chemical potential μc of 0.3, 0.7 and 1.3 ev is investigated. The presented results in Figure 5.7 indeed confirm the previously stated conclusions; the introduced graphene chemical potential enhances

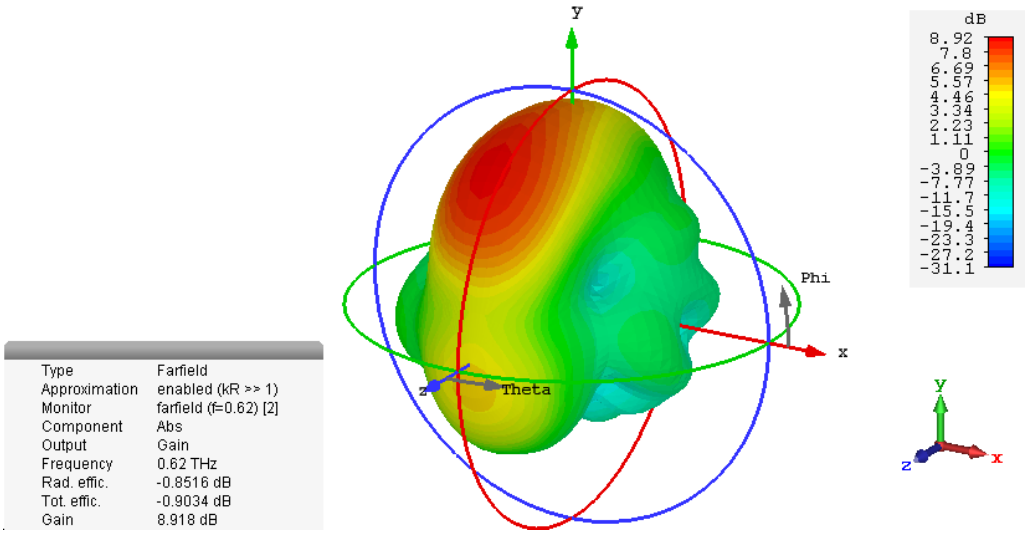

Figure 5.6: 2D far field radiation pattern of MIMO Antenna 3

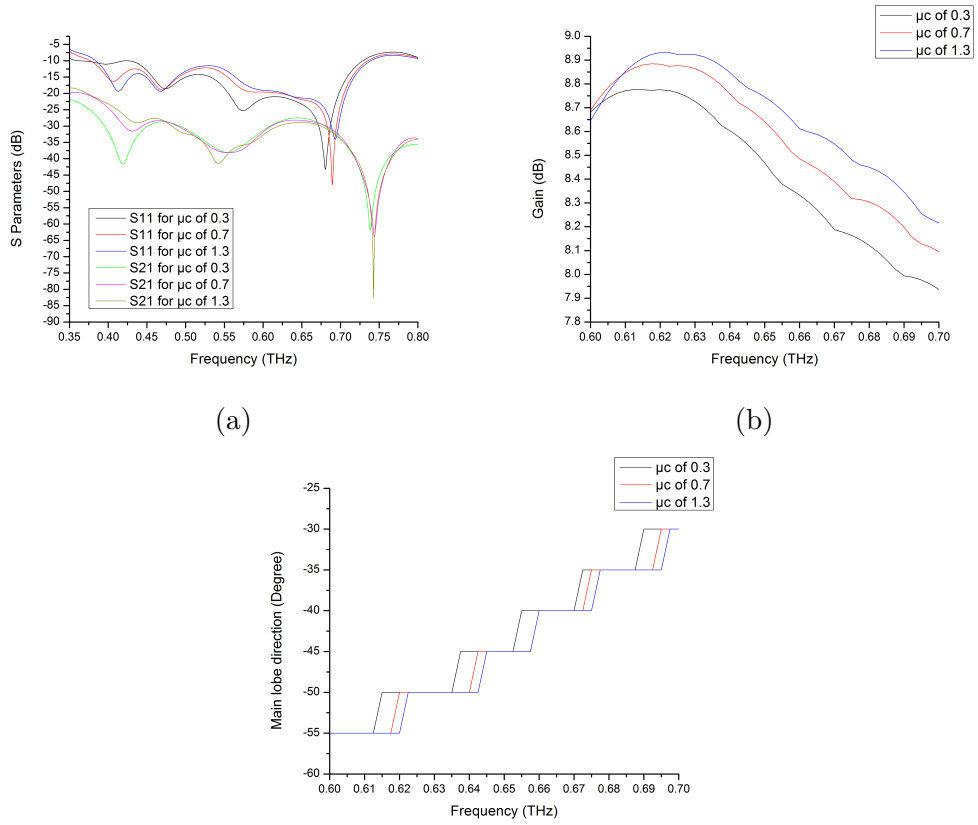

(a) (b)

(c)

Figure 5.7: Performance of the designed MIMO antenna based on optimized PBG for muc=0.3, 0.7, 1.3 (a) the Scattering parameters (b) Gain versus frequency (c) Main lobe direction

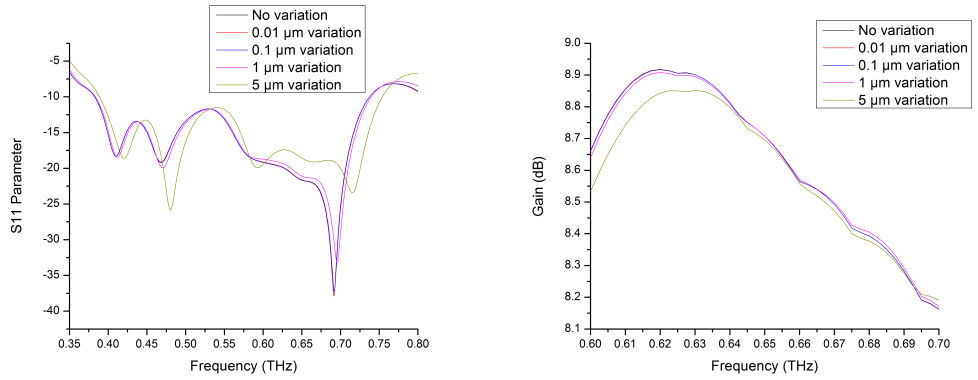

(a) (b)

Figure 5.8: Performance of the designed MIMO antenna based on optimized PBG for different hole radii variations (a) Reflection coefficient (b) Gain versus frequency

the bandwidth and the gain. Besides, the main lobe direction curve with respect to frequency is shifted forward with the increase in graphene chemical potential.

Although the hole radii of the MIMO antenna based on optimized PBG are with a precision on the second digit, i.e. 10 nm, the fabrication tolerance is in the scale of micrometers according to Figure 5.8 which presents the scattering parameters and the gain versus frequency of the presented MIMO antenna based on optimized PBG. By varying the holes radii by $0.01, 0.1, 1$ and $5\mu m$, similar results are obtained with several micrometers as a threshold where a considerable deterioration in the performance is noticed.

5.4 MIMO system design

The terahertz channel has been studied by several researchers and gains their interests due to the promising features it offers after banishing its main challenge, which is the path loss. The losses in terahertz waves includes spreading loss and molecular absorption loss for line of sight communication systems. However, when there is no direct path, which is the common situation for T rays, a fading exists and an introduced extra loss is presented in such situation. The spreading loss, the molecular absorption loss and the reflection loss formulas are defined as [182]:

$$A_{spread}(f,d) = 20log\left(\frac{4\pi fd}{c}\right) \tag{5.4}$$

$$A_{abs} = k(f)d10log_{10}e \tag{5.5}$$

where A_{spread} is the spread loss in dB, d is the travelled distance, c is the light speed and f is the operating frequency; the molecular absorption loss A_{abs} is related to the medium absorption coefficient $K(f)$ for the different existing gases in air. In spite of that, the absorption loss includes windows where the loss is very small and can be ignored. One of these windows is around $0.65THz$ as the operating frequency of the presented MIMO antennas in previous section. Besides, the reflection loss A_{ref} which is due to the collision of waves with the indoor rough surfaces as terahertz wavelengths are comparable with indoor surfaces. In this work, the scenario shown

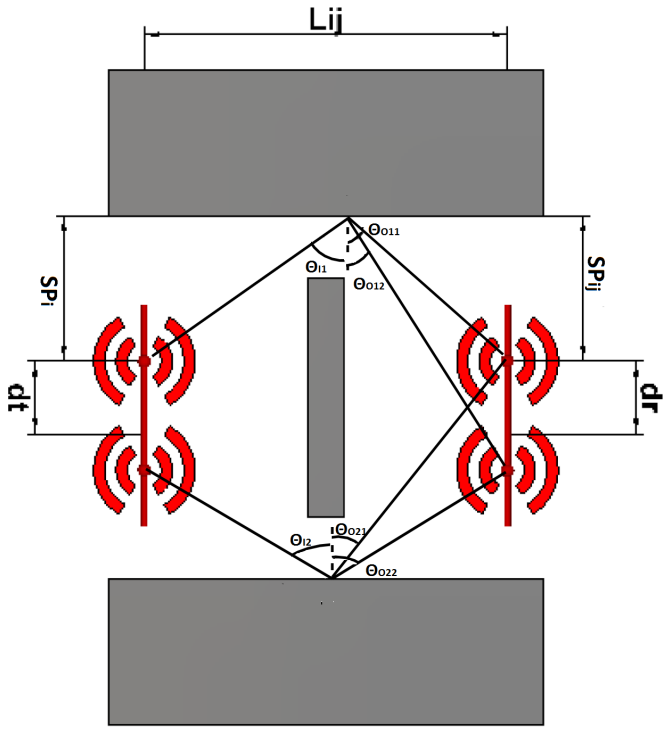

Figure 5.9: A scenario of MIMO system model for three MIMO antennas.

in Figure 5.9 is considered due to the fact that moving objects in real word are quite slow compared to terahertz waves. Thus, it is safely assumed that the moving object to be static between the transmitters and receivers. Therefore, it prohibits line of sight communications and allows fadings. According to the scenario of Figure 5.9, Sp_i is the distance between the transmitter and the corresponding indoor wall, Sp_{ij} is the distance between the receiver j and indoor wall i, L_{ij} is the horizontal distance between transmitters and receivers, d_t and d_r are the spacing between

transmitters and between receivers, respectively. Different system configurations are studied including SISO (1×1), MISO (2×1), SIMO (1×2) and MIMO (2×2). In addition to the mentioned losses, there is also the loss of wave's collision with the indoor surfaces. Theses variations in the surfaces are in the range of several hundred of microns. Thus, the wavelength of the radiated waves in terahertz frequencies is comparable with the roughness of the indoor surfaces [182]. The roughness factor ρ is approximately as follows [181]:

$$\rho = e^{-\frac{g}{2}} \tag{5.6}$$

$$g = \left(\frac{2\pi\Delta(cos(\Theta_I) + cos(\Theta_O)}{\lambda} \right)^2 \tag{5.7}$$

where the surface deviation coefficient Δ is set to $88\mu m$ [179] for plaster indoor walls, λ is the wavelength, g is the surface variation intensity and the angle of incidence Θ_I and refection Θ_O are expressed as follows for the presented scenario in Figure 5.9:

$$Sp_i tan(\Theta_{Ii}) + Sp_{ij} tan(\Theta_{Oij}) = Lij \tag{5.8}$$

In this part, as the system is considered with M transmit antennas and N receive antennas, the time invariant channel can be modeled as an $M \times N$ gain matrix H as follows:

$$y = Hx + w \tag{5.9}$$

Where x and y are transmit and receive signals, respectively and w is the white Gaussian noise. The gain matrix elements, the gain h_{ij} between the i_{th} transmitter and the j_{th} receiver, can be computed based on the following formula [202]:

$$h_{ij} = -A_{spread} - A_{abs} + \rho + G_T + G_R \tag{5.10}$$

Where G_t is the transmitter gain and G_r is the gain of the receiver at the angle of incidence Θ_I and the angle of reflection Θ_O, respectively. The aforementioned angles with the travelling distance in the presented scenario are calculated by using

the following formulas [182]:

$$\frac{Sp_i}{cos(\Theta_I)} + \frac{Sp_{ij}}{cos(\Theta_O)} = d_{ij} \tag{5.11}$$

After that, the capacity can be calculated by maintaining the singular values λ_i of the gain matrix H as follows [182]:

$$C = \sum_{i=1}^{n_{min}} log_2 \left(1 + \frac{P_i \lambda_i^2}{N_0}\right) b/s/Hz \tag{5.12}$$

Where N_0 is the noise power spectral density, P_i is the transmitted power from the i_{th} MIMO antenna and n_{min} is the rank of the gain matrix H.

To investigate the degree of mutual coupling, several simulations have been performed by using two MIMO antennas based on optimized PBG with distinct spacing distances d_t of $3000, 6000$, and $10000\mu m$ between them. Figure 5.10 presents differ-

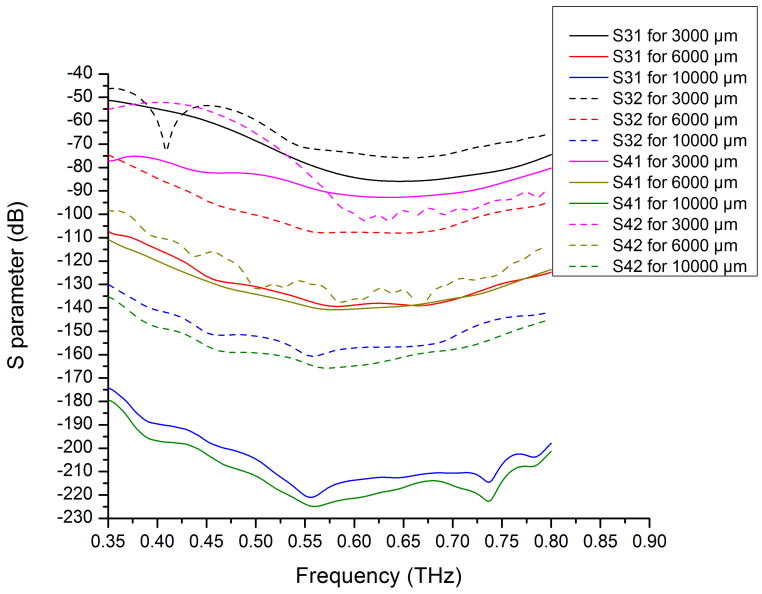

Figure 5.10: Degree of mutual coupling between the ports of two MIMO antennas based on optimized PBG for different spacing distances.

ent transmission coefficients between port 3 and 4 of Antenna 2 with ports 1 and 2 of Antenna 1. The results show a quite reduced level of coupling as the spacing distance is increased. Concerning the condition number, which indicates how well channel matrix is conditioned, practical results are obtained as $dt > 0.05m$ with

18.10 dB for $0.1m$ and very good performance as the spacing $dt > 0.2m$ with 9.92 dB for $0.2m$ and 7.84 dB for $0.3m$. However, by sweeping the distance parameter d_r through $0.1, 0.6$, and $1.2m$, the condition number is $86.87, 86.22$, and $85.68dB$ respectively. Furthermore, as the distance lij is varied between $1, 2.5$, and $4m$, the maintained condition numbers are $97.78, 87.72$, and 96.17 dB with the minimum being 85.54 dB for $1.5m$.

For the first system configuration, a single transmitter with a single receiver are employed, 1×1 system, where $Sp_1 = 1m$, $Sp_{11} = 1m$, and $l_{ij} = 2m$. The spreading loss, reflection loss and total loss versus the incidence angle of transmission are shown in Figure 5.11. It is clearly seen the best incidence angle, where the loss is minimum, is at 45° with $37.32, 11.34$ and $48.66dB$ for the spreading loss, reflection loss and total loss, respectively.

After computing the different losses and employing the 2D radiation pattern of

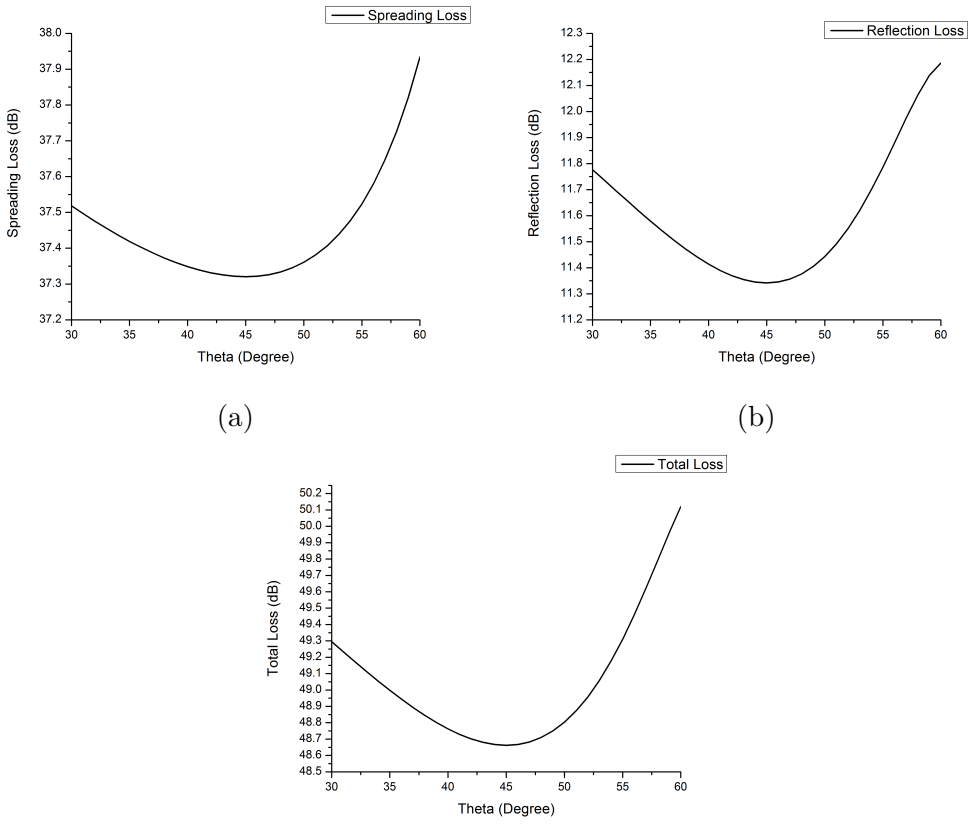

Figure 5.11: path loss of (1×1) configuration, namely spread loss, reflection loss, and total loss

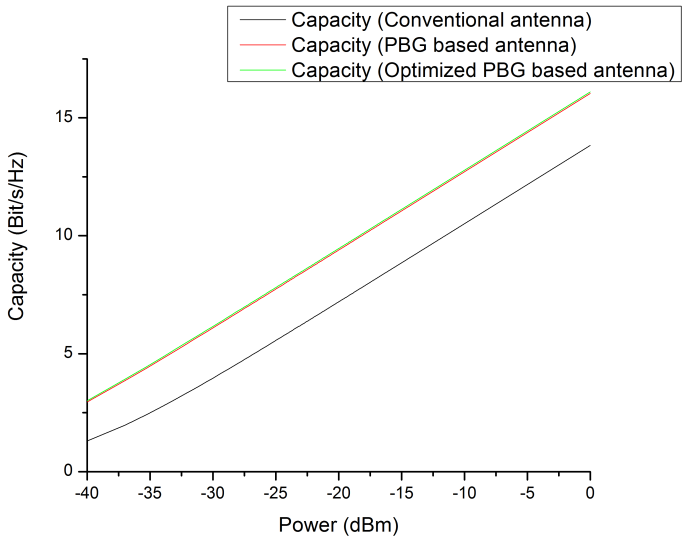

Figure 5.12: Capacity of the designed MIMO (1×1) configuration.

the presented MIMO antennas, namely Antenna 1 based on homogeneous substrate, Antennas 2 and 3 based on photonic crystal substrate, the capacity (c) is calculated for SISO system. The results are shown in Figure 5.12 where the enhancement in the performance is clearly seen when PCs are employed in Antennas 3 and 2 of 16.1 and $16.03 bit/s/Hz$, respectively compared to $13.83 bit/s/Hz$ for MIMO Antenna 1.

For MISO system, two transmitters and a single receiver are utilized, namely 2×1 configuration, where $Sp_1 = 1m$, $d_t = 0.1mm$, $Sp_{11} = 1m$, and $l_{ij} = 2m$. The spreading loss, reflection loss and total loss versus the incidence angle of transmission are shown in Figure 5.13. It is clearly seen the best incidence angle, where the loss is minimum, is also at 45° with $37.32, 11.34$ and $48.66 dB$ for the spreading loss, reflection loss and total loss, respectively.

After computing the gain matrix for each antenna from the presented MIMO antennas, the capacity is calculated for MISO system. The results are shown in Figure 5.14 where the enhancement in the performance is clearly seen when PCs are employed of 17.10 and $17.03 bit/s/Hz$ compared to $14.83 bit/s/Hz$ for MIMO Antenna 1 and slight overall improvement is noticed due to MISO configuration. For SIMO system, a single transmitter and double receivers are utilized, namely 1×2 configuration, where $Sp_1 = 1m, Sp_{11} = 0.75m, d_r = 0.5m$ and $l_{ij} = 2m$. The spreading loss, reflection loss and total loss versus the incidence angle of transmis-

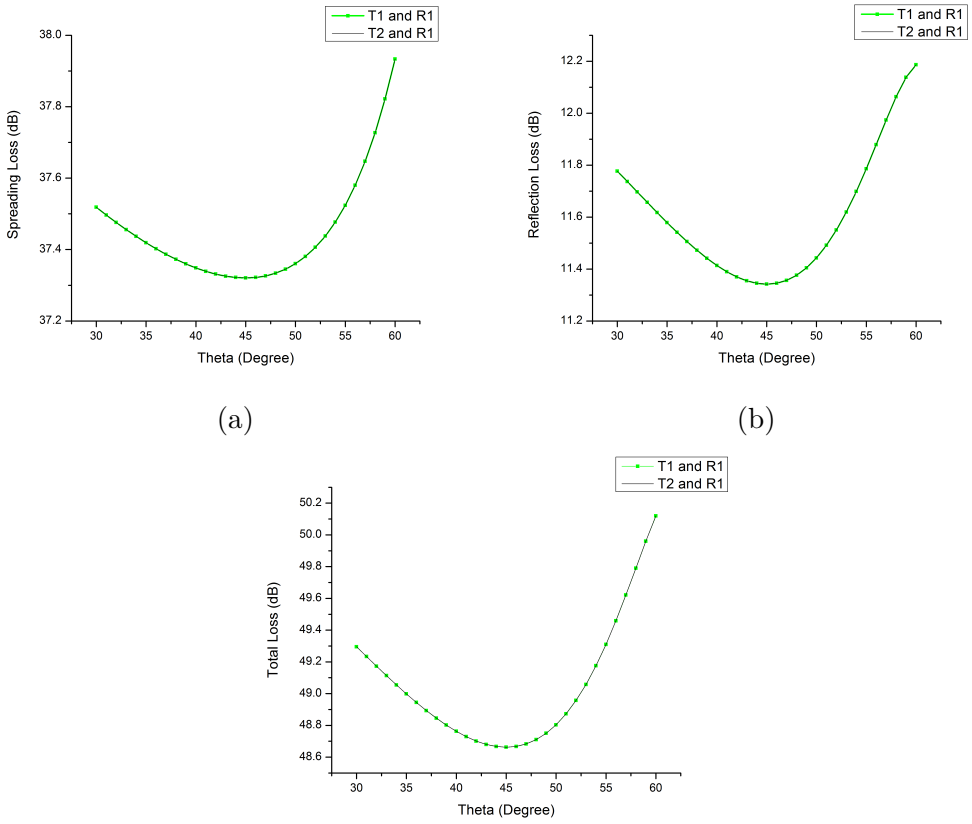

Figure 5.13: path loss of (2×1) configuration, namely spread loss, reflection loss, and total loss

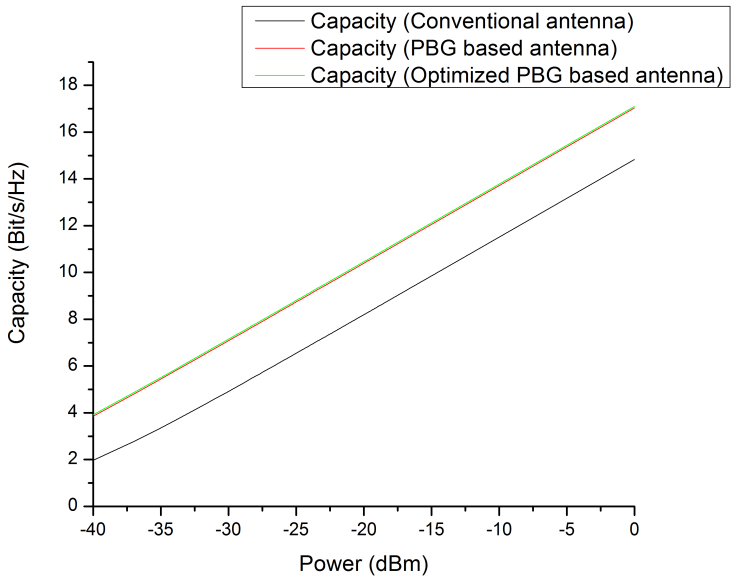

Figure 5.14: Capacity of the designed MIMO (2×1) configuration.

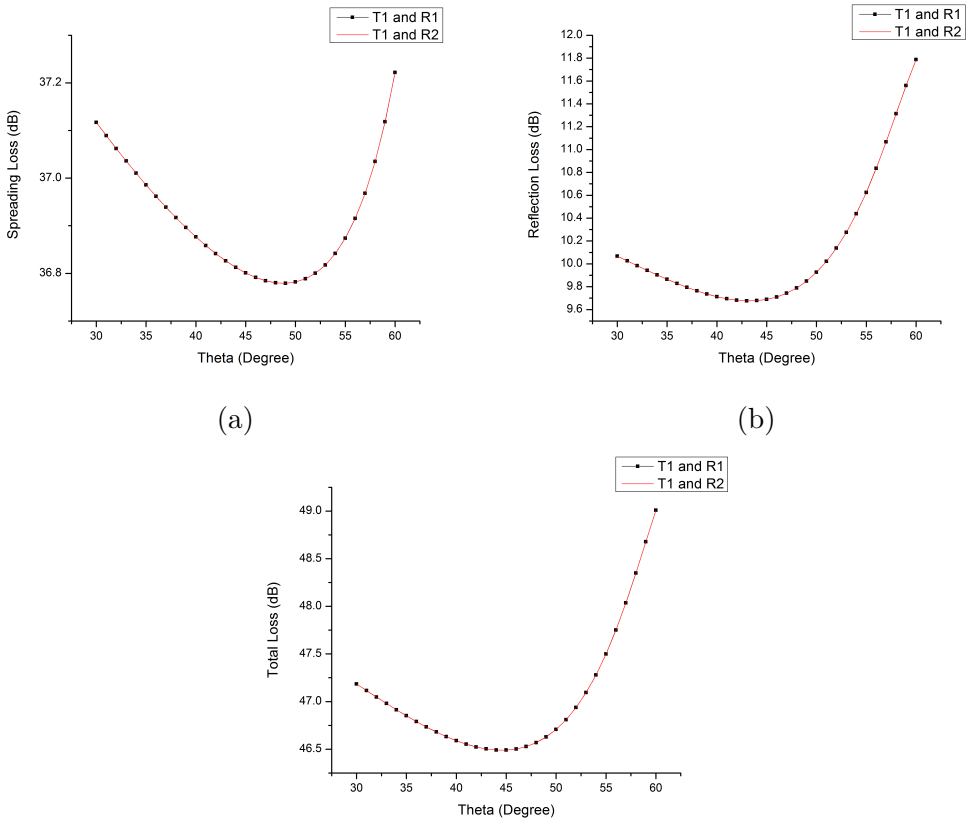

Figure 5.15: path loss of (1×2) configuration, namely spread loss, reflection loss, and total loss

sion are shown in Figure 5.15. It is clearly seen the best incidence angle, where the loss is minimum, is located around 45° with $36.77, 9.67$ and $46.48dB$ for the spreading loss, reflection loss and total loss, respectively. The capacity is calculated for SIMO system. The results are shown in Figure 5.16 where the improvement in the performance is clearly seen when PCs are employed of 18.21 and $17.80bit/s/Hz$ compared to $16.06bit/s/Hz$ for MIMO Antenna 1.

For MIMO system, two transmitters and two receivers are employed, namely 2×2 configuration, where $Sp_1 = 1m, d_t = 0.1mm, Sp_{11} = 0.75m, d_r = 0.5m$ and $l_{ij} = 2m$. The spreading loss, reflection loss and total loss versus the incidence angle of transmission are shown in Figure 5.17. It is clearly seen the best incidence angle, where the loss is minimum, is also around 47° with $36.77, 9.68$ and $46.48dB$ for the spreading loss, reflection loss and total loss, respectively.

The capacity is calculated for MIMO (2×2) system configuration. The results

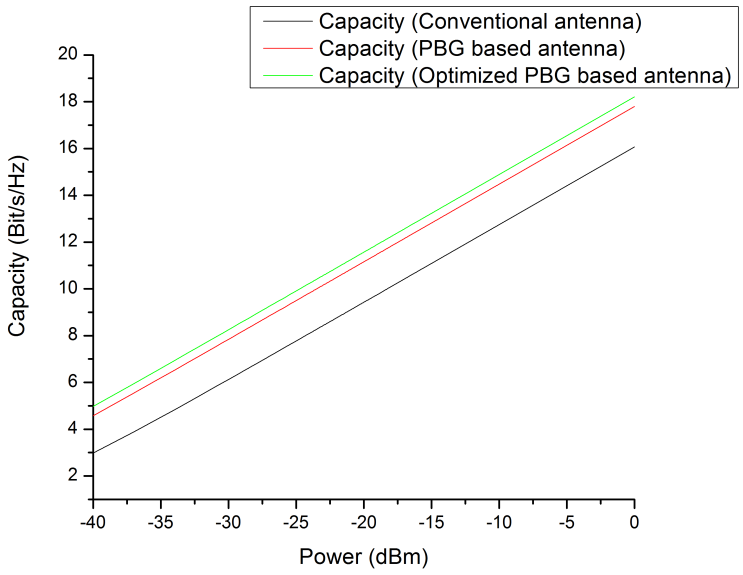

Figure 5.16: Capacity of the designed MIMO (1×2) configuration.

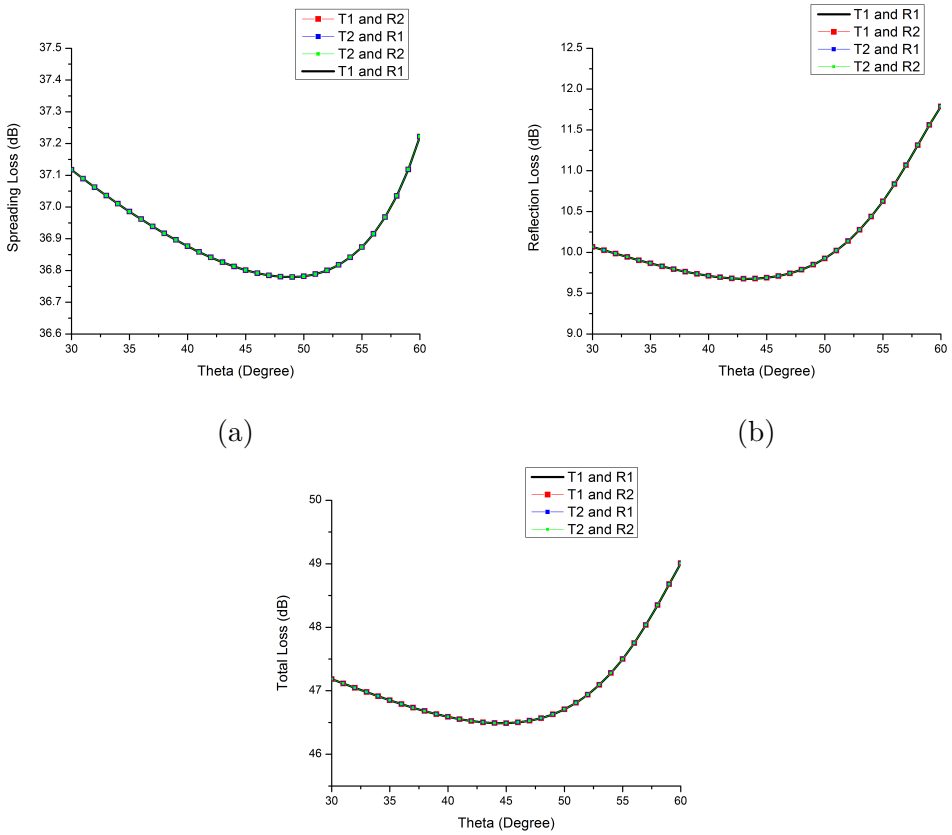

Figure 5.17: path loss of (2×2) configuration, namely spread loss, reflection loss, and total loss

are shown in Figure 5.18 where the enhancement in the performance is clearly seen when PCs are employed of 17.91 and 17.8$bit/s/Hz$ compared to 16.06$bit/s/Hz$ for MIMO Antenna 1. An overall improvement is noticed due to MIMO configuration.

Moreover, the impact of the distance between the receiving antennas in 2×2 MIMO system is studied by sweeping d_r from $0.1m$ to $1.2m$. The total loss versus

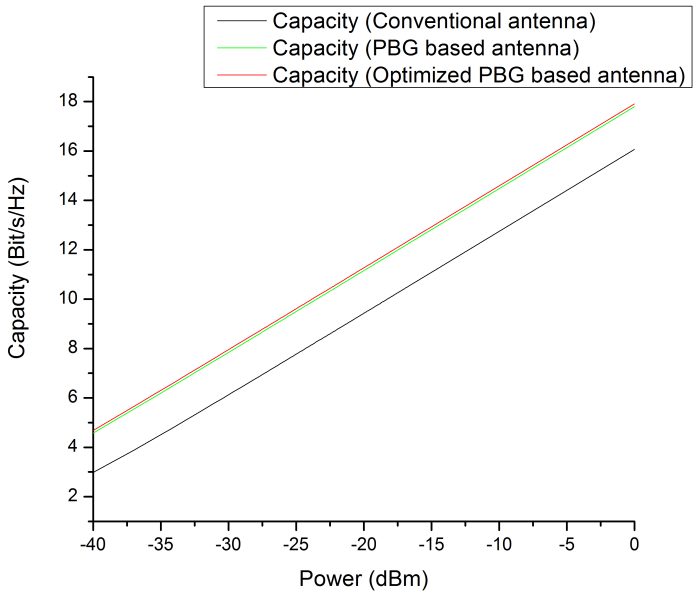

Figure 5.18: Capacity of the designed MIMO (2×2) configuration.

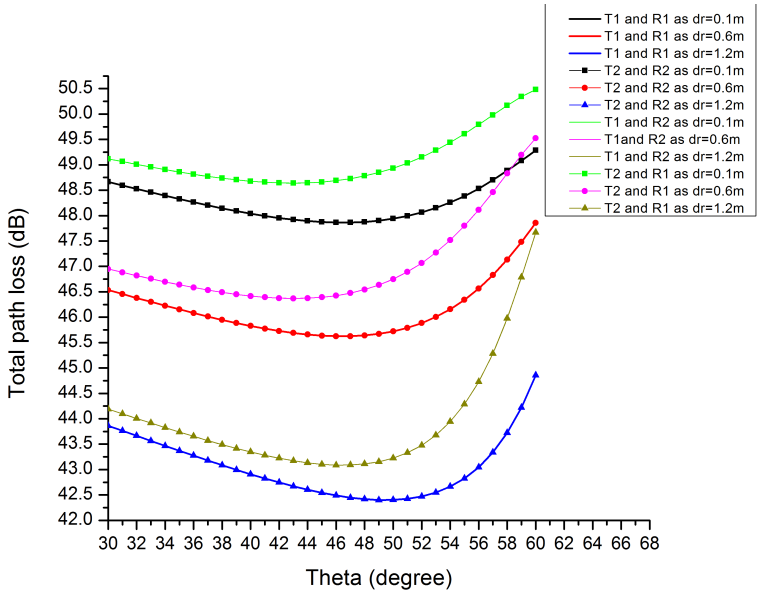

Figure 5.19: Total path loss of (2×2) configuration for different receiver's spacing.

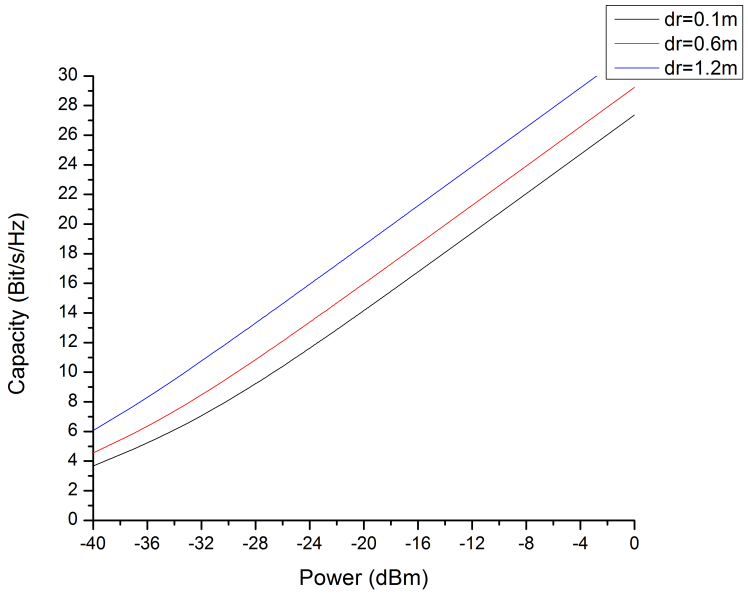

Figure 5.20: Capacity of the designed MIMO (2×2) configuration for different receiver's spacing.

the incidence angle of transmission is shown in Figure 5.19 between each transmit antenna and receive antenna within the system. It is also noticed the conformance between several paths due to symmetry in the scenario such as the total path loss between transmit Antenna 1 and receive Antenna 1 with transmit Antenna 2 and receive Antenna 2. The results in Figure 5.19 reveals that the total loss is reduced by increasing the spacing between the receivers due to the added diversity scheme with a slight increase in the best incident angle of transmission. The capacity is calculated and presented in Figure 5.20, the achieved capacities are $31.85, 29.21$ and $27.37 bit/s/Hz$ at the $0 dBm$ transmission power using MIMO Antenna 3.

Furthermore, the effect of the distance between the transmit antennas in 2×2 MIMO system using MIMO Antenna 3 is studied by sweeping d_t from $0.1m$ to $0.3m$. The total loss versus the incidence angle of transmission is shown in Figure 5.21 for every transmit antenna and receive antenna. It is also obtained the coincidence between different paths due to symmetry scheme in the scenario. The results in Figure 5.21 affirm that the total loss is reduced by increasing the spacing between the transmitters also due to the added diversity scheme. A slight increase in the best incident angle of transmission is noticed. The capacity is calculated and presented in Figure 5.22, the obtained capacities are $31.5, 30.77$ and $28.86 bit/s/Hz$ at the trans-

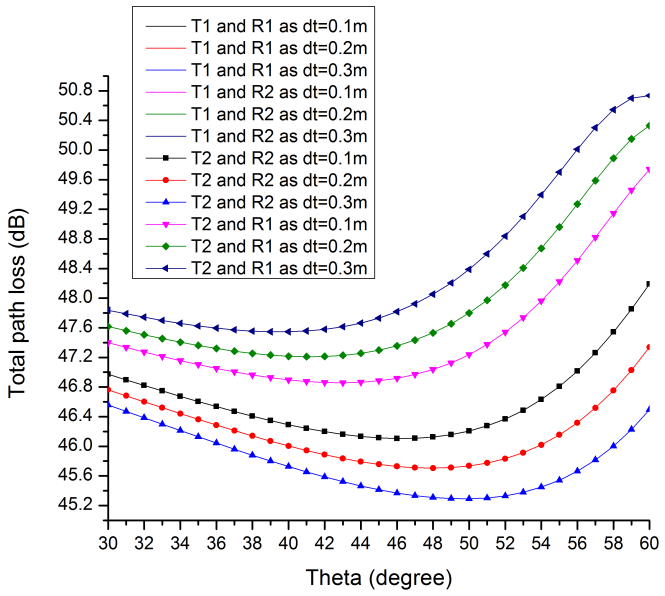

Figure 5.21: Total path loss of (2×2) configuration for different transmitter's spacing.

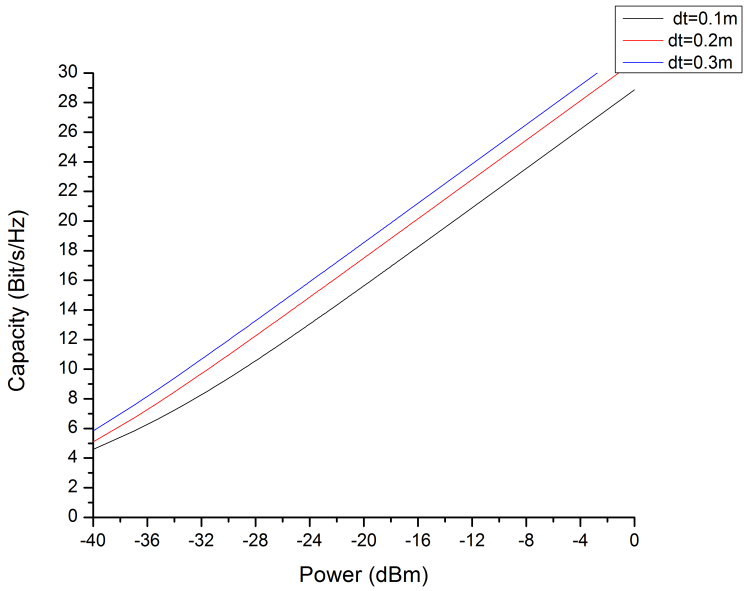

Figure 5.22: Capacity of the designed MIMO (2×2) configuration for different transmitter's spacing.

mission power of $0dBm$. Finally, the impact of the horizontal distance between the transmit antennas and the receive antennas using MIMO Antenna 3 is studied by sweeping l_{ij} through $1, 2.5$, and $4m$. The total loss versus the incidence angle of transmission is shown in Figure 5.23 between transmitters and receivers. It is also maintained the similarity between different paths due to the symmetry scheme.

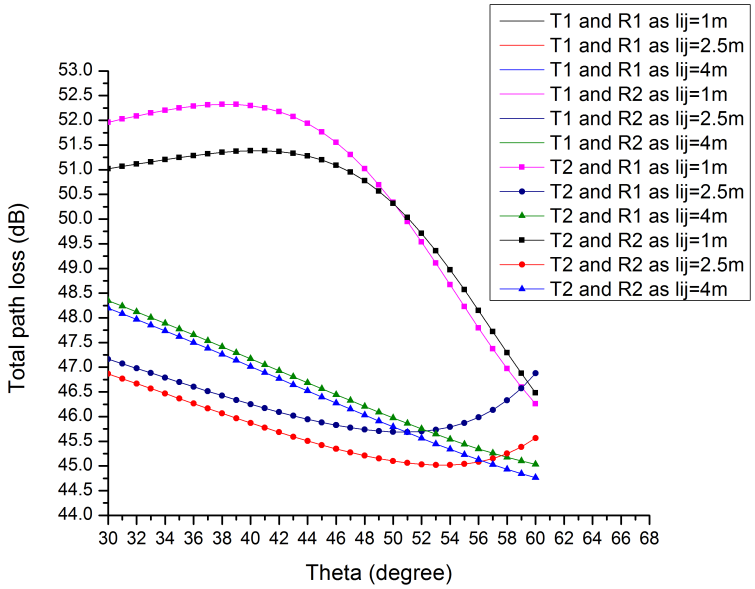

Figure 5.23: Total path loss of (2×2) configuration for different lij distances.

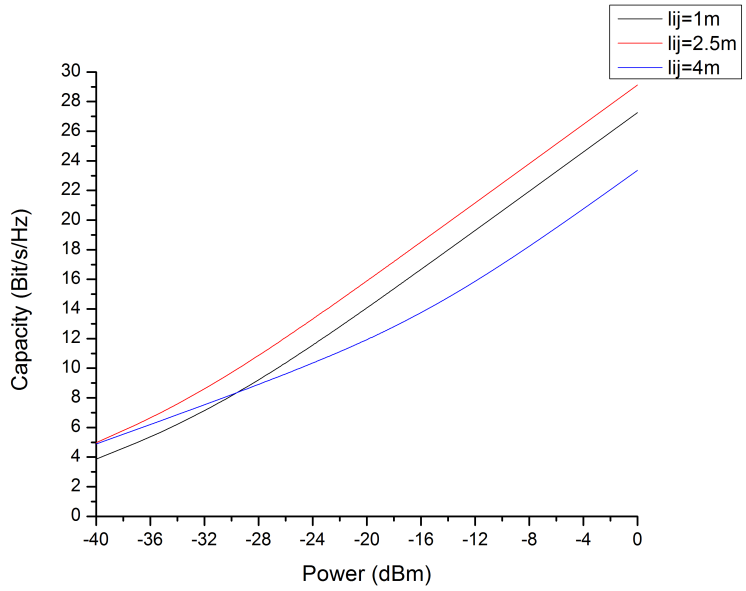

Figure 5.24: Capacity of the designed MIMO (2×2) configuration for different lij distances.

The results in Figure 5.23 confirm that the total loss can be smaller in a scenario where the horizontal distance is larger with some ceiling. A slight increase in the best incident angle of transmission is also noticed. The capacity is calculated and it is shown in Figure 5.24, the achieved capacities at the transmission power of $0dBm$ are $29.10, 27.25$ and $23.36bit/s/Hz$. The achieved maximum capacity with trans-

mit power of $0dBm$ for the presented scenario is $18.21bit/s/Hz$ and $17.91bit/s/Hz$ compared to a capacity around $11.5bit/s/Hz$ in [182] for the same scenario of 2×2 MIMO terahertz indoor communication system. The aforementioned capacities can be improved further by manipulating the studied spacings and distances.

5.5 Summary

A novel MIMO antennas based on homogeneous and Photonic Band Gap PBG substrates with graphene load and fed by two different ports are designed and analyzed for MIMO terahertz communications. The radiation pattern of the antennas exhibits a symmetrical pattern for port 1 and port 2 which is exploited in a challenging scenario within terahertz communication. Besides, the results reveal in a noticeable enhancement in the bandwidth as it reaches $356GHz$ with the achieved gain of $8.92dB$. The MIMO system scenario is studied using different configurations including SISO, MISO, SIMO, and MIMO. The results have revealed that the proposed MIMO system (2×2) with antennas based on the optimized photonic crystal substrate has the highest capacity and the lowest total loss where the capacity of $18.21bit/s/Hz$ is established with a remarkable enhancement of 58.35% compared with literature. Furthermore, a conducted study is performed concerning the effect of the spacing between transmit antennas, receive antennas, and the horizontal distance between transmit and receive antennas.

Chapter 6

General Conclusion

6.1 Conclusion

In this thesis, a terahertz antenna technology literature review is provided with its probable impacts and key features and obstacles. The terahertz channel is then explored and its additional benefits are contrasted to its neighboring bands. Besides, several cutting-edge terahertz technologies are presented in the fields of revolutionary wireless communication systems, biology, farming, defense, and security. A survey on terahertz components was then presented starting from terahertz sources and detectors to the need for planar antennas such as microstrip antennas and some developments and amelioration techniques were discussed. Then, the researcher provided an outline of the photonic crystal and simulation utilizing the CST microwave studio simulator. The photonic crystal structure is formed for exhibiting the band gap at $0.6THz$ separately using direct transmission method. Then, it is employed to boost microstrip antennas performance, while a small atmospheric attenuation gap enables extra efficiency for wireless communications systems. Simulated data for this antenna show that the photonic crystal substrate effectively enhances the directivity of the conventional antenna on the desired frequency range.

A technique based on a hybrid Binary Particle Swarm Optimization (BPSO) algorithm with a CST studio simulator has been used to enhance microstrip patch antennas based on a synthesized photonic crystal substrate. A study of air cylinders embedded in a thick silicon substrate with high permittivity is used to build the ini-

tial antenna. PBG substrate, nevertheless, may be more beneficial when the CST microwave studio has been combined with BPSO because it has proved useful for synthesizing a splendid built photonic crystal substrate for the terahertz microstrip antenna with the desired features according to its potential usage. In fact, Antenna 2 has been found to be appropriate for dual-band employment around 0.65 THz and 0.6 THz with a return loss enhancement of 5.39% compared with the initial Antenna 1. In comparison, it has dramatically enhanced the fractional bandwidth for the patch antenna, based on the synthesized photonic crystal substrate, Antenna 3, by 128% relative to the original antenna (Antenna 1). Their bandwidth is substantially increased. Furthermore, both optimization results decrease side lobes levels. The improved antenna features are attributed to the introduced photonic crystal substrates. The antennas have resonance around $0.65THz$, which are the request for the next wireless networking technologies.

A variety of microstrip terahertz patch antennas are built and studied upon an engineered photonic crystal substrate. First of all, the antenna is designed based on a photonic crystal substrate in order to increase its efficiency by blocking the unnecessary surface wave. The analysis of simulated photonic crystal substrates demonstrates that the characteristics of the classic microstrip antenna in this frequency band are effectively enhanced. Furthermore, many other antennas, that have been studied based on a modified photonic crystal structure, will result in substantial and beneficial incremental changes to antenna return loss, bandwidth, gain and radiation efficiency that would produce significant enhancements as high as $279\%, +64.29\%, 50.41\%$ and 15.1%, respectively.

Finally, a novel MIMO antenna is developed and analyzed for MIMO terahertz indoor communications fed by two separate ports on the basis of homogeneous and photonic crystal substrates with a small graphene load. The antennas provide a symmetrical pattern of radiation for port 1 and port 2, which is employed inside indoor terahertz communication in a challenging situation. Various schemes like SISO, MISO, SIMO, and MIMO are being utilized with the MIMO system scenario. These findings demonstrated the highest spectral efficiency of the proposed MIMO (2×2) device with antennas based on an enhanced photonic crystal. Furthermore, a study

is conducted on the influence of the space between transmitting antennas, receiving antennas, and transmit-receive antennas, horizontally, with respect to spectral efficiency and channel condition number.

6.2 Suggestions

During research progresses, some interesting suggestions and extensions of this thesis can be outlined as follows for the future:

- Application of terahertz microstrip antenna on different communication scenarios
- Design of terahertz array antennas based on PCs.
- Design of new photonic crystal structures that further enhances antenna features and system performance.
- Design of new terahertz antennas based on PCs with graphene.

Bibliography

[1] A. Redo-Sanchez and X.-C. Zhang, "Terahertz science and technology trends," *IEEE Journal of Selected topics in quantum electronics*, vol. 14, no. 2, pp. 260–269, 2008.

[2] W. L. Chan, J. Deibel, and D. M. Mittleman, "Imaging with terahertz radiation," *Reports on progress in physics*, vol. 70, no. 8, p. 1325, 2007.

[3] M. Tonouchi, "Cutting-edge terahertz technology," *Nature photonics*, vol. 1, no. 2, p. 97, 2007.

[4] V. Bratman, M. Glyavin, T. Idehara, Y. Kalynov, A. Luchinin, V. Manuilov, S. Mitsudo, I. Ogawa, T. Saito, Y. Tatematsu *et al.*, "Review of subterahertz and terahertz gyrodevices at iap ras and fir fu," *IEEE Transactions on Plasma Science*, vol. 37, no. 1, pp. 36–43, 2008.

[5] J. A. Zeitler and L. F. Gladden, "In-vitro tomography and non-destructive imaging at depth of pharmaceutical solid dosage forms," *European Journal of Pharmaceutics and Biopharmaceutics*, vol. 71, no. 1, pp. 2–22, 2009.

[6] P. H. Siegel, "Terahertz technology in biology and medicine," *IEEE transactions on microwave theory and techniques*, vol. 52, no. 10, pp. 2438–2447, 2004.

[7] R. Appleby and H. B. Wallace, "Standoff detection of weapons and contraband in the 100 ghz to 1 thz region," *IEEE transactions on antennas and propagation*, vol. 55, no. 11, pp. 2944–2956, 2007.

[8] J. Yinon, *Counterterrorist detection techniques of explosives*. Elsevier, 2011.

[9] Y. L. Hor, J. F. Federici, and R. L. Wample, "Nondestructive evaluation of cork enclosures using terahertz/millimeter wave spectroscopy and imaging," *Applied Optics*, vol. 47, no. 1, pp. 72–78, 2008.

[10] C.-H. Chen, *Ultrasonic and advanced methods for nondestructive testing and material characterization*. World Scientific, 2007.

[11] K. R. Jha and G. Singh, "Terahertz planar antennas for future wireless communication: A technical review," *infrared physics & Technology*, vol. 60, pp. 71–80, 2013.

[12] M. N. E. Temmar, A. Hocini, D. Khedrouche, and M. Zamani, "Analysis and design of a terahertz microstrip antenna based on a synthesized photonic bandgap substrate using bpso," *Journal of Computational Electronics*, vol. 18, no. 1, pp. 231–240, 2019.

[13] A. Hocini, M. Temmar, D. Khedrouche, and M. Zamani, "Novel approach for the design and analysis of a terahertz microstrip patch antenna based on photonic crystals," *Photonics and Nanostructures - Fundamentals and Applications*, vol. 36, p. 100723, 2019.

[14] M. N. eddine Temmar, A. Hocini, D. Khedrouche, and T. A. Denidni, "Enhanced flexible terahertz microstrip antenna based on modified silicon-air photonic crystal," *Optik*, vol. 217, p. 164897, sep 2020.

[15] M. N. eddine Temmar, A. Hocini, and D. Khedrouche, "Design and analysis of terahertz microstrip circular patch antenna based on an optimized polyimide photonic crystal substrate." in *The Second International Conference on Electrical Engineering (ICEEB'2018)*, December 2018.

[16] ——, "Design and analysis of terahertz microstrip patch antenna based on optimized photonic crystal substrate," in *Third International Conference on Technological Advances in Electrical Engineering (ICTAEE'18)*, December 2018.

[17] M. N. E. Temmar, A. Hocini, D. Khedrouche, and T. A. Denidni, "Analysis and design of MIMO indoor communication system using terahertz patch antenna based on photonic crystal with graphene," *Photonics and Nanostructures - Fundamentals and Applications*, vol. 43, p. 100867, feb 2021.

[18] M. Koch, "Terahertz communications: A 2020 vision," in *Terahertz frequency detection and identification of materials and objects*. Springer, 2007, pp. 325–338.

[19] J. Laskar, S. Pinel, D. Dawn, S. Sarkar, B. Perumana, and P. Sen, "The next wireless wave is a millimeter wave," *Microwave Journal*, vol. 50, no. 8, p. 22, 2007.

[20] R. C. Daniels and R. W. Heath, "60 ghz wireless communications: Emerging requirements and design recommendations," *IEEE Vehicular technology magazine*, vol. 2, no. 3, pp. 41–50, 2007.

[21] R. C. Daniels, J. N. Murdock, T. S. Rappaport, and R. W. Heath, "60 ghz wireless: Up close and personal," *IEEE Microwave magazine*, vol. 11, no. 7, pp. 44–50, 2010.

[22] I. Frigyes, J. Bitó, B. Héder, and L. Csurgai-Horváth, "Applicability of the 50–90 ghz frequency bands in feeder networks," in *2009 3rd European Conference on Antennas and Propagation*. IEEE, 2009, pp. 336–340.

[23] S. S. Dhillon, M. S. Vitiello, E. H. Linfield, A. G. Davies, M. C. Hoffmann, J. Booske, C. Paoloni, M. Gensch, P. Weightman, G. P. Williams, E. Castro-Camus, D. R. S. Cumming, F. Simoens, I. Escorcia-Carranza, J. Grant, S. Lucyszyn, M. Kuwata-Gonokami, K. Konishi, M. Koch, C. A. Schmuttenmaer, T. L. Cocker, R. Huber, A. G. Markelz, Z. D. Taylor, V. P. Wallace, J. A. Zeitler, J. Sibik, T. M. Korter, B. Ellison, S. Rea, P. Goldsmith, K. B. Cooper, R. Appleby, D. Pardo, P. G. Huggard, V. Krozer, H. Shams, M. Fice, C. Renaud, A. Seeds, A. Stöhr, M. Naftaly, N. Ridler, R. Clarke, J. E. Cunningham, and M. B. Johnston, "The 2017 terahertz science and technology roadmap," *Journal of Physics D: Applied Physics*, vol. 50, no. 4, p. 043001, jan 2017.

[24] *Article 2.1: Frequency and wavelength bands.*, Radio regulations 2016 edition ed., International Telecommunications Union, Jan. 2017.

[25] K. R. Jha and G. Singh, *Terahertz planar antennas for next generation communication.* Springer, 2014.

[26] J. Chamberlain, "Where optics meets electronics: recent progress in decreasing the terahertz gap," *Philosophical Transactions of the Royal Society of London. Series A: Mathematical, Physical and Engineering Sciences*, vol. 362, no. 1815, pp. 199–213, 2004.

[27] S. Cherry, "Do telecom data rates mimic moore's law?" *IEEE Spectrum*, vol. 41, no. 7, pp. 50–50, 2004.

[28] R. E. Miles, X.-C. Zhang, H. Eisele, and A. Krotkus, *Terahertz frequency detection and identification of materials and objects.* Springer Science & Business Media, 2007.

[29] C. Mann, "Towards terahertz communications systems," in *Terahertz Sources and Systems.* Springer, 2001, pp. 261–267.

[30] R. Piesiewicz, J. Jemai, M. Koch, and T. Kurner, "Thz channel characterization for future wireless gigabit indoor communication systems," in *Terahertz and Gigahertz Electronics and Photonics IV*, vol. 5727. International Society for Optics and Photonics, 2005, pp. 166–176.

[31] A. Hirata, M. Harada, and T. Nagatsuma, "120-ghz wireless link using photonic techniques for generation, modulation, and emission of millimeter-wave signals," *Journal of Lightwave Technology*, vol. 21, no. 10, pp. 2145–2153, 2003.

[32] A. Hirata, T. Nagatsuma, T. Kosugi, H. Takahashi, R. Yamaguchi, N. Shimizu, N. Kukutsu, K. Murata, Y. Kado, H. Ikegawa *et al.*, "10-gbit/s wireless communications technology using sub-terahertz waves," in *Terahertz Physics, Devices, and Systems II*, vol. 6772. International Society for Optics and Photonics, 2007, p. 67720B.

[33] J. Federici and L. Moeller, "Review of terahertz and subterahertz wireless communications," *Journal of Applied Physics*, vol. 107, no. 11, p. 6, 2010.

[34] D. L. Woolard, J. O. Jensen, and R. J. Hwu, *Terahertz science and technology for military and security applications*. world scientific, 2007, vol. 46.

[35] M. J. Rosker and H. B. Wallace, "Imaging through the atmosphere at terahertz frequencies," in *2007 IEEE/MTT-S International Microwave Symposium*. IEEE, 2007, pp. 773–776.

[36] R. Piesiewicz, T. Kleine-Ostmann, N. Krumbholz, D. Mittleman, M. Koch, J. Schoebei, and T. Kurner, "Short-range ultra-broadband terahertz communications: Concepts and perspectives," *IEEE Antennas and Propagation Magazine*, vol. 49, no. 6, pp. 24–39, 2007.

[37] M. Toyoshima, "Trends in satellite communications and the role of optical free-space communications," *Journal of Optical Networking*, vol. 4, no. 6, pp. 300–311, 2005.

[38] T. Kleine-Ostmann and T. Nagatsuma, "A review on terahertz communications research," *Journal of Infrared, Millimeter, and Terahertz Waves*, vol. 32, no. 2, pp. 143–171, 2011.

[39] B. Bowden, J. A. Harrington, and O. Mitrofanov, "Fabrication of terahertz hollow-glass metallic waveguides with inner dielectric coatings," *Journal of Applied Physics*, vol. 104, no. 9, p. 093110, 2008.

[40] K. Wang and D. M. Mittleman, "Metal wires for terahertz wave guiding," *Nature*, vol. 432, no. 7015, pp. 376–379, 2004.

[41] R. Piesiewicz, T. Kleine-Ostmann, N. Krumbholz, D. Mittleman, M. Koch, and T. Kürner, "Terahertz characterisation of building materials," *Electronics Letters*, vol. 41, no. 18, pp. 1002–1004, 2005.

[42] C. Jansen, S. Wietzke, and M. Koch, "Terahertz spectroscopy of polymers," in *Terahertz spectroscopy and imaging*. Springer, 2012, pp. 327–353.

[43] D. Turchinovich, A. Kammoun, P. Knobloch, T. Dobbertin, and M. Koch, "Flexible all-plastic mirrors for the thz range," *Applied Physics A*, vol. 74, no. 2, pp. 291–293, 2002.

[44] N. Krumbholz, K. Gerlach, F. Rutz, M. Koch, R. Piesiewicz, T. Kürner, and D. Mittleman, "Omnidirectional terahertz mirrors: A key element for future terahertz communication systems," *Applied Physics Letters*, vol. 88, no. 20, p. 202905, 2006.

[45] I. A. Ibraheem, N. Krumbholz, D. Mittleman, and M. Koch, "Low-dispersive dielectric mirrors for future wireless terahertz communication systems," *IEEE microwave and wireless components letters*, vol. 18, no. 1, pp. 67–69, 2008.

[46] S. Wietzke, C. Jansen, F. Rutz, D. Mittleman, and M. Koch, "Determination of additive content in polymeric compounds with terahertz time-domain spectroscopy," *Polymer Testing*, vol. 26, no. 5, pp. 614–618, 2007.

[47] V. Jungnickel, T. Haustein, A. Forck, and C. Von Helmolt, "155 mbit/s wireless transmission with imaging infrared receiver," *Electronics Letters*, vol. 37, no. 5, pp. 314–315, 2001.

[48] N. Cvijetic, D. Qian, and T. Wang, "Optical fiber conference, 2008 feb. 24–28, 2008 san diego osa," *Washington, DC*.

[49] D. Kedar and S. Arnon, "Urban optical wireless communication networks: the main challenges and possible solutions," *IEEE Communications Magazine*, vol. 42, no. 5, pp. S2–S7, 2004.

[50] J. M. Jornet and I. F. Akyildiz, "Channel modeling and capacity analysis for electromagnetic wireless nanonetworks in the terahertz band," *IEEE Transactions on Wireless Communications*, vol. 10, no. 10, pp. 3211–3221, 2011.

[51] V. Petrov, J. Kokkoniemi, D. Moltchanov, J. Lehtomaki, Y. Koucheryavy, and M. Juntti, "Last meter indoor terahertz wireless access: Performance insights and implementation roadmap," *IEEE Communications Magazine*, vol. 56, no. 6, pp. 158–165, 2018.

[52] G. Ducournau, P. Szriftgiser, A. Beck, D. Bacquet, F. Pavanello, E. Peytavit, M. Zaknoune, T. Akalin, and J.-F. Lampin, "Ultrawide-bandwidth single-channel 0.4-thz wireless link combining broadband quasi-optic photomixer and coherent detection," *IEEE transactions on terahertz science and technology*, vol. 4, no. 3, pp. 328–337, 2014.

[53] V. Petrov, A. Pyattaev, D. Moltchanov, and Y. Koucheryavy, "Terahertz band communications: Applications, research challenges, and standardization activities," in *2016 8th International Congress on Ultra Modern Telecommunications and Control Systems and Workshops (ICUMT)*. IEEE, 2016, pp. 183–190.

[54] A. Abdelaziz, K. Yang, K. Qaraqe, J. Boutros, Q. H. Abbasi, and A. Alomainy, "Multiple antenna techniques for terahertz nano-bio communication," in *2018 IEEE 4th Middle East Conference on Biomedical Engineering (MECBME)*. IEEE, 2018, pp. 67–71.

[55] C. Jördens, M. Scheller, B. Breitenstein, D. Selmar, and M. Koch, "Evaluation of leaf water status by means of permittivity at terahertz frequencies," *Journal of biological physics*, vol. 35, no. 3, pp. 255–264, 2009.

[56] P. INITIATIVE, "Federal strategic spectrum plan," Ph.D. dissertation, National Aeronautics and Space Administration, 2008.

[57] E. Brown, K. McIntosh, K. Nichols, and C. Dennis, "Photomixing up to 3.8 thz in low-temperature-grown gaas," *Applied Physics Letters*, vol. 66, no. 3, pp. 285–287, 1995.

[58] S. Matsuura, M. Tani, and K. Sakai, "Generation of coherent terahertz radiation by photomixing in dipole photoconductive antennas," *Applied Physics Letters*, vol. 70, no. 5, pp. 559–561, 1997.

[59] S. Verghese, K. McIntosh, and E. Brown, "Optical and terahertz power limits in the low-temperature-grown gaas photomixers," *Applied Physics Letters*, vol. 71, no. 19, pp. 2743–2745, 1997.

[60] I. Gregory, W. Tribe, B. Cole, M. Evans, E. Linfield, A. Davies, and M. Missous, "Resonant dipole antennas for continuous-wave terahertz photomixers," *Applied Physics Letters*, vol. 85, no. 9, pp. 1622–1624, 2004.

[61] S. Schiller, B. Roth, F. Lewen, O. Ricken, and M. Wiedner, "Ultra-narrow-linewidth continuous-wave thz sources based on multiplier chains," *Applied Physics B*, vol. 95, no. 1, pp. 55–61, 2009.

[62] I. Mehdi, P. Siegel, D. Humphrey, T. Lee, R. Dengler, J. Oswald, A. Pease, R. Lin, H. Eisele, R. Zimmermann *et al.*, "An all solid-state 640 ghz subharmonic mixer," in *1998 IEEE MTT-S International Microwave Symposium Digest (Cat. No. 98CH36192)*, vol. 2. IEEE, 1998, pp. 403–406.

[63] M. Dyakonov, M. Shur, and R. Miles, "Terahertz sources and systems," *Kluwer Academic, The Netherlands*, pp. 187–207, 2001.

[64] G. Carr, M. Martin, W. McKinney, K. Jordan, G. Neil, and G. Williams, "Very high power thz radiation sources," *Journal of biological physics*, vol. 29, no. 2-3, pp. 319–325, 2003.

[65] G. P. Gallerano, S. Biedron *et al.*, "Overview of terahertz radiation sources," in *Proceedings of the 2004 FEL Conference*, vol. 1, 2004, pp. 216–221.

[66] G. P. Williams, "Filling the thz gapï¿½high power sources and applications," *Reports on Progress in Physics*, vol. 69, no. 2, p. 301, 2005.

[67] P. Mukherjee and B. Gupta, "Terahertz (thz) frequency sources and antennas-a brief review," *International Journal of Infrared and Millimeter Waves*, vol. 29, no. 12, pp. 1091–1102, 2008.

[68] T. Minotani, A. Hirata, and T. Nagatsuma, "A broadband 120-ghz schottky-diode receiver for 10-gbit/s wireless links," *IEICE transactions on electronics*, vol. 86, no. 8, pp. 1501–1505, 2003.

[69] H.-J. Song, K. Ajito, A. Hirata, A. Wakatsuki, Y. Muramoto, T. Furuta, N. Kukutsu, T. Nagatsuma, and Y. Kado, "8 gbit/s wireless data transmission at 250 ghz," *Electronics Letters*, vol. 45, no. 22, pp. 1121–1122, 2009.

[70] M. Mukherjee, N. Mazumder, S. K. Roy, and K. Goswami, "Gan impatt diode: a photo-sensitive high power terahertz source," *Semiconductor Science and Technology*, vol. 22, no. 12, p. 1258, 2007.

[71] M. Mukherjee, N. Mazumder, and S. K. Roy, "Prospects of 4h-sic double drift region impatt device as a photo-sensitive high-power source at 0.7 terahertz frequency regime," *Active and Passive Electronic Components*, vol. 2008, 2008.

[72] Y. Ren, J. Hovenier, R. Higgins, J. Gao, T. Klapwijk, S. Shi, A. Bell, B. Klein, B. Williams, S. Kumar *et al.*, "Terahertz heterodyne spectrometer using a quantum cascade laser," *Applied Physics Letters*, vol. 97, no. 16, p. 161105, 2010.

[73] M. A. Belkin, F. Capasso, F. Xie, A. Belyanin, M. Fischer, A. Wittmann, and J. Faist, "Room temperature terahertz quantum cascade laser source based on intracavity difference-frequency generation," *Applied Physics Letters*, vol. 92, no. 20, p. 201101, 2008.

[74] B. S. Williams, S. Kumar, Q. Hu, and J. L. Reno, "Operation of terahertz quantum-cascade lasers at 164 k in pulsed mode and at 117 k in continuous-wave mode," *Optics Express*, vol. 13, no. 9, pp. 3331–3339, 2005.

[75] T. Kleine-Ostmann, K. Pierz, G. Hein, P. Dawson, and M. Koch, "Audio signal transmission over thz communication channel using semiconductor modulator," *Electronics Letters*, vol. 40, no. 2, pp. 124–126, 2004.

[76] A. Hirata, T. Kosugi, H. Takahashi, R. Yamaguchi, F. Nakajima, T. Furuta, H. Ito, H. Sugahara, Y. Sato, and T. Nagatsuma, "120-ghz-band millimeter-wave photonic wireless link for 10-gb/s data transmission," *IEEE transactions on microwave theory and techniques*, vol. 54, no. 5, pp. 1937–1944, 2006.

[77] C. Jastrow, K. Mu, R. Piesiewicz, T. Ku, M. Koch, T. Kleine-Ostmann *et al.*, "300 ghz transmission system," *Electronics Letters*, vol. 44, no. 3, pp. 213–214, 2008.

[78] M. J. Fitch and R. Osiander, "Terahertz waves for communications and sensing," *Johns Hopkins APL technical digest*, vol. 25, no. 4, pp. 348–355, 2004.

[79] B. Thomas, A. Maestrini, J. Gill, C. Lee, R. Lin, I. Mehdi, and P. de Maagt, "A broadband 835–900-ghz fundamental balanced mixer based on monolithic gaas membrane schottky diodes," *IEEE Transactions on Microwave Theory and Techniques*, vol. 58, no. 7, pp. 1917–1924, 2010.

[80] K. Cooper, R. Dengler, G. Chattopadhyay, E. Schlecht, J. Gill, A. Skalare, I. Mehdi, and P. Siegel, "A high-resolution imaging radar at 580 ghz," *IEEE Microwave and wireless components letters*, vol. 18, no. 1, pp. 64–66, 2008.

[81] G. M. Rebeiz, "Millimeter-wave and terahertz integrated circuit antennas," *Proceedings of the IEEE*, vol. 80, no. 11, pp. 1748–1770, 1992.

[82] R. Mendis, C. Sydlo, J. Sigmund, M. Feiginov, P. Meissner, and H. Hartnagel, "Spectral characterization of broadband thz antennas by photoconductive mixing: toward optimal antenna design," *IEEE Antennas and Wireless Propagation Letters*, vol. 4, pp. 85–88, 2005.

[83] N. Shimizu and T. Nagatsuma, "Photodiode-integrated microstrip antenna array for subterahertz radiation," *IEEE photonics technology letters*, vol. 18, no. 6, pp. 743–745, 2006.

[84] K.-i. Maki and C. Otani, "Terahertz beam steering and frequency tuning by using the spatial dispersion of ultrafast laser pulses," *Optics express*, vol. 16, no. 14, pp. 10 158–10 169, 2008.

[85] A. Hirata, T. Kosugi, N. Meisl, T. Shibata, and T. Nagatsuma, "High-directivity photonic emitter using photodiode module integrated with hemt amplifier for 10-gbit/s wireless link," *IEEE transactions on microwave theory and techniques*, vol. 52, no. 8, pp. 1843–1850, 2004.

[86] G.-J. Kim, W.-K. Han, J.-I. Kim, and S.-G. Jeon, "High resolution terahertz imaging (t-ray) with a horn antenna," in *35th International Conference on Infrared, Millimeter, and Terahertz Waves*. IEEE, 2010, pp. 1–2.

[87] D. F. Filipovic, W. Y. Ali-Ahmad, and G. M. Rebeiz, "Millimeter-wave double-dipole antennas for high-gain integrated reflector illumination," *IEEE transactions on microwave theory and techniques*, vol. 40, no. 5, pp. 962–967, 1992.

[88] J. Van Rudd and D. M. Mittleman, "Influence of substrate-lens design in terahertz time-domain spectroscopy," *JOSA B*, vol. 19, no. 2, pp. 319–329, 2002.

[89] J. Kim, C. S. Cho, and F. S. Barnes, "Dielectric slab rotman lens for microwave/millimeter-wave applications," *IEEE transactions on microwave theory and techniques*, vol. 53, no. 8, pp. 2622–2627, 2005.

[90] A. V. Boriskin, R. Sauleau, and A. I. Nosich, "Performance of hemielliptic dielectric lens antennas with optimal edge illumination," *IEEE Transactions on Antennas and Propagation*, vol. 57, no. 7, pp. 2193–2198, 2009.

[91] F. Formanek, M.-A. Brun, T. Umetsu, S. Omori, and A. Yasuda, "Aspheric silicon lenses for terahertz photoconductive antennas," *Applied Physics Letters*, vol. 94, no. 2, p. 021113, 2009.

[92] A. Neto, "Uwb, non dispersive radiation from the planarly fed leaky lens antennaï¿½part 1: Theory and design," *IEEE Transactions on Antennas and Propagation*, vol. 58, no. 7, pp. 2238–2247, 2010.

[93] A. Karttunen, J. Ala-Laurinaho, R. Sauleau, and A. V. Räisänen, "A study of extended hemispherical lenses for a high-gain beam-steering antenna," in *Proceedings of the Fourth European Conference on Antennas and Propagation*. IEEE, 2010, pp. 1–5.

[94] S. S. Gearhart, C. C. Ling, G. M. Rebeiz, H. Davee, and G. Chin, "Integrated 119-mu m linear corner-cube array," *IEEE microwave and guided wave letters*, vol. 1, no. 7, pp. 155–157, 1991.

[95] G. M. Rebeiz and D. B. Rutledge, "Integrated horn antennas for millimeter-wave applications," in *Annales des télécommunications*, vol. 47, no. 1-2. Springer, 1992, pp. 38–48.

[96] Y. Lan, B. Zeng, H. Zhang, B. Chen, and Z. Yang, "Simulation of carbon nanotube thz antenna arrays," *International Journal of Infrared and Millimeter Waves*, vol. 27, no. 6, pp. 871–877, 2006.

[97] G. W. Hanson, "Fundamental transmitting properties of carbon nanotube antennas," *IEEE Transactions on antennas and propagation*, vol. 53, no. 11, pp. 3426–3435, 2005.

[98] P. J. Burke, S. Li, and Z. Yu, "Quantitative theory of nanowire and nanotube antenna performance," *IEEE transactions on nanotechnology*, vol. 5, no. 4, pp. 314–334, 2006.

[99] C. Fumeaux, G. D. Boreman, W. Herrmann, F. K. Kneubühl, and H. Rothuizen, "Spatial impulse response of lithographic infrared antennas," *Applied optics*, vol. 38, no. 1, pp. 37–46, 1999.

[100] H. Röser, E. Durwen, R. Wattenbach, and G. Schultz, "Investigation of a heterodyne receiver with open structure mixer at 324 ghz and 693 ghz," *International journal of infrared and millimeter waves*, vol. 5, no. 3, pp. 301–314, 1984.

[101] J. Zmuidzinas, A. Betz, and R. Boreiko, "A corner-reflector mixer mount for far infrared wavelengths," *Infrared physics*, vol. 29, no. 1, pp. 119–131, 1989.

[102] W. Miao, Y. Delorme, F. Dauply, R. Lefevre, B. Lecomte, A. Feret, G. Beaudin, J. Krieg, W. Zhang, S. Cheng *et al.*, "Investigation of a 600-ghz membrane-based twin slot antenna for heb mixers," in *Proceedings of 19th international symposium on space terahertz technology*, 2008, pp. 28–30.

[103] A. Sharma, V. K. Dwivedi, and G. Singh, "Thz rectangular patch microstrip antenna design using photonic crystal as substrate," in *Progress in Electromagnetic Research Symposium, Cambridge, USA*, 2008, pp. 161–165.

[104] A. Sharma and G. Singh, "Rectangular microstirp patch antenna design at thz frequency for short distance wireless communication systems," *Journal of Infrared, Millimeter, and Terahertz Waves*, vol. 30, no. 1, p. 1, 2009.

[105] K. R. Jha and G. Singh, "Improved performance analysis of square patch microstrip antenna at terahertz frequency," in *2009 International Conference on Advances in Recent Technologies in Communication and Computing*. IEEE, 2009, pp. 676–679.

[106] ——, "Performance analysis of an open-loop resonator loaded terahertz microstrip antenna," in *Terahertz Planar Antennas for Next Generation Communication*. Springer, 2014, pp. 125–145.

[107] G. Singh, "Design considerations for rectangular microstrip patch antenna on electromagnetic crystal substrate at terahertz frequency," *Infrared physics & technology*, vol. 53, no. 1, pp. 17–22, 2010.

[108] K. R. Jha and G. Singh, "Dual-band rectangular microstrip patch antenna at terahertz frequency for surveillance system," *Journal of computational electronics*, vol. 9, no. 1, pp. 31–41, 2010.

[109] A. K. Bhattacharyya, "Characteristics of space and surface waves in a multilayered structure (microstrip antennas)," *IEEE Transactions on Antennas and Propagation*, vol. 38, no. 8, pp. 1231–1238, 1990.

[110] R. Gonzalo, I. Ederra, C. Mann, and P. De Maagt, "Radiation properties of terahertz dipole antenna mounted on photonic crystal," *Electronics Letters*, vol. 37, no. 10, pp. 613–614, 2001.

[111] K. R. Jha and G. Singh, "Analysis and design of enhanced directivity microstrip antenna at terahertz frequency by using electromagnetic bandgap material," *International Journal of Numerical Modelling: Electronic Networks, Devices and Fields*, vol. 24, no. 5, pp. 410–424, 2011.

[112] A. Sharma, V. K. Dwivedi, and G. Singh, "Thz rectangular microstrip patch antenna on multilayered substrate for advance wireless communication systems," in *Progress in electromagnetics research symposium, Beijing, China*, 2009, pp. 627–631.

[113] V. Lubecke, K. Mizuno, and G. Rebeiz, "Micromachining for terahertz applications," *IEEE Transactions on Microwave Theory and Techniques*, vol. 46, no. 11, pp. 1821–1831, 1998.

[114] S. C. Nemat-Nasser, A. V. Amirkhizi, W. J. Padilla, D. N. Basov, S. Nemat-Nasser, D. Bruzewicz, and G. Whitesides, "Terahertz plasmonic composites," *Physical Review E*, vol. 75, no. 3, p. 036614, mar 2007.

[115] Y. Kadoya, "Thz wave propagation on strip lines: Devices, properties, and applications," in *2007 19th International Conference on Applied Electromagnetics and Communications*. IEEE, 2007, pp. 1–4.

[116] K. R. Jha and G. Singh, "Prediction of highly directive probe-fed microstrip antenna at terahertz frequency," *International Journal of Numerical Modelling: Electronic Networks, Devices and Fields*, vol. 25, no. 2, pp. 175–191, aug 2011.

[117] A. Raisanen, "Challenges of terahertz," in *2nd European Conference on Antennas and Propagation (EuCAP 2007)*, IET. Institution of Engineering and Technology, 2007, pp. 1–4.

[118] A. Räisänen, J. Ala-Laurinaho, A. Karttunen, J. Mallat, P. Pousi, and A. Tamminen, "Recent activities on antenna measurements at mm-and submm-wavelengths at aalto university," in *Proceedings of the 5th European*

Conference on Antennas and Propagation (EUCAP). IEEE, 2011, pp. 3543–3545.

[119] D. Grieg and H. Engelmann, "Microstrip-a new transmission technique for the klilomegacycle range," *Proceedings of the IRE*, vol. 40, no. 12, pp. 1644–1650, 1952.

[120] C. A. Balanis, *Antenna theory: analysis and design*. John wiley & sons, 2016.

[121] R. Waterhouse, *Microstrip patch antennas: a designer's guide*. Springer Science & Business Media, 2013.

[122] E. Yablonovitch, "Photonic crystals: semiconductors of light," *Scientific American*, vol. 285, no. 6, pp. 46–55, 2001.

[123] H. Zheng and S. Ravaine, "Bottom-up assembly and applications of photonic materials," *Crystals*, vol. 6, no. 5, p. 54, may 2016.

[124] P. R. Villeneuve and M. Piché, "Photonic band gaps in two-dimensional square lattices: Square and circular rods," *Physical Review B*, vol. 46, no. 8, p. 4973, 1992.

[125] M. Plihal and A. Maradudin, "Photonic band structure of two-dimensional systems: The triangular lattice," *Physical Review B*, vol. 44, no. 16, p. 8565, 1991.

[126] J. Bueno, V. Murugesan, K. Karatsu, D. J. Thoen, and J. J. A. Baselmans, "Ultrasensitive kilo-pixel imaging array of photon noise-limited kinetic inductance detectors over an octave of bandwidth for thz astronomy," *Journal of Low Temperature Physics*, vol. 193, pp. 96–102, 2018.

[127] Z. Li, L. Guan, C. Li, and A. Radwan, "Secure intelligent spectrum control strategy for future thz mobile heterogeneous networks," *EEE Communications Magazine*, vol. 56, no. 6, pp. 116–123, 2018.

[128] K. Murate and K. Kawase, "Terahertz wave parametric generator and its applications," *Journal of Applied Physics*, vol. 124, no. 16, p. 901, 2018.

[129] C. Wu, X. Miao, and K. Zhao, "Identifying pm2.5 samples collected in different environment by using terahertz timedomain spectroscopy," *Frontiers of Optoelectronics*, vol. 11, pp. 256–260, 2018.

[130] M. H. Y.-M. O. S. J. B., Seo, "Study of molecular structure change of d - and l -glucose by proton irradiation using terahertz spectroscopy," *Infrared Physics and Technology*, vol. 93, pp. 154–157, 2018.

[131] H. Zhang, Z. Li, F. Hu, B. Qin, Y. Zhao, T. Chen, and C. Hu, "Sensitive distinction between herbs by terahertz spectroscopy and a metamaterial resonator," *Spectroscopy Letters*, vol. 51, pp. 174–178, 2018.

[132] W. Zhang, Y. Tang, A. Shi, L. Bao, Y. Shen, R. Shen, and Y. Ye, "Recent developments in spectroscopic techniques for the detection of explosives," *Materials*, vol. 11, 2018.

[133] G. S. Kumud Ranjan Jha, "Dual-band rectangular microstrip patch antenna at terahertz frequency for surveillance system," *J Comput Electron*, vol. 9, no. 1, pp. 31–41, 2009.

[134] I. F. Akyildiz, J. M. Jornet, and C. Han, "Terahertz band next frontier for wireless communications," *Physical Communication*, vol. 12, pp. 16–32, 2014.

[135] J. Federici and L. Moeller, "Review of terahertz and subterahertz wireless communications," *J. Appl. Phys*, vol. 107, no. 1, p. 11110, 2010. [Online]. Available: https://doi.org/10.1063/1.3386413

[136] K. R. Jha and G. S. A. and, "and design of rectangular microstrip antenna on two-layer substrate materials at terahertz frequency," *J Comput Electron*, vol. 9, no. 2, pp. 68–78, 2010.

[137] M. Singh, J. Rai, and A. Mrwaha., "Design of a triangular patch microstrip antenna on a substrate of photonic crystal material," *International Journal of Computer Applications*, vol. 96, no. 8, pp. 26–29, 2014.

[138] H. Kim, W. Choe, and . A. Jinho Jeong, "Terahertz cmos v-shaped patch antenna with defected ground structure," *Sensors.*, vol. 18, no. 8, p. 2432, 2018.

[139] D. M. Pozar., "Considerations for millimeter wave printed antennas," *IEEE Transactions on Antennas and Propagation*, vol. 31, no. 5, pp. 740–747, 1983.

[140] A. Sharma, V. K. Dwivedi, and G. Singh., "Thz rectangular microstrip patch antenna on multilayered substrate for advanced wireless communication systems," *Progress in Electromagnetics Research Symposium, Beijing, China*, pp. 627–631, 2009.

[141] K. Wu, Y. J. Cheng, T. Djerafi, and W. Hong., "Substrate-integrated millimeter-wave and terahertz antenna technology," in *Proc. IEEE*, 2012, pp. 2219–2232.

[142] R. Bala and A. Marwaha, "Analysis of graphene based triangular nano patch antenna using photonic crystal as substrate for wireless applications." in *2nd International Conference on Recent Advances in Engineering and Computational Sciences (RAECS)*, 2015, 2nd International Conference on Recent Advances in Engineering and Computational Sciences (RAECS).

[143] G. M. Yang, R. H. Jin, G. B. Xiao, C. Vittoria, V. G. Harris, and N. X. Sun, "Ultra wideband (uwb) antennas with multi-resonant splitring loops." *IEEE Trans Antennas Propag.*, vol. 57, no. 1, pp. 56–260, 2009.

[144] D. Grischkowsky, I. N. I. Duling, T. C. Chen, and C.-C. Chi, "Electromagnetic shock waves from transmission lines," *Phys. Rev Lett(15)*, vol. 59, no. 15, pp. 1663–1666, 1987.

[145] K. R. Jha and G. S. . A. and, "and design of terahertz microstrip antenna on photonic bandgap material," *J. Comput Electron*, vol. 11, no. 4, pp. 364–373, 2012.

[146] A. Singh and S. Singh, "A trapezoidal microstrip patch antenna on photonic crystal substrate for high speed thz applications," *Photonics and Nanostructures-Fundamentals and applications*, vol. 14, pp. 52–62, 2015.

[147] R. K. Kushwaha, P. Karuppanan, and L. D. Malviya, "Design and analysis of novel microstrip patch antenna on photonic crystal in thz," *Physica B: Condensed Matter*, vol. 545, pp. 107–112, 2018.

[148] A. Nejatia, R. AliSadeghzadeh, and F. Geran, "Effect of photonic crystal and frequency selective surface implementation on gain enhancement in the microstrip patch antenna at terahertz frequency," *Physica B: Condensed Matter*, vol. 449, p. 113, 2014.

[149] M. Dadras, P. Rezaei, and M. Danaie, "Planar double-band monopole antenna with photonic crystal structure," *Indian Journal of Science and Technology*, vol. 8, 2016.

[150] K. R. Jha and G. Singh., "Effect of unit-cells of the frequency selective surface as superstrate on the directivity of rectangular microstrip antenna," *J Comput Electron*, vol. 13, no. 2, pp. 496–502, 2014.

[151] S. Noda, K. Tomoda, N. Yamamoto, and A. Chutinan., "Full three-dimensional photonic bandgap crystals at near-infrared wavelengths," *Science.*, vol. 289, no. 5479, p. 604, 2000.

[152] Y. A. Vlasov, X.-Z. Bo, J. C. Sturm, and D. J. Norris., "On-chip natural assembly of silicon photonic bandgap crystals," *Nature.*, vol. 414, no. 6861, p. 289, 2001.

[153] M. Qi, E. Lidorikis, P. T. Rakich, S. G. Johnson, J. D. Joannopoulos, E. P. Ippen, and . A. H. I. Smith, "three-dimensional optical photonic crystal with designed point defects," *Nature.*, vol. 429, no. 6991, p. 538, 2004.

[154] A. Razmjou, M. Asadnia, O. Ghaebi, H.-C. Yang, E. Warkiani, H. M., and C. J., "V.:preparation of iridescent 2d photonic crystals by using a mussel-inspired spatial patterning of zif-8 with potential applications in optical switch and chemical sensor," *ACS Applied Materials and Interfaces*, vol. 9, no. 43, pp. 38 076–38 080, 2017.

[155] A. I. Il'in, V. T. Volkov, O. V. Trofimov, and M. Y. Barabanenkov, "Technological problems in forming si waveguide lamellar diffraction gratings and 2d photonic crystals by plasma and wet etching of si," in *2015 IEEE 15th*

International Conference on Nanotechnology (IEEE-NANO). IEEE, 2015, pp. 983–986.

[156] V. Rajpoot, D. K. Srivastava, and . Arun K. Saurabh, "Optimization of i-shape microstrip patch antenna using pso and curve fitting," *J Comput Electron*, vol. 13, no. 4, pp. 1010–1013, 2014.

[157] O. B. . M. and, "and optimization of radiation characteristics of triangular superconducting microstrip antenna array," *J Comput Electron*, vol. 13, no. 3, pp. 657–665, 2014.

[158] K. Fertas, H. Kimouche, M. Challal, H. Aksas, R. Aksas, and . A. Azrar, "Design and optimization of a cpw-fed tri-band patch antenna using genetic algorithms," *ACES JOURNAL*, vol. 30, no. 7, pp. 754–759, 2015.

[159] A. Recioui, A. Azrar, H. Bentarzi, M. Dehmas, and . Mouloud Chalal, "synthesis of linear arrays with sidelobe level reduction constraint using genetic algorithms." *international journal of microwave and optical technology.*, vol. 3, no. 5, pp. 524–530, 2008.

[160] R. Hassan, B. Cohanim, O. De Weck, and G. Venter, "A comparison of particle swarm optimization and the genetic algorithm," in *46th AIAA/ASME/ASCE/AHS/ASC structures, structural dynamics and materials conference*, 2012.

[161] S. Anand *et al.*, "Graphene nanoribbon based terahertz antenna on polyimide substrate," *Optik-International Journal for Light and Electron Optics*, vol. 125, no. 19, pp. 5546–5549, 2014.

[162] B. Ferguson and X.-C. Zhang, "Materials for terahertz science and technology," *Nature materials*, vol. 1, pp. 26–33, 2002.

[163] Z. Li, L. Guan, C. Li, and A. Radwan, "A secure intelligent spectrum control strategy for future thz mobile heterogeneous networks," *IEEE Communications Magazine*, vol. 56, no. 6, pp. 116–123, 2018.

[164] K. Murate and K. Kawase, "Perspective: Terahertz wave parametric generator and its applications," *Journal of Applied Physics*, vol. 124, p. 901, 2018.

[165] D. L. Woolard, R. Brown, M. Pepper, and M. Kemp, "Terahertz frequency sensing and imaging: A time of reckoning future applications?" in *Proc. IEEE 93*, 2005, pp. 1722–1743.

[166] R. Gonzalo, "Modelling of photonic band gap structures," ESTEC, working paper, 2008.

[167] M. N. Temmar, A. Hocini, D. Khedrouche, and M. Zamani, "Analysis and design of terahertz microstrip antenna based on synthesized photonic band gap substrate using bpso," *J. Comput Electron*, 2019.

[168] L. Yang, X. Shi, K. Chen, K. Fu, and B. Zhang, "Analysis of photonic crystal and multi-frequency terahertz microstrip patch," *Physica B: Condensed Matter*, vol. 431, pp. 11–14, 2013.

[169] D. Mittala and E. Sidhu, "Thz rectangular microstrip patch antenna employing polyimide substrate for video rate imaging and homeland defence applications," *Optik-International Journal for Light and Electron Optics*, vol. 144, pp. 634–641, 2017.

[170] R. K. Kushwaha, P. Karrupanan, and L. D. Malviya, *Design and analysis of novel microstrip patch antenna on photonic crystal in THz.* Physica B: Physics of Condensed Matter, 2018.

[171] G. Varamini, A. Keshtkar, and M. Nasser-Moghadasi, "Miniaturization of microstrip loop antenna for wireless applications based on metamaterial metasurface," *International Journal of Electronics and Communications*, 2017.

[172] G. Varamini, A. Keshtkar, and M. Naser-Moghadasi, "Compact and miniaturized microstrip antenna based on fractal and metamaterial loads with reconfigurable qualification," *International Journal of Electronics and Communications*, 2017.

[173] M. Naderi, F. B. Zarrabi, F. S. Jafari, and S. Ebrahimi, "Fractal ebg structure for shielding and reducing the mutual coupling in microstrip patch antenna array," *International Journal of Electronics and Communications*, 2018.

[174] R. Yadav and P. N. Patel, "Ebg-inspired reconfigurable patch antenna for frequency diversity application," *International Journal of Electronics and Communications*, 2017.

[175] M. N. Mollah, N. C. Karmakar, and J. S. Fu., "Uniform circular photonic bandgap structures (pbgss) for harmonic suppression of a bandpass filte," *International Journal of Electronics and Communications*, vol. 62, pp. 717–724, 2008.

[176] K. R. Jha and G. Singh, "Analysis and design of terahertz microstrip antenna on photonic bandgap material," *J. Comput Electron*, vol. 11, no. 4, pp. 364–373, 2012.

[177] K. M. S. Huq, S. A. Busari, J. Rodriguez, V. Frascolla, W. Bazzi, and D. C. Sicker, "Terahertz-enabled wireless system for beyond-5g ultra-fast networks: A brief survey," *IEEE Network*, vol. 33, no. 4, pp. 89–95, 2019.

[178] S. Dash, A. Patnaik, and B. K. Kaushik, "Performance enhancement of graphene plasmonic nanoantennas for THz communication," *IET Microwaves, Antennas & Propagation*, vol. 13, no. 1, pp. 71–75, jan 2019.

[179] C. Jansen, S. Priebe, C. Moller, M. Jacob, H. Dierke, M. Koch, and T. Kurner, "Diffuse scattering from rough surfaces in thz communication channels," *IEEE Transactions on Terahertz Science and Technology*, vol. 1, no. 2, pp. 462–472, 2011.

[180] R. Piesiewicz, C. Jansen, D. Mittleman, T. Kleine-Ostmann, M. Koch, and T. Kurner, "Scattering analysis for the modeling of thz communication systems," *IEEE Transactions on Antennas and Propagation*, vol. 55, no. 11, pp. 3002–3009, 2007.

[181] P. Beckmann and A. Spizzichino, *The scattering of electromagnetic waves from rough surfaces*. Artech House, 1963.

[182] Z. Xu, X. Dong, and J. Bornemann, "Design of a reconfigurable mimo system for thz communications based on graphene antennas," *IEEE Transactions on Terahertz Science and Technology*, vol. 4, no. 5, pp. 609–617, 2014.

[183] D. Tse and P. Viswanath, *Fundamentals of Wireless Communication*. Cambridge University Press, 2005.

[184] A. Sharma Thakur, V. Dwivedi, and G. Singh, "Thz rectangular microstrip patch antenna on multilayered substrate for advance wireless communication systems," *Progress In Electromagnetics Research Symposium, Beijing, China*, vol. 1, 01 2009.

[185] K. Wu, Y. J. Cheng, T. Djerafi, and W. Hong, "Substrate-integrated millimeter-wave and terahertz antenna technology," *Proceedings of the IEEE*, vol. 100, no. 7, pp. 2219–2232, July 2012.

[186] R. Bala and A. Marwaha, "Analysis of graphene based triangular nano patch antenna using photonic crystal as substrate for wireless applications," in *2015 2nd International Conference on Recent Advances in Engineering Computational Sciences (RAECS)*, Dec 2015, pp. 1–7.

[187] G. M. Yang, R. H. Jin, G. B. Xiao, C. Vittoria, V. G. Harris, and N. X. Sun, "Ultrawideband (uwb) antennas with multiresonant split-ring loops," *IEEE Transactions on Antennas and Propagation*, vol. 57, no. 1, pp. 256–260, Jan 2009.

[188] D. Grischkowsky, I. N. D. III, J. C. Chen, and C. C. Chi, "Electromagnetic shock waves from transmission lines," *Physical Review Letters*, vol. 59, no. 15, pp. 1663–1666, Oct. 1987.

[189] K. R. Jha and G. Singh, "Analysis and design of rectangular microstrip antenna on two-layer substrate materials at terahertz frequency," *Journal of Computational Electronics*, vol. 9, no. 2, pp. 68–78, Jun. 2010.

[190] V. Kumar and M. Kumar, "Photonic crystal assisted multiband compact terahertz antenna on engineered silicon-on-insulator," *IET Optoelectronics*, vol. 10, no. 1, pp. 7–10, feb 2016.

[191] A. S. Arezoomand, M. Naser-Moghadasi, I. Arghand, P. Jahangiri, and F. B. Zarrabi, "Photonic band gap implementation for phase centre controlling in vivaldi antenna," *IET Microwaves, Antennas & Propagation*, vol. 11, no. 13, pp. 1880–1886, oct 2017.

[192] M. Qi, E. Lidorikis, P. T. Rakich, S. G. Johnson, J. D. Joannopoulos, E. P. Ippen, and H. I. Smith, "A three-dimensional optical photonic crystal with designed point defects," *Nature*, vol. 429, no. 6991, pp. 538–542, Jun. 2004.

[193] K. S. Novoselov, "Electric field effect in atomically thin carbon films," *Science*, vol. 306, no. 5696, pp. 666–669, Oct. 2004.

[194] M. Esfandiyari, M. Norouzi, P. Haghdoust, and S. Jarchi, "Study of a surface plasmon resonance optical fiber sensor based on periodically grating and graphene," *Silicon*, vol. 10, no. 6, pp. 2711–2716, Apr. 2018.

[195] C. Liu, L. Qi, and X. Zhang, "Broadband graphene-based metamaterial absorbers," *AIP Advances*, vol. 8, no. 1, p. 015301, Jan. 2018.

[196] S. Mrunalini and A. Manoharan, "Dual-band re-configurable graphene-based patch antenna in terahertz band for wireless network-on-chip applications," *IET Microwaves, Antennas & Propagation*, vol. 11, no. 14, pp. 2104–2108, nov 2017.

[197] F. Kazemi, "Dual band compact fractal THz antenna based on CRLH-TL and graphene loads," *Optik*, vol. 206, p. 164369, mar 2020.

[198] N. Kiani, F. T. Hamedani, P. Rezaei, M. J. Chashmi, and M. Danaie, "Polarization controling approach in reconfigurable microstrip graphene-based antenna," *Optik*, vol. 203, p. 163942, feb 2020.

[199] J. Wang, W.-B. Lu, Z.-G. Liu, A.-Q. Zhang, and H. Chen, "Graphene-based microwave antennas with reconfigurable pattern," *IEEE Transactions on Antennas and Propagation*, vol. 68, no. 4, pp. 2504–2510, apr 2020.

[200] M. Grande, G. V. Bianco, D. Laneve, P. Capezzuto, V. Petruzzelli, M. Scalora, F. Prudenzano, G. Bruno, and A. D. Orazio, "Gain and phase control in a graphene loaded reconfigurable antenna," *Applied Physics Letters*, vol. 115, no. 13, p. 133103, sep 2019.

[201] M. Grande, G. V. Bianco, D. Laneve, P. Capezzuto, V. Petruzzelli, M. Scalora, F. Prudenzano, G. Bruno, and A. D'Orazio, "Optically transparent wideband CVD graphene-based microwave antennas," *Applied Physics Letters*, vol. 112, no. 25, p. 251103, jun 2018.

[202] M. Esfandiyari, S. Jarchi, and M. Ghaffari-Miab, "Channel capacity enhancement by adjustable graphene-based MIMO antenna in THz band," *Optical and Quantum Electronics*, vol. 51, no. 5, Apr. 2019.

[203] G. W. Hanson, "Dyadic green's functions and guided surface waves for a surface conductivity model of graphene," *Journal of Applied Physics*, vol. 103, no. 6, p. 064302, mar 2008.

[204] J. Zhao, M. Wang, H. Li, X. Zhang, L. You, S. Qiao, B. Gao, X. Xie, and M. Jiang, "Lithium-ion-based solid electrolyte tuning of the carrier density in graphene," *Scientific Reports*, vol. 6, no. 1, oct 2016.

[205] J. Zhao, M. Wang, X. Zhang, Y. Lv, T. Wu, S. Qiao, S. Song, and B. Gao, "Application of sodium-ion-based solid electrolyte in electrostatic tuning of carrier density in graphene," *Scientific Reports*, vol. 7, no. 1, jun 2017.

PhD thesis: *Analysis and Design of Terahertz Microstrip Antenna based on Photonic Band Gap Substrate.*

By: *Mohamed Nasr eddine TEMMAR*

Supervisor: *Abdesselam HOCINI*

Co-supervisor : *Djamel KHEDROUCHE*

الملخص

تركز هذه الرسالة على تحليل وتصميم هوائيات تيراهيرتز الميكروستريب القائمة على الركيزة البلورية الضوئية. تم تصميم وتحليل الركيزة البلورية الضوئية المركبة باستخدام تقنية تعتمد على مزيج من خوارزمية التحسين التطوري مع المحاكي CST Microwave Studio ومقارنتها مع أداء الهوائي القائم على الركيزة المتجانسة و البلورية الضوئية التقليدية. بعد ذلك ، تم تصميم وتحليل العديد من هوائيات تيراهيرتز بناءً على ركائز فجوة الحزمة الضوئية المعدلة والمهندسة. تم كذلك مقارنة النتائج التي تم الحصول عليها من الهوائيات المذكورة مع أوراق بحثية مختلفة. أخيرًا ، تم التحقيق في نظام اتصال داخلي MIMO باستخدام هوائي مصغر مصمم على أساس ركيزة بلورية ضوئية محسنة مع الجرافين في نطاق التيراهيرتز متبوعًا بدراسة سيناريو اتصال داخلي شائع لأنظمة SISO و SIMO و MISO و MIMO ومقارنتها مع أعمال بحثية أخرى.

الكلمات المفتاحية

تيراهيرتز ، هوائي الميكروستريب، البلورة الضوئية ، خوارزمية التحسين ، CST، MIMO

Abstract

This thesis focuses on the analysis and design of terahertz microstrip antennae based on photonic crystal substrate. A synthesized photonic crystal substrate is designed and analyzed by using a technique based on the combination of an evolutionary heuristic optimization algorithm with the CST Microwave Studio simulator and compared with homogeneous and conventional photonic crystal substrate-based antennae performance. Then, several terahertz antennae are designed and analyzed based on different engineered modified photonic bandgap substrates. The obtained results from the aforementioned antennae are compared with different research papers in literature. Finally, a MIMO indoor communication system is investigated using a designed microstrip antenna based on an optimized photonic crystal substrate with a graphene load at the terahertz band followed by a common indoor communication scenario, which is studied for SISO, SIMO, MISO, and MIMO systems and compared with other researches in literature.

Keywords: Terahertz, Microstrip antenna, Photonic crystal, Heuristic algorithm, CST, MIMO.

Résumé

Cette thèse se concentre sur l'analyse et la conception d'antennes microruban térahertz basées sur un substrat de cristal photonique. Un substrat de cristal photonique synthétisé est conçu et analysé en utilisant une technique basée sur la combinaison d'un algorithme d'optimisation heuristique évolutive avec le simulateur CST Microwave Studio et comparé aux performances d'antennes basées sur un substrat homogène et de cristal photonique conventionnel. Ensuite, plusieurs antennes térahertz sont conçues et analysées sur la base de différents substrats de bande interdite photonique modifiés. Les résultats obtenus à partir des antennes susmentionnées sont comparés à différents articles de recherche dans la littérature. Enfin, un système de communication intérieur MIMO est étudié à l'aide d'une antenne microruban conçue basée sur un substrat de cristal photonique optimisé avec une charge de graphène dans la bande térahertz suivie d'un scénario de communication intérieur commun qui est étudié pour les systèmes SISO, SIMO, MISO et MIMO et comparé avec d'autres recherches dans la littérature.

Mots clés : Terahertz, Antenne Microruban, Cristal photonique, Algorithme heuristique, CST, MIMO.